Application of bio-based FRP on a road traffic bridge

by

Georgios Zarifis

in partial fulfillment of the requirements for the degree of

Master of Science

at the Delft University of Technology,
to be defended publicly January, 2018.

Thesis Committee:	Prof. Dr. M.Veljkovic,	TU Delft
	Dr. M.Pavlović,	TU Delft
	Dr. M.A.N. Hendriks,	TUDelft
	Ir. W.Claassen,	Witteveen + Bos

TU Delft

Witteveen + Bos

Acknowledgements

This report is the result of the research I conducted at Witteveen + Bos for the master degree in Structural Engineering at Delft University of Technology. In order to complete this study, I received support from many people. I would like to thank every person that helped me during this graduation thesis.

First and foremost, I want to thank W+B, for offering the interesting topic and supporting me with the space and knowledge which was needed throughout the writing of this thesis. Especially I would like to thank Ir. W. Claassen who advised, supervised, helped and guided me throughout this project. In addition I would like to thank Ir. P. Bosman who gave me together with W+B the opportunity to get involved with some experimental work on bio-based FRP. I would like to express my sincere gratitude to Dr. M.Pavlović for his guidance throughout this period as well as for the valuable time he spent for our countless discussions on the subject. In addition I would like to thank Prof. Dr. M.Veljkovic for his critical feedback and guidance along the way.

Furthermore, I want to thank my friends in Greece and in Delft for their encouragement, patience and support. Lastly, I would like to thank my family for constantly supporting me all these years. Their love and encouragement helped me to finish this graduation study.

Georgios Zarifis
Delft, January 2018

Abstract

The last decades Fiber Reinforced Polymer (FRP) structures start to find their own place in the field of civil engineering applications and quite lately in bridge engineering. Composites are considered highly versatile materials that offer great tailoring on their design. Synthetic fibers and resins are already quite popular especially in applications where low weight, construction speed and high performance are the objectives.

However, environmental concerns over the disposability of non-recycle composites is driving the engineering world towards the use of natural composites. Certain natural fibers appear to be advantageous not only in terms of mechanical properties but also in terms of sustainability compared to synthetic ones. However, environmental performance of bio materials is difficult to assess and predict due to their large natural variability.

Durability assessment through literature review and optimization of the superstructure of an FRP bridge, accounting for failure modes mostly deriving from high concentrated vertical loading (wheel loading), are the main objectives of this report. In order to deal with the large amount of variables and constraints for the design according to existing structural standards, advanced optimization algorithms are employed. In addition, due to lack of analytical formulas for local buckling resistance prediction, Finite Element (FE) analysis is used since it offers a better insight into buckling failure of composite laminates. Finally, an optimization workflow is developed that accounts for all variables and constraints and minimizes the objective, which in this case is the weight of the superstructure. The obtained results form recommendations for the optimum design of a flax and glass FRP bridge, regarding the thicknesses and orthotropy of the cross section's laminates with $L/300$ and $L/500$ maximum deflection requirement, providing a deck slenderness $L/16$ and a spacing of the web $s_w = h_{SP}/3$. The assessment and the optimization reveals that flax or BioMid FRP could be promising candidates in replacing synthetic fibers for a bridge application as they can compete in performance and weight the synthetic glass FRP for the case of single span bridge and a span range of $10 - 30m$.

Contents

List of abbreviations

BC Boundary Condition. viii, 37, 50, 72

DFBR Defined Before each Run. 71

FE Finite Element. v, viii, xiv, 2, 3, 23, 36, 37, 40, 42–51, 54, 61, 80, 88

FFRP Flax Fiber Reinforced Polymer. 19, 69, 75, 76, 78, 79, 81, 82, 86–88

FRP Fiber Reinforced Polymer. v, viii, xvi, 1, 5, 18, 23, 24, 27, 29, 30, 32, 33, 35–37, 40, 55, 58, 60, 67–69, 72, 74, 76, 78, 85, 87

GFRP Glass Fiber Reinforced Polymer. vii, xvi, 6, 21, 23–25, 30, 37, 76, 78, 79, 81, 82, 84, 87

LM-1 Load Model 1. ix, xiv, xvi, 38, 61, 62, 65, 66, 79

LM-2 Load Model 2. ix, xiv, 38, 61, 63, 65, 66

LSS Laminate Stacking Sequence. xiv, 23, 55, 68, 69

NFRP Natural Fiber Reinforced Polymer. 20, 21

PE Polyethylene. 8

PHA Polyhydroxyalkanoates. 8

PHB Polyhydroxybutyrates. 8

PLA Poly Lactic Acid. 8

PP Polypropylene. 8

PS Polystyrene. 8

PVC Polyvinyl Chloride. 8

RH Relative Humidity. 18, 24

RLM Random Laid Laminate. 22

RTM Resin Transfer Moulding. 11, 12

SLS Serviceability Limit State. ix, xvi, 22–24, 27, 63, 64, 72, 84

SP Sandwich Panel. xiii, xiv, 36, 37, 43–46, 55, 70, 71

TS Tandem System. xiv, 38, 62–66, 73, 79, 80

UD Unidirectional. vii, ix, xvi, 18, 19, 23, 25, 67–69, 78

UDL Uniformly Distributed Loading. xiv, 39, 55, 62, 64

ULS Ultimate Limit State. ix, 22–24, 27, 63–65, 84

UTS Ultimate Tensile Strain. 27

VARTM Vacuum Assisted Resin Transfer Moulding. 12, 19, 20, 22, 33, 34, 36, 60

List of symbols

δ	The quantity that accounts for the mass portion of fibers in the loading direction
η_{cf}	The conversion factor for fatigue effects
η_{cm}	The conversion factor for humidity effects
η_{ct}	The conversion factor for temperature effects
η_{cv}	The conversion factor for creep effects
γ_G	The partial safety factor for permanent actions
γ_M	The partial safety factor
γ_P	The partial safety factor for prestressing actions
γ_Q	The partial safety factor for variable actions
γ_{M1}	The partial material factor linked to uncertainties in obtaining the correct material properties
γ_{M2}	The partial material factor linked to uncertainties due to the nature of the constituent parts and the production method
ψ_0	Factor for combination value of a variable action
ψ_1	Factor for frequent value of a variable action
ψ_2	Factor for quasi-permanent value of a variable action
n_w	Number of longitudinal webs integrated in the sandwich panel
s_w	Spacing of longitudinal webs integrated in the sandwich panel
T_d	The service temperature
T_g	The glass transition temperature
V_f	Fiber volume content in a composite laminate
X_k	The characteristic value of the property
X_k	The design value of the property

List of Figures

List of Tables

Chapter 1

Scope-Objectives

1.1 Introduction

By the term composite material we mean the combination of at least two different materials. Those materials have to interact and cooperate with each other in order to ensure the composite action. The point at which the composite action stops existing, one can consider the failure of the composite material.

After failure of the composite action (interface) composite's constituents work individually. However, since the composite action offers advanced properties to the composite material, its constituents cannot always withstand by themselves the loading or environmental actions held by the entire composite.

Quite early in the construction history, engineers realized that materials can be combined, cooperate and thus produce a system of materials with enhanced properties compared to the sum of its individual components. Great and quite known examples of modern composites are reinforced concrete (steel/concrete) and timber (cellulose fibers/ lignin matrix) structures.

Fiber reinforced polymers consist of a relatively new composite material in which a polymer plays the role of the matrix and the fibers (continuous or discontinuous) the role of the reinforcement. FRP have already an extensive application in aerospace, marine, automobile and electrical product industries. Their advanced properties like high strength to weight ratio and corrosion resistance triggered lately civil engineers to explore FRP's possibilities in their applications. A revolutionary step, was the application of FRP in bridge engineering which first appear in 1976 in Israel and till now huge developments have been noticed. Low weight, low need for maintenance and rapid installation are some of the advantages that lead engineers to the choice of FRP when facing a bridge design project and even more when replacement of an old bridge is the objective. Almost all FRP bridge applications till now involve synthetic fibers and resins.

However, environmental concerns over the disposability of existing non-recyclable composites is driving nowadays the engineering world towards the use of bio-composites. Considering also the increasing application of composites the last decades, the first statement is being further supported by the need of surpassing the dependence on petroleum resources for FRP production. Up until now, there have been applications of bio-FRP in the civil engineering field. However, in bridge applications those are still limited to pedestrian and bicycle bridges [15]. The main reason for this is the long-term behavior of natural composites, which cannot be easily controlled and predicted. The scope of this project is to assess the applicability of bio-composites in a road traffic bridge and will be limited to the most promising bio-fibers (flax and BioMid). Advanced optimization algorithms will be employed for the design of the bridge.

The structure of the current thesis consists mainly of the research question which will

be met by two objectives. Sequencially, each of the objectives will be met by more specific tasks.

1.2 Research question

How can bio-based FRP be used for the application of a road traffic bridge

1.3 Objective 1

Investigate the durability of bio-based FRP

The application of bio-based materials in a road traffic bridge is one of the most aggressive and demanding cases in terms of environmental exposure, strength and stiffness demands. For this reason, the most promising material will be selected that will be asked to meet the design citeria for the bridge application.

1.3.1 Parameters that influence the durability

The main parameters that influence the durability of bio-composites are:

- Moisture absorption
- Elevated temperature
- Creep effect
- Fatigue resistance

1.3.2 Approach method

The way durability issues will be accounted in this thesis, is identical to the one the structural codes have adapted for synthetic FRP. More specifically, as prescribed in chapter 2.3.5 of [9] *"Approach to special problems by using conversion factors"*, those factors are used to determine the reduced values of the design parameters due to environmental degradation or load duration effect. Conversion factors for the case of bio-composites will be based on available literature which is however quite limited.

1.3.3 Goal of Objective 1

The aim of this literature study is to define conversion factors for the selected promising material, which will account for durability for the design process. This outcome will be used as input for the structural optimization of the design that follows in Objective 2.

1.4 Objective 2

Optimize the design of single span, single deck FRP bridge with integrated webs

Design of the bridge will be dealt employing finite element analysis using Abaqus. For the optimization of the design advanced optimization algorithms will be used. Abaqus and modeFrontier will be employed and combined for the FE based optimization process. ModeFrontier is a software that gives the opportunity to combine different softwares into a workflow an make use of advanced optimization algorithms. The outline of objective 2 is briefly presented below:

- Decision for the cross section to be used and discussion on its parameters
- Define design criteria and failure modes
- FE modelling verification in comparison to the analytical approach
- Define and run optimization processes
- Discussion on the results

1.4.1 Definition of optimum design

Especially in case of fiber reinforced polymers the optimum design is not trivial even considering a specific structural configuration. The reasoning behind this, lies in the manufacturing freedom that FRP offers and on the tailored end material properties. The selected structural configuration of the bridge will be a longitudinally stiffened sandwich panel. However, as already mentioned, this choice does not constrain the freedom and variables like thicknesses of laminates, orientation of plies into the laminates etc. The approach for the optimization in the scope of this thesis will account for reasonable assumptions based on current industry manufacturing techniques and limitations for the optimum design.

Part I

Bio-Composites literature review

Chapter 2

Bio-composites overview

2.1 Introduction

The era of using composite materials for building structural elements, starts centuries ago with the use of natural materials. Findings from ancient civilizations reveals the use of clay together with straw fibers for building walls approximately 3000 years ago. However, later on, natural fibers lost their interest and more durable construction materials took their place like concrete, steel etc.. During the sixties though, a rise for composite materials took place incorporating glass fibers and synthetic resins. It is only the last two decades that natural fibers are regaining their interest for structural applications, because of the increasing environmental concern and their comparable to synthetic fibers properties, and quite recently for a road traffic bridge application.

The environmental impact of natural fiber composites is considerably lower compared to glass or carbon composites. This can be justified if one considers the production energy of natural fibers, which is less than half compared to synthetic fibers see Figure 2.1.

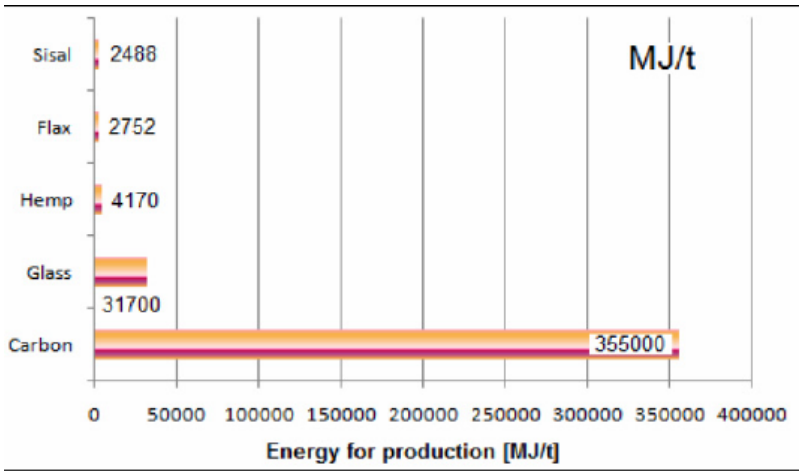

Figure 2.1: Energy for production of some natural fibers (adopted from [1])

As already mentioned, the interest in bio-based composites is constantly increasing nowadays from all different kind of parties (governments, companies, etc.). Although different parties may have different motivation, the point where everybody meet is the potential of bio-based composites to replace synthetic FRPs, offering not only lower cost but also improved sustainability. Pros and cons of bio-based composites compared to synthetic FRPs are summarized in Table 2.1.

Table 2.1: Benefits and drawbacks of bio-based composites compared to conventional GFRP [10, 11, 12, 13]

Benefits	Drawbacks
• Lower pollution and energy needed during production • Less abrasive to processing equipment • Low density and relatively high specific strength and stiffness • Higher damping coefficient • Low emission of toxic fumes when subjected to heat and during incineration at the end of their life	• Quality of end-product is difficult to be standardized due to great variability of properties • Sensitive for moisture absorption which results in degradation • Lowering processing temperatures limiting matrix options due to exothermic curing process • Durability needs to be enhanced for civil engineering applications making them not always cost effective

2.2 Factors affecting mechanical properties

A great advantage of composites, is that they offer not only tailoring of shape and material properties but also design freedom. However, this freedom and especially when it comes for bio-based composites, arises many aspects that need to be taken into consideration in order to obtain a robust end material. Below, factors that affect mechanical properties of those composites and explain at the same time their variability are listed.

- Fiber selection (type, harvest time, extraction method, treatment and fiber content)
- Resin selection
- Interfacial strength
- Fiber dispersion and orientation
- Composite manufacturing process

One by one those effects will be discussed below. A extensive review on those, has been given in [16].

2.2.1 Fiber selection

Natural fibers can be categorized based on their origin namely, plant, animal or mineral. It has been observed that, plant and wood fibers, exhibit greater stiffness and strength properties. Those fibers are complex polymers themselves mainly composed of cellulose, hemicellulose, lignin and pectin [14, 17].

Cellulose

Cellulose is the main component of plant 63wt% and wood fibers 49wt% and is responsible for the strength and stability of the cell wall. Cellulose microfibrils consist of

amorphous and crystalline regions. The former, have in general more exposed hydroxyl groups which tend to bond with water molecules while the latter are closely packed having less hydroxyl groups exposed and available for bonding. It can be concluded thus, that amorphous is relatively more hydrophilic compared to crystalline cellulose.

Hemicellulose

Hemicellulose plays the role of the connecting mean between lignin and cellulose, is rarely crystalline and is mostly responsible for the water absorption of the fiber.

Lignin

Lignin acts as a gluing agent together with hemicellulose for cellulose microfibrils and enhances fiber's microbial and UV resistance.

Pectin

Pectin forms the interface where the fibers are connected. Pectin is the most hydrophillic substance in the fibers.

It is reasonable thus to state that, fiber types that have high cellulose content, have also greater structural performance. This makes cellulose based fibers attractive and suitable for structural applications. In addition to that, the more aligned the cellulose microfibrils are to the fiber's direction, the greater their performance gets. This appears to occur mostly in bast fibers. Below, the presented chart summarizes the mostly used cellulosic fibers while Tables 2.2 and 2.3 present their chemical composition and indicative mechanical properties.

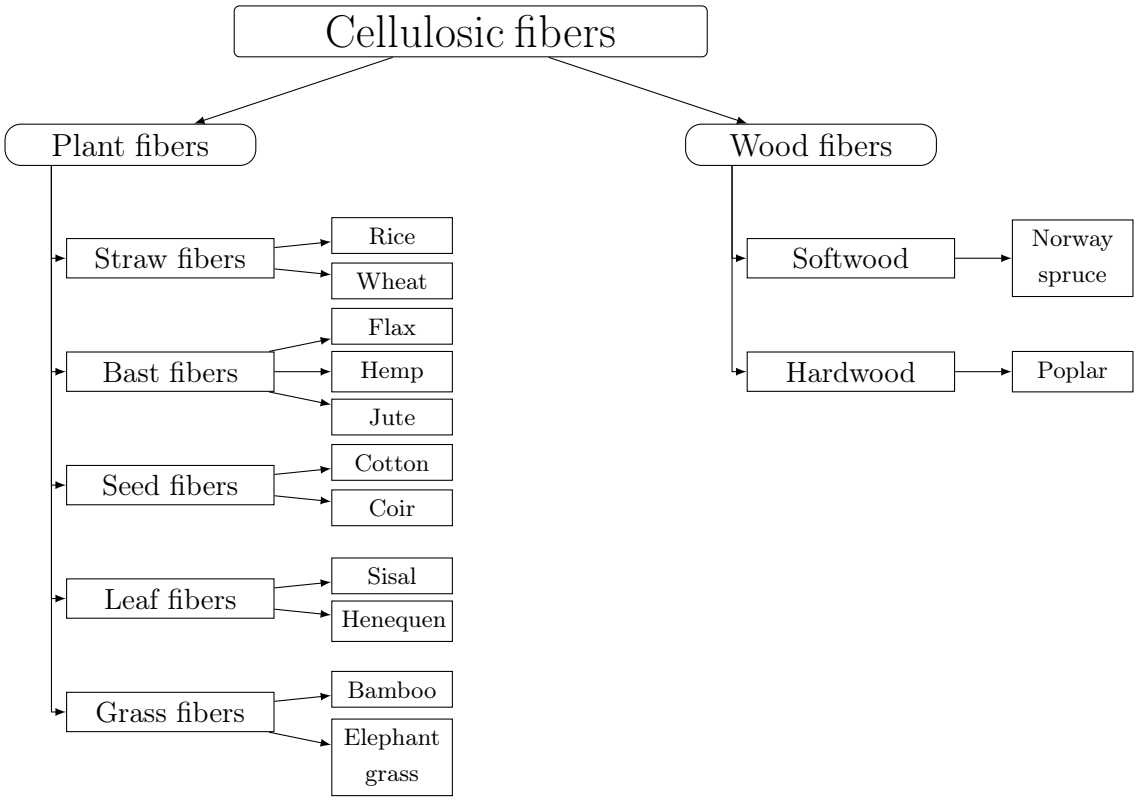

Table 2.2: Cellulosic fibers properties [13]

Fiber type	Density (g/cm^3)	Tensile strength (MPa)	Tensile modulus (GPa)	Specific modulus (approx)
E-glass	$2.5-2.6$	$2000-3500$	$70-76$	29
Bamboo	$0.6-1.1$	$140-800$	$11-32$	25
Coir	$1.1-1.5$	$95-230$	$2.8-6$	4
Cotton	$1.5-1.6$	$287-800$	$5.5-12.6$	6
Flax	$1.4-1.5$	$343-2000$	$27.6-103$	45
Hemp	$1.4-1.5$	$270-900$	$23.5-90$	40
Henequen	1.2	$430-570$	$10.1-16.3$	11
Jute	$1.3-1.5$	$320-800$	$8-78$	30

Table 2.3: Cellulosic fibers chemical composition [13]

Fiber type	Cellulose (wt%)	Hemi-celluose (wt%)	Lignin (wt%)	Pectin (wt%)
E-glass	–	–	–	–
Bamboo	$26-65$	30	$5-31$	–
Coir	$32-43.8$	$0.15-20$	$40-45$	$3-4$
Cotton	$82.7-90$	5.7	<2	$0-1$
Flax	$62-72$	$18.6-20.6$	$2-5$	
Hemp	$68-74.4$	$15-22.4$	$3.7-10$	0.9
Henequen	$60-77.6$	$4-28$	$8-13.1$	–
Jute	$59-71.5$	$13.6-20.4$	$11.8-13$	$0.2-0.4$

2.2.2 Resin selection

The resin in a composite material is equally important as the fibers. It mainly serves for i) protection against environmental effects, ii) keeping the fibers straight, iii) transferring stresses between fibers and iv) protecting the fibers' surface. The resin in the composite material is the ingredient with the highest environmental impact. Governments, companies and scientists are working towards developing an alternative to conventional petroleum-based resins, which follow the environmental concern that is rapidly gaining attention nowadays but also the depletion of fossil fuels.

Resins can be categorized in two families namely, thermoplastics and thermo-settings. Thermosets, are polymers that experience an irreversible chemical reaction called cross-linking or curing with the aid of heat and/or chemical additives. Broadly used thermosets for natural fiber composites are epoxy, phenolic, polyester, vinyl, acrylate resins and polyurethanes. On the other hand, thermoplastics are non toxic and repeatedly meltable at a specific temperature. Examples of thermosets are Polypropylene (PP), Polyethylene (PE), Polystyrene (PS) and Polyvinyl Chloride (PVC). Lately also bio-thermoplastics have been used like Poly Lactic Acid (PLA), Polyhydroxyalkanoates (PHA) and Polyhydroxy-butyrates (PHB) but only on a small scale. Both of the aforementioned categories have been used as matrices for natural fiber composites. The biggest limitation of resin application when choosing a natural fiber is the curing temperature. In fact, most of natural fibers cannot sustain temperatures above $200°C$ [16].

Recyclability of thermoplastics has attracted the interest of developing a biocomposite making use of them rather than thermosetting resins. However, thermosets are generally superior than thermoplastics in terms of mechanical properties, a fact that still limits the latter's broader structural application. A detailed review on biocomposites has been given by [18, 19]. In Figure 2.2 the different, up to now used, resins are listed based on their bio-content and biodegrability.

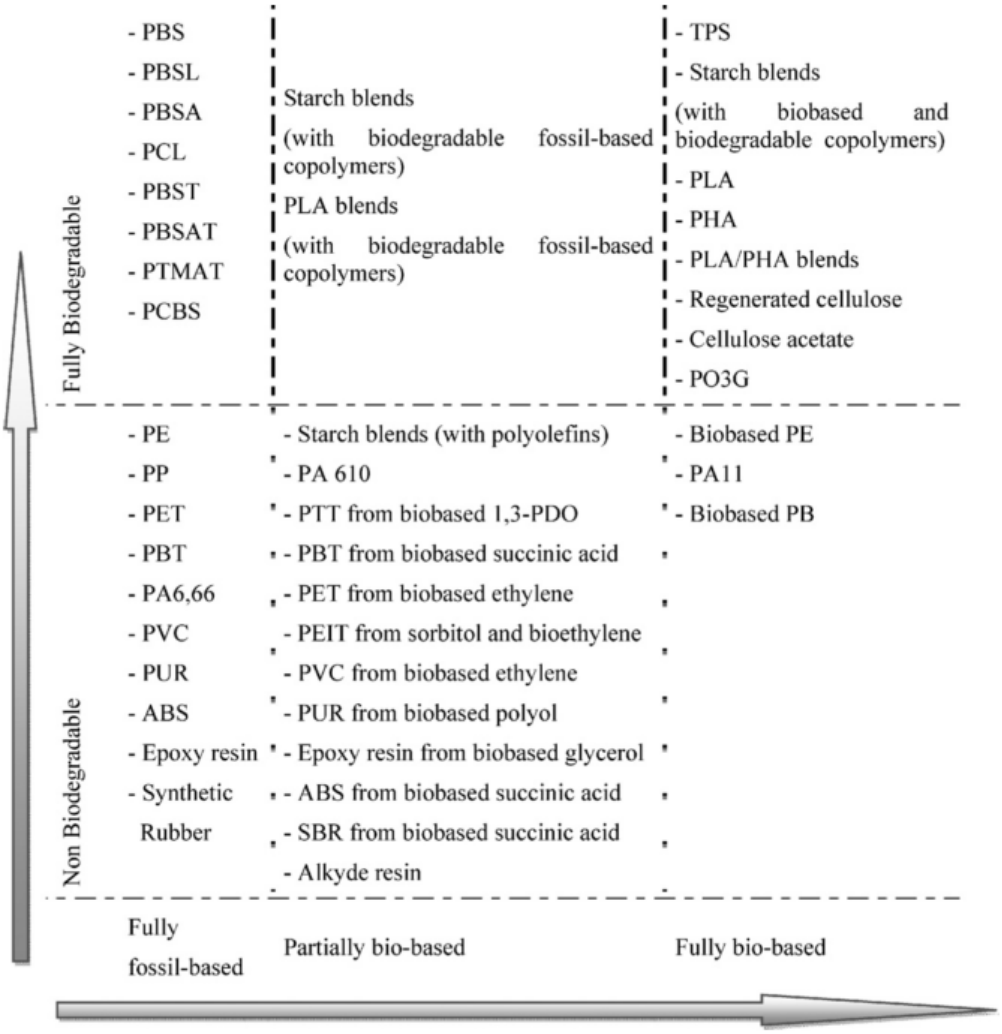

Figure 2.2: Plastics and their biodegrability

2.2.3 Interfacial strength

Interfacial bonding of fibers and matrix is a crucial point and plays a decisive role for the mechanical properties of the composite material since stress transfer takes place between the two substances. However, the fact that plant and wood fibers are hydrophilic while matrices are usually hydrophobic is a drawback for the performance of the interface, affecting moisture resistance and long term properties. Extensive research has been carried out focusing on how to to enhance the interfacial properties of natural fibers and resins and many different techniques have been developed. Those methods, chemical, natural or mechanical aim mostly at reducing the hydrophilicity of natural fibers in order to enhance the compatibility with the matrix. A review on those modification methods is given by [16] and [20].

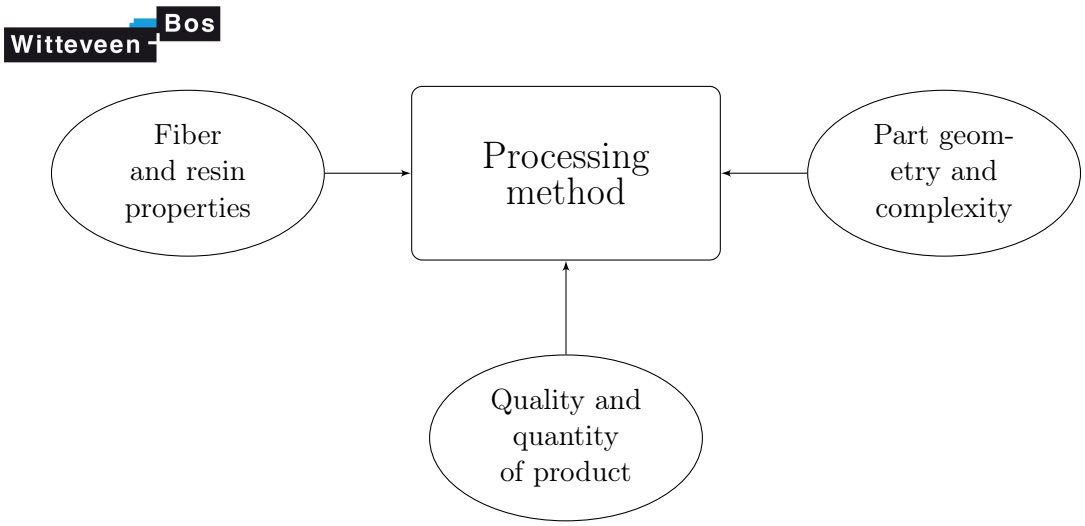

Figure 2.3: Manufacturing process dependencies

2.2.4 Fiber dispersion and orientation

Fiber dispersion has proven to be a major reason that affects the mechanical properties of the composite material. As already discussed, the hydrophilic nature of natural fibers in contradiction to the hydrophobic matrices tends to reduce the fiber dispersion, fibers tend to agglomerate, ending up with fibers not fully surrounded by resin, sabotaging thus interfacial bonding and finally mechanical properties. On the other hand, as far as fiber orientation is conserned, the optimum mechanical properties are obtained when the fibers are alligned parallel to the direction of the applied load. However, in case of natural fibers, who are usually discontinuous compared to synthetic fibers, such an allignment is rather difficult to achieve during the manufacturing process of the composite material. Different fiber processing techniques and manufacturing methods have been employed and developed to cope this difficulty [16].

2.2.5 Composite manufacturing process

During the last decades extensive research has been carried out on different processing and manufacturing techniques of composites. However, in case of natural fibers and bio-based material the choice of the right process depends on several parameters. The ideal choice of manufacturing method depends in fact on complexity, size, fiber's and resin's properties, quality and quantity of the product see Figure 2.3. Some of the most used techniques for composite processing are discussed below.

Compression moulding

Compression moulding is the most popular process in the automotive industry. The process can be briefly described as follows see also Figure 2.4:

- The moudling compound or the semi-finished product is placed in an open mold cavity
- The mold is closed and pressure is then applied forcing the material to fill up the entire mold cavity. At this stage pressure and heat are maintained until full curing of the matrix
- The final part is then removed of the mold

Apart from two dimensional parts, also three dimensional parts are able to be produced using compression moulding with a maximum depth of 15-20cm. This technique appears to

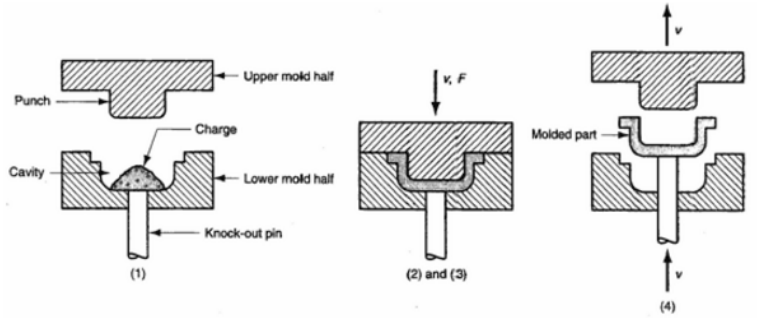

Figure 2.4: Compression moulding process

be more suitable when medium size quantities and larger scale parts are desired, compared to injection moulding for the economical point of view [21].

Pultrusion

The term pultrusion derives from the combination of words "pull" and "extrusion". The distinct difference of this method compared to the quite known extrusion is that instead of being pushed, the composite material is pulled, using pulling devices like grippers or pads, through the shaped dye in order to form the desired profiles. In this way, continuous lengths of reinforced composite with a constant cross section can be produced while a cutter at the end forms the final length of the products. In the pultrusion process, fibers

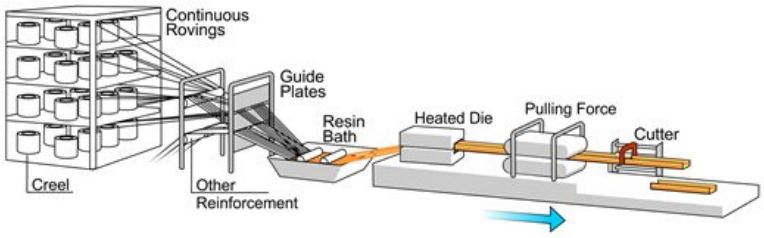

Figure 2.5: Pultrusion process

are present in the form of yarn, roving or reel and are doffed from bobbins. The fibers then sequentially are guided through a resin bath where they are fully impregnated and then the composite passes through a heated die where curing of the resin takes place. Finally the cured material needs some time to cool down and is cut into desired length. The process is depicted in Figure 2.5. Application of the pultrusion manufacturing method has limitation when natural fibers are used mostly because of minimun fiber strength needed to avoid tearing [21].

Resin Transfer Moulding (RTM)

The RTM is a closed mould manufacturing process operating using low pressure up to 5 bar. A great advantage of closed mould processed is the reduction of worker's exposure to harmful volatiles. The process can be described briefly as follow. First, a thermoset resin is injected with pressure aid into the closed cavity where the fibers are already placed in the form of felts or fabrics. The enclosed air is slowly pushed out of the mould, the resin fills the whole cavity and curing reaction begins. Finally, the thickness of the component is being controled by the distance between the mould tools. In Figure 2.6 a schematic representation of RTM is depicted. However, RTM turns out not being cost effective as the component gets bigger. In addition, in case of natural fibers research reveals that difficulties are faced

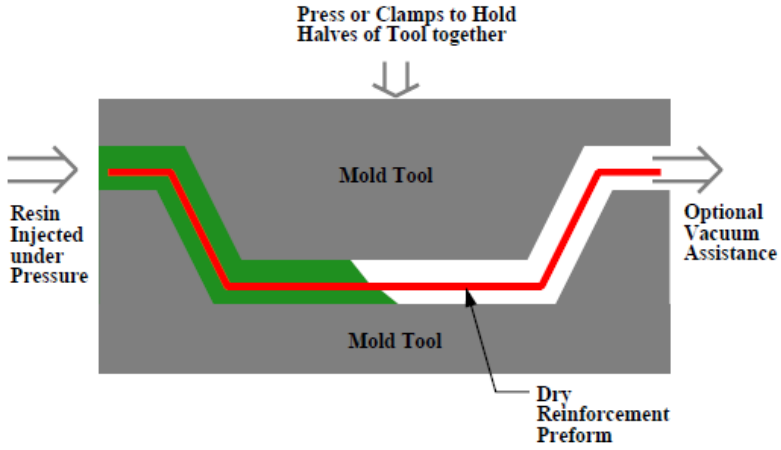

Figure 2.6: Resin transfer moulding process

with the use of RTM on smoothly distributing the resin into the mold, retaining the fiber's arrangement and avoiding unwetted fibers and air voids. The additional assistance of vacuum has been proven to be very helpful regarding the aforementioned issues [21, 22].

Vacuum Assisted Resin Transfer Moulding (VARTM)

VARTM has been developed as an alternative to cope the difficulties that RTM was facing and to reduce the cost coming from large metal tools when the component gets bigger. In VARTM the upper mould metal tool is replaced by a vacuum bag which is completely sealed to the lower surface of the mould. In this way, the need of creating a perfectly matched metal part is eliminated. Figure 2.7 shows a schematic representation of VARTM. The process begins by turning on the vacuum pump and making sure that the vacuum bag is perfectly sealed so as the air can be expelled from the air bag. Then, the resin flow is released and the vacuum pressure of usually 1 atm smoothly drives the resin into the sealed bag. The resin impregnates the already placed fibers and the vacuum pump remains on until the whole component has been impregnated. Finally, curing may take place at room temperature or using an oven. An extensive report on VARMT has been conducted by [22].

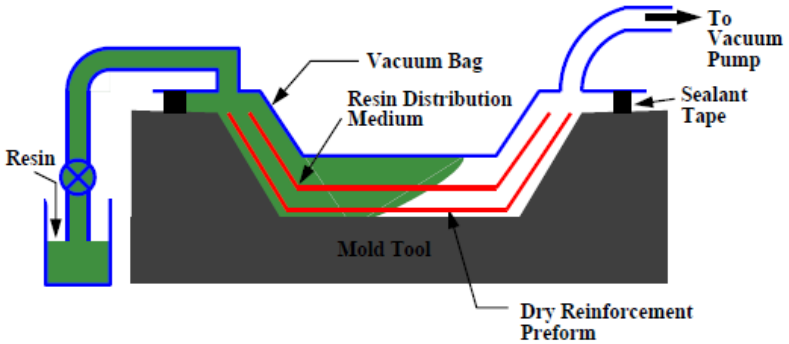

Figure 2.7: Vacuum assisted resin transfer moulding process

Chapter 3

Selection of promising fibers

The application of bio-based materials in a road traffic bridge is one of the most aggressive and demanding cases in terms of environmental exposure, strength and stiffness demands. For this reason, flax and bio-mid fibers will be considered for this project. Criteria for this choice are presented below together with a detailed description of the structure and origin of those selected fibers.

3.1 Selection of flax fiber

In the previous chapter, properties of various natural fibers are presented. After comparison of mechanical strength and stiffness, it can be stated that flax fibers have the most promising properties for a structural application, see table 2.2. Although straight comparison of absolute values of flax properties coincide with those of glass fibers, when comparing specific properties the advantage of flax fibers becomes more easily obvious due to its low density, see Figures 3.1 and 3.2. The specific properties of flax become even more striking when plotting bending stiffness of stiff plates over fiber volume fraction for $V_f > 30$ according to [2], see Figure 3.3.

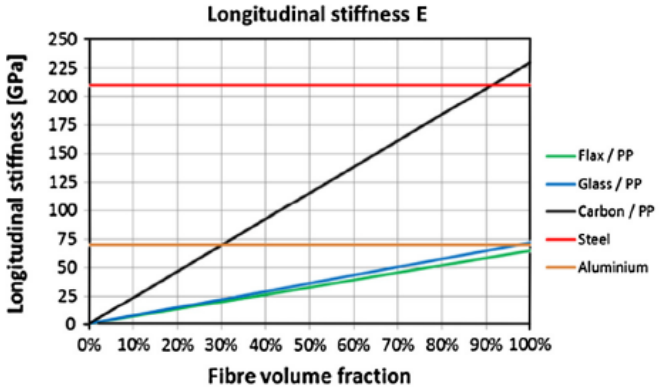

Figure 3.1: Absolute values comparison (adopted from [2])

In addition, flax fiber's surface is more uniform compared to the other natural fibers which confines the large scattering on the material properties that natural fibers experience. Lastly, flax fibers have better vibration absorption behavior and are cheaper and easier to procure than other natural fibers [23]. Therefore the flax is selected as a natural fiber to be applied to the eco-friendly structure. In the following subsections a review of flax fiber is presented.

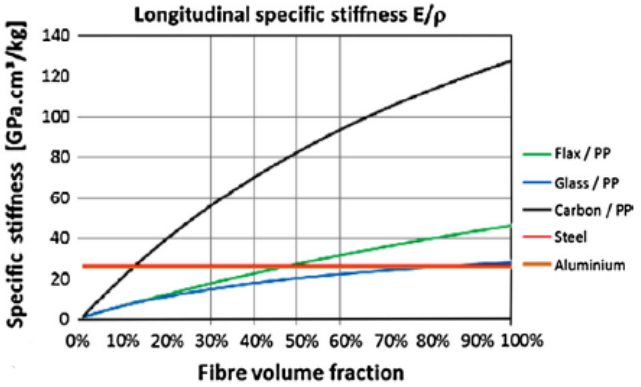

Figure 3.2: Specific values comparison (adopted from [2])

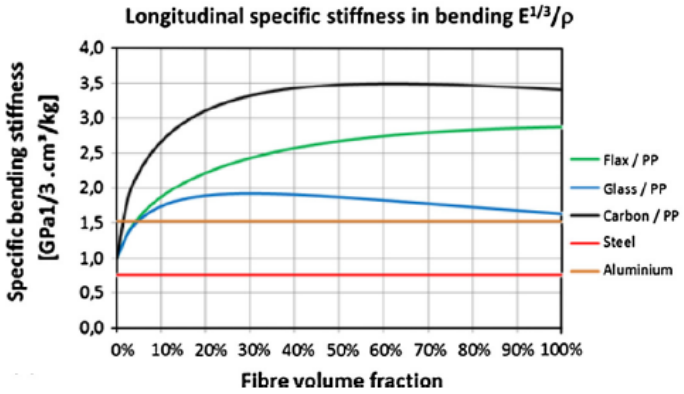

Figure 3.3: Specific bending stiffness of plates comparison (adopted from [2])

3.1.1 Origin and environmental impact

Flax or *linum usitatissimum* is one of the most utilized natural fiber as an alternative to synthetic reinforcement for composites. Flax fibers are found in the stems of flax plant and are not a recent invention. Flax textiles have been found in graves in Egypt that date back to 5000BC. Canada is considered the leading worldwide producer while Belgium, France and Netherlands follow [11].

Flax fibers reduce the production energy of the end composite. They appear to be to be advantageous in all environmental indicators (excluding land use) compared to synthetic fibers see Figure 3.4.

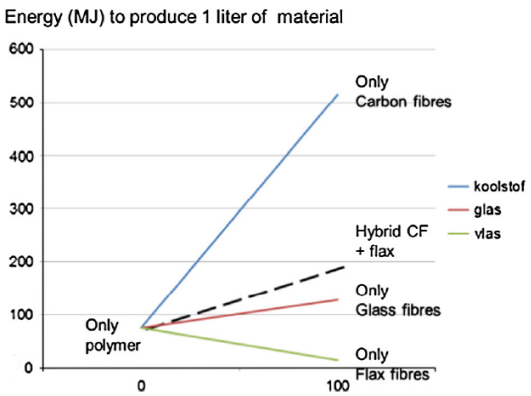

Figure 3.4: Production energy over fiber volume content,V_f (adopted from [2])

3.1.2 Structure

The fibers are found in the form of bundles in the outer ring area of the plant stem, called bast, inner bark or skin see Figure 3.5. They belong thus, to the family of bast fibers which are mostly cellulosic, a substance that is responsible for their strength, stiffness and structural stability [24]. The chemical composition of flax fibers is presented in Table 3.1.

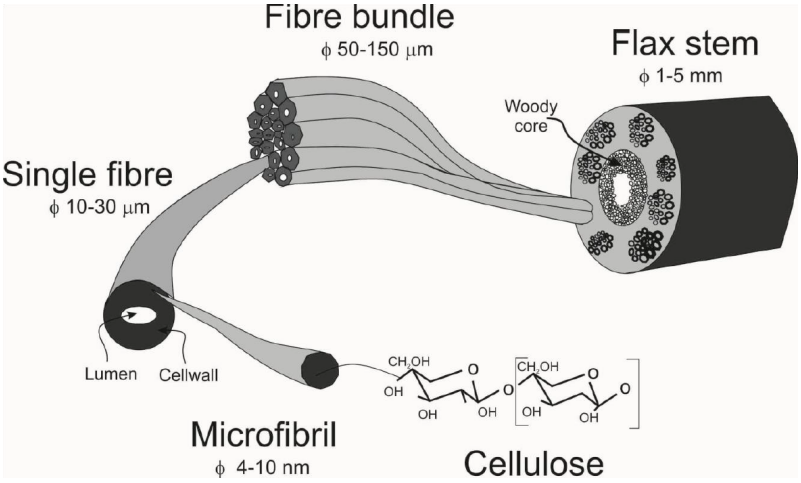

Figure 3.5: Flax cross section and fibers

3.1.3 From plant to fiber

In order to obtain a high quality flax structural fiber from the stem plant, a multistep manufacturing process is required see Figure 3.6. This multi-step procedure also justifies by itself why it is difficult to standardize the material properties of flax. This process involves:

- Rippling of the straw flax plant in order to remove the flower heads.
- Retting of the rippled straw flax. In this step, moisture or micro-organisms are employed to dissolve or rot away the surroundings of the bast fiber bundles in order to isolate the fiber bundles from the stem.
- Scutching follows which involves, complete removal of the wooden parts of the retted fiber bundles. Scutching turbines using knives, scrape the bundles and thus remove the broken wooden stem parts, a process also known as decortication.
- Hackling is the final step before obtaining the technical fibers. Coarse fiber bundles are being combed and as a result thinner and finer fibers are obtained.

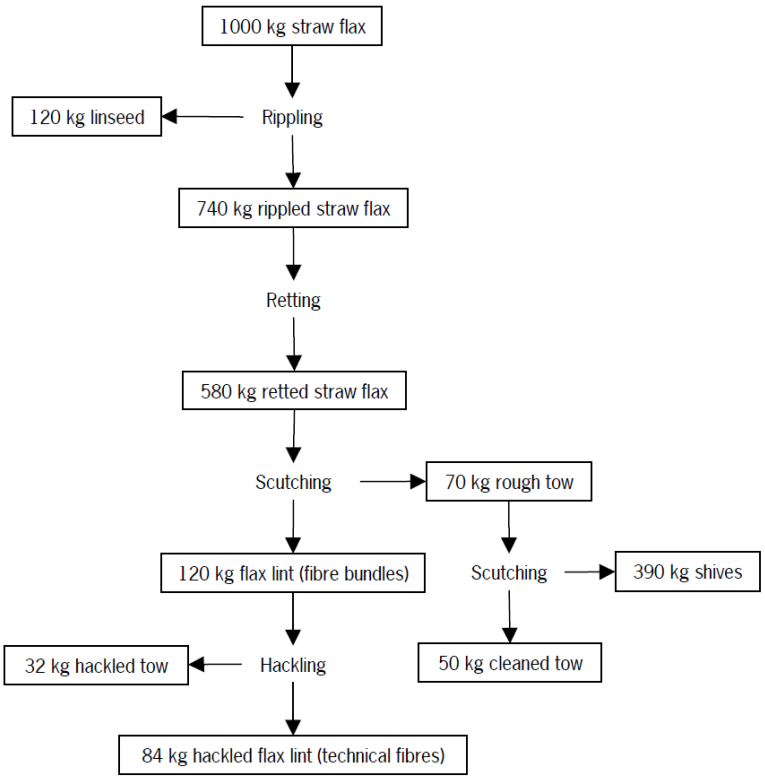

Figure 3.6: Multistep manufacturing process (adopted from [3])

3.1.4 Fiber's properties dependencies

Flax, as a natural fiber, exhibits a great variability in its properties. Difficulties in standardizing the final structural properties with a certain consistency are attributed to [25]:

- Location of harvest and climatic conditions.
- Processing conditions that can introduce defects on the end fibers in every step as described above.
- Sensitivity to temperature moisture and UV radiation.

3.2 Biomid-fibers

Constantly, civil engineers are looking for candidate bio-fibers that could meet the design needs for infrastructure applications with minimum needed modification [14].

3.2.1 Origin - structure

Unlike most bio-based fibers, BioMid is white in color (see Figure 3.8) and becomes transparent when used in a composite laminate. Biomid fibers are secondary bio-based fibers made from by-products of the lumber industry. As a result, it is arguable if they are natural, although they are 100% renewable and biodegradable. Unlike other natural fibers, Biomid are continuous and have very small scattering on their properties. That can be attributed to the fact that the have already experienced some processing.

Figure 3.7: BioMid Fibers

3.3 Properties

In the following table, the mechanical properties of Flax and BioMid compared to E-Glass fibers are presented.

Table 3.1: Flax-BioMid Chemical composition[14]

Substance	Flax [18] [%]	BioMid [%]
Cellulose (wt%)	71	100
Hemi-cellulose (wt%)	18.6-20.6	-
Lignin (wt%)	2.2	-
Waxes (wt%)	1.5	-

Table 3.2: Flax, BioMid and E-Glass mechanical properties [14]

Property	Flax ≤ 100% cellulose	BioMid 100% cellulose	E-Glass	Unit
Modulus of elasticity	55000-75000	52000	72400	MPa
Shear modulus	1600	1600	30200	MPa
Tensile strength	800-1500	1100	2800	MPa
Compression strength	830-1570	1100	2800	MPa
Tensile fracture strain	1.5-2.0	1.5	3.9	%
Poisson ratio	0.25	0.25	0.2	-
Density	1.4-1.5	1.45	2.44	kg/dm^3
Thermal expansion coefficient	5.0	5.0	2.8	$10^{-6}/°C$
Heat conduction coefficient	0.06	0.06	1.05	W/mK

3.4 First results of UD laminates and selected natural fibers

The first results of a large ongoing investigation for the sake of an upcoming project are presented in this section. Those experiments took place in the Windesheim University of Applied Sciences in September & October 2017. The main issues examined are the relative comparison of flax, BioMid and glass for:

1. Fiber moisture content in room temperature and Relative Humidity (RH)
2. Density of the fibers and FRP laminates
3. Fiber volume content of the produced laminates

3.4.1 Fiber moisture content and density

The purpose of the following results is the relative comparison of glass, BioMid and glass fibers regarding the moisture content in room temperature and RH.

Table 3.3: Moisture content of fabrics considered

N_0	Fabric type	Moisture content % per mass	Moisture content % per volume
1	Glass	1.2	3.0
2	Flax (terre prlin UD)	12.7	17.8
3	Flax (Selcom ±45, stitched)	11.0	15.4
4	Flax (comp 0/90 EVO woven)	10.6	14.8
5	BioMid UD (7% vol cross glass)	10.2	14.2

Figure 3.8: Fabrics examined, from left to right, 1,2,3,4 and 5, see Table 3.3

3.4.2 Density of fibers and produced laminates

The production method of the laminates was a hand layup method applying the resin with a roller handle, see Figure 3.9 (a). The type of resin used was a typical polyester /vinyl ester type of resin with a density of $\rho_r = 1191 kg/m^3$. After full impregnation of the fibers with the resin, a sealing tape was used and with the aid of a vacuum pump the resin was removed while curing to achieve a high fiber volume content, see Figure 3.9 (b).

Figure 3.9: (a) Hand layup method, (b) Sealing tape for vacuum application while curing

In Table 3.4 the calculated densities of both the fabrics and the laminates produced are presented.

Table 3.4: Densities and volumetric characteristics of fabrics and laminates

N_0	Fabric type	ρ_f (kg/m^3)	ρ_{lam} (kg/m^3)	V_f (%)	Water (%) vol
1	Glass	2525	2011	60	1.53
2	Flax	1218	1197	20	3.64
3	Biomid	1260	1234	55	7.70

Fiber volume content is quite low in case of flax UD laminate, see Table 3.4. However, such a low V_f is not representative for Flax Fiber Reinforced Polymer (FFRP). Data possessed by W+B reveal that with VARTM higher fiber volume fractions of $40-50\%$ can be achieved. The higher water volumetric percentage of the BioMid laminate compared to the flax laminate can be explained considering the relative V_f contents and the similar

hydrophilicity and moisture absorption of the 2 selected natural fibers, see Table 3.3.

3.5 Conclusion/Notes

The properties of BioMid fibers as presented in Table 3.2 are derived from initial testing of pultruted samples. The first impression is that BioMid's properties have been underestimated, especially the shear modulus which appears to be quite low. At the moment a large investigation of Natural Fiber Reinforced Polymer (NFRP) for the sake of an upcoming project is being performed which includes flax and BioMid fibers in combination with different types of resin. A first impression of this experimental session is presented in Section **??**. Finally, for the sake of this thesis the manufacturing process that has been considered for the design of the bridge is the VARTM. This can easily be justified considering the large component's dimensions, and the benefits of this method as presented in 2.2.5.

As far as the resin is concerned, a 100% bio-based resin cannot yet be applied for a bridge structure and thus a polyester or vinylester type of resin is going to be considered. The main issue for this matter is the low durability of bio-resins and if one considers that the main action of the resin is to protect the fibers from degradation mechanism arising from the interaction with the environment.

Chapter 4

Conversion factors of selected materials

The way durability issues will be accounted in this thesis, is identical to the one the structural codes have adapted for synthetic FRP. More specifically, as prescribed in chapter 2.3.5 of [9] *"Approach to special problems by using conversion factors"*, those factors are used to determine the reduced values of the design parameters due to environmental degradation or load duration effect. The current MSc project will be limited to the examination of the conversion factor that accounts for the degradation of bio-composites caused by the moisture absorption effect. The design value, X_d, of a generic property of resistance or deformation of a material can be expresses as follows:

$$X_d = \eta_c \frac{X_k}{\gamma_M} \tag{4.1}$$

where:

$$\eta_c = \eta_{ct} \cdot \eta_{cm} \cdot \eta_{cv} \cdot \eta_{cf} \tag{4.2}$$

$$\gamma_M = \gamma_{M1} \cdot \gamma_{M2} \tag{4.3}$$

In this chapter, first a detailed calculation of the conversion factors used for a typical GFRP laminate is presented and later an estimation of the conversion factors that should be used for the selected NFRP, see Chapter **??**, is presented based on engineering practice and literature.

4.1 Conversion and material safety factor of GFRP

In this section the conversion and material safety factors for the case of an anisotropic GFRP laminate $[55\%0°/15\%90°/15\% + 45°/15\% - 45°]$ with a fiber volume content of $V_f = 50\%$ as prescribed in Table 11.13 [9]GFRP are presented. The choice for the aforementioned factors accounts for the design of a road traffic bridge, glass fibers and vinyl-ester type of resin.

4.1.1 Temperature η_{ct}

For strength verification the proposed conversion factor for temperature is 0.9, while for deformability and stability the proposed factor is depended on the glass transition temperature (T_g) of the resin used:

- $\eta_{ct} = 1.0$, for service temperature $T_d = T_g - 40$
- $\eta_{ct} = 0.9$, for service temperature $T_g - 40 < T_d < T_g - 20$

The T_g of vinylester is approximately $100°C$. The actual value of T_g depends on the polymerisation process applied and in particular on the temperature applied during post-curing. Based on the T_g of vinyl ester the temperature conversion factor can be taken as 1.0.

4.1.2 Humidity η_{cm}

The conversion factor that accounts for humidity - moisture effects is divided in 3 media classes according to JRC2016 [9] based on the severity of the influence and exposure. The selected media class for the case of the road traffic bridge is number III whose influence is described as: *"Small influence, continuously exposed to water, strong UV exposure, 30-40°C "*. The proposed value for this class is 0.8.

4.1.3 Creep η_{cv}

The creep conversion factor depends on the load duration of each type of loading acting on the structure. Thus, different creep conversion factor has to be considered for each load combination. In addition to that, since the manufacturing process considered throughout this project is the VARTM, the conversion factor used is the one corresponding to the Random Laid Laminate (RLM) as specified in ANNEX A in JRC2016 [9]. In the aforementioned ANNEX A conversion factors are given for a reference load duration of 20 years. Time duration transformation follows the rule below:

$$n_{c\nu}(t_\nu) = (n_{c\nu,20})^T, \qquad T = 0.253 + 0.141 \cdot \log(t_\nu), \qquad t_\nu[h] \tag{4.4}$$

The creep conversion factor differs between ULS and SLS verification.

ULS

The reference conversion factor for strength verification for RLM is:

$$n_{c\nu,20} = 0.63 \tag{4.5}$$

According to Table 2.7 of JRC2016, Classification of loads, the duration of vertical loads on bridges is considered as *long* which means a duration of 6 months. Finally the ULS creep conversion factor can be calculated according to equation 4.4 :

$$T_{6months} = 0.253 + 0.141 \log(0.5 \cdot 365 \cdot 24) = 0.77$$

$$n_{c\nu,ULS} = (n_{c\nu,20})^{T_{6months}} = 0.63^{0.77} = 0.70 \tag{4.6}$$

SLS

The reference creep conversion factor for SLS verification and RLM is:

$$n_{c\nu,20} = \frac{1}{2.4 - 2\delta_i}, \qquad \delta = \frac{1}{1 + \frac{1/V_{fi} - 1}{\gamma_f/\gamma_r}} \tag{4.7}$$

Where:

- δ_i accounts for the V_{fi} in each direction
- $\gamma_r = 1100kg/m^3$ is the density of vinyl ester
- $\gamma_f = 2570kg/m^3$ is the density of glass fibers

Table 4.1: Creep conversion factors for SLS verification

	Direction 1 0°	Direction 2 90°	Direction 12 45°&-45°
V_{fi}	27.5%	7.5%	15%
δ_{fi}	0.47	0.16	0.29
$\eta_{c\nu,20i}$	0.68	0.48	0.55
$\eta_{c\nu,50i}$	0.67	0.46	0.54

That means that for the case of the selected anisotropic GFRP laminate, one has 3 different creep conversion factors. Those are summarized in the Table 4.1.

This approach for accounting for creep for long term deflection is applicable when the engineering constants of the equivalent FRP laminate are considered considered. Also for FE modeling when FRP laminates are modeled as equivalent orthotropic sections, according to E.J.Barbero [26] by using engineering constants.

However, the actual creep effect applies on UD properties and not in the final properties of the laminate. As in the Design optimization chapter, the material is going to be modeled as composite layup (LSS according to E.J.Barbero [26]) , the following procedure is going to be used to account for reduced stiffness due to creep effect. Reduction of the stiffness on UD ply stage is going to take place.
For parallel to fibers:

$$n_{c\nu,20} = \frac{1}{2.4 - 2\delta} = 1.00, \qquad \delta = \frac{1}{1 + \frac{1/V_f - 1}{\gamma_f/\gamma_r}} = 0.7, \qquad V_f = 50\% \tag{4.8}$$

For perpendicular to fibers:

$$n_{c\nu,20} = \frac{1}{2.4 - 2\delta} = 0.42, \qquad \delta = \frac{1}{1 + \frac{1/V_f - 1}{\gamma_f/\gamma_r}} = 0, \qquad V_f = 0\% \tag{4.9}$$

Assumption is made that the shear modulus is reduced by the same factor as the stiffness in the perpendicular of the fiber's direction.

Table 4.2: UD laminate stiffness of GFRPa and creep conversion factors

Composite	V_f (%)	$E_{1,UD}$ (MPa)	$E_{2,UD}$ (MPa)	$G_{12,UD}$ (MPa)	$\nu_{12,UD}$	Density (kg/m^3)
Glass-Vinylester	50	37200	11400	3800	0.29	1835
δ	-	0.7	0	0	-	-
$\eta_{c\nu,50i}$	-	1	0.4	0.4	-	-

4.1.4 Fatigue η_{cf}

Fatigue has an effect on both stiffness and strength. According to JRC2016 [9], for SLS verification, a conversion factor of 0.9 should be taken into account for reduced stiffness. However, for ULS verification the fatigue creep conversion factor needs further examination including testing, something that is beyond the scope of this MSc project. Full scale testing is planned to be done for the project of the bridge in Ritsumasyl in mid 2018.

4.2 Conversion factors for Flax FRP

The degradation process of flax FRP resulting from UV radiation, wear and chemicals, does not differ from glass FRP, since the fibers are protected by the cured resin and the

Table 4.3: Material safety and conversion factors for anisotropic GFRP [9]

Factor	Strength (ULS)	Stability (ULS)	Local stability (ULS)	Creep (SLS)	Momentary deflection (SLS)
γ_{M1}	1.0	1.0	1.0	1.0	1.0
γ_{M2}	1.35	1.35	1.5	1.0	1.0
η_{ct}	0.9	1.0	1.0	1.0	1.0
η_{cm}	0.8	0.8	0.8	0.8	0.8
$\eta_{c\nu}$	0.7	0.7	0.7	-	-
$\eta_{c\nu,1}$	-	-	-	0.67/1	-
$\eta_{c\nu,2}$	-	-	-	0.46/0.4	-
$\eta_{c\nu,12}$	-	-	-	0.54/0.4	-
η_{cf}	-	0.9	0.9	0.9	0.9

degradation mechanism is matrix dominated [15]. Further to that, the durability can be enhanced using paints or coatings at the end product which is a common practice on real applications. However, the distinctive different degradation mechanism that appears in natural FRPs, is that caused by micro-organisms under humid environment. In this section the conversion factors, as found in literature, for a flax FRP are presented. For ease of comparison the same anisotropic laminate as in Section 4.1 is considered, anisotropic laminate $[55\%0°/15\%90°/15\% + 45°/15\% - 45°]$ with a fiber volume content of $V_f = 50\%$.

4.2.1 Temparature η_{ct}

The conversion factor that takes into account temperature effect for glass FRP is 0.9 for strength and 1 for stability and deformability verification. As discussed above and based on experimental work of [15], the temperature conversion factor for flax FRP is taken 0.9 both for SLS and ULS verification.

4.2.2 Creep η_{cv}

At this point there are no quantitative data in literature for creep conversion factor in case of flax FRP. Having in mind flax's origin and following the approach used in [15], the assumption that creep effect in flax FRP is similar to plywood. Thus, the k_{mod} and k_{def} factors are going to be adopted as presented in Eurocode 5 Part 1.1 Tables 3.1 and 3.2 for ULS and SLS verification respectively.

Eurocode 5 presents 3 different service classes:

- Service Class 1: Corresponds to a temperature of 20°C and an air RH that only exceeds 65% for a few weeks per year

  NOTE: In Service Class 1 the average moisture content in the member will not exceed 12%.

- Service class 2: Corresponds to a temperature of 20°C and an air RH that only exceeds 85% for a few weeks per year

  NOTE: In Service Class 2 the average moisture content in the member will not exceed 20%.

- Service Class 3: Corresponds to higher moisture contents than in Service Class 2.

Taking into account also the moisture percentages as presented in Tables 3.3 and 3.4, the estimate for Service Class 2 is made and the relevant values are presented below.

$$\eta_{cv.ULS} = k_{mod} = 0.6 \tag{4.10}$$

$$\eta_{cv.SLS} = \frac{1}{1 + k_{def}} = \frac{1}{1+1} = 0.5 \tag{4.11}$$

The assumption that this creep conversion factor applies for the stiffness parallel to the fiber orientation and being consistent with the assumptions made for GFRP UD properties, the following table presents the adopted creep conversion factors for flax UD properties for long term deflections.

Table 4.4: UD laminate stiffness of GFRPa and creep conversion factors

Composite	V_f (%)	$E_{1,UD}$ (MPa)	$E_{2,UD}$ (MPa)	$G_{12,UD}$ (MPa)	$\nu_{12,UD}$	Density (kg/m^3)
Flax-Vinylester	50	28400	10750	1425	0.32	1175
δ	-	-	0	0	-	-
$\eta_{c\nu,50i}$	-	0.5	0.4	0.4	-	-

4.2.3 Humidity, η_{cm}

Moisture Absorption effect

The moisture effect in combination with that of temperature is an issue of top priority. The reasoning for its importance lies in the incompatibility between the hydrophilic fibers and the hydrophobic matrices which results in the polymer's degradation by sabotaging the interfacial strength as discussed in Section 2.2.3. The degradation mechanism can be briefly described in the following steps and can be depicted in Figure 4.1.

- Water uptake of natural fibers
- Fibers swell
- Micro-cracking of the polymer due to swelling
- The more the composite cracks the more capillarity is being activated
- Capillary mechanism involves the flow of water through fiber-matrix interface
- Water molecules attack the interface causing de-bonding and degradation of the composite structure

The effect of elevated temperatures accelerates the above degradation process.

Literature data

Also for the case of the humidity effect, there is no quantitative conversion factor in literature. Looking into mechanical properties of fibers only, literature findings concerning the humidity effect on them are not always consistent. The reason for this diversity is related to the test conditions and variability factors of natural fibers (growth conditions, extraction condition, storage condition...), see Figure 4.2.

Comparison of glass and flax composites and how the moisture absorption affect their mechanical properties is given in [5]. Testing of unidirectional plates for an immersing period of 40 days until saturation of the specimens took place, see Figure 4.3.

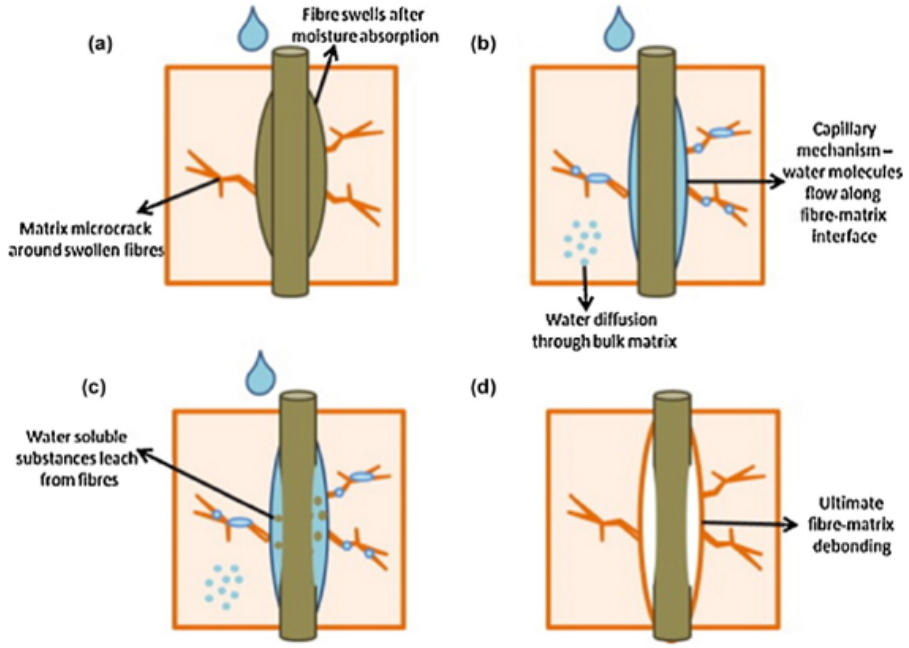

Figure 4.1: Degradation mechanism due to moisture absorption

Kind of fiber	Hygroscopic conditions	Young's modulus evolution	Failure strength evolution	Elongation at break evolution	References
Flax and nettle	30, 40, 50, 60, and 70%	Decreases	Not significative effect		Davies and Bruce, 1998
Flax and sisal			Maximum for RH = 70%		Van Voorn et al., 2001
Flax	30, 66, 93%		Increases and stabilizes at RH = 66%		Stamboulis et al., 2001
Jute, flax, sisal, hemp, coir, agave	65, 90% et immersion	Increases until a threshold, then decreases (depend on the fiber)	Not significative effects	increases	Symington et al., 2009

Figure 4.2: Moisture absorption effect on natural fibers (adopted from [4])

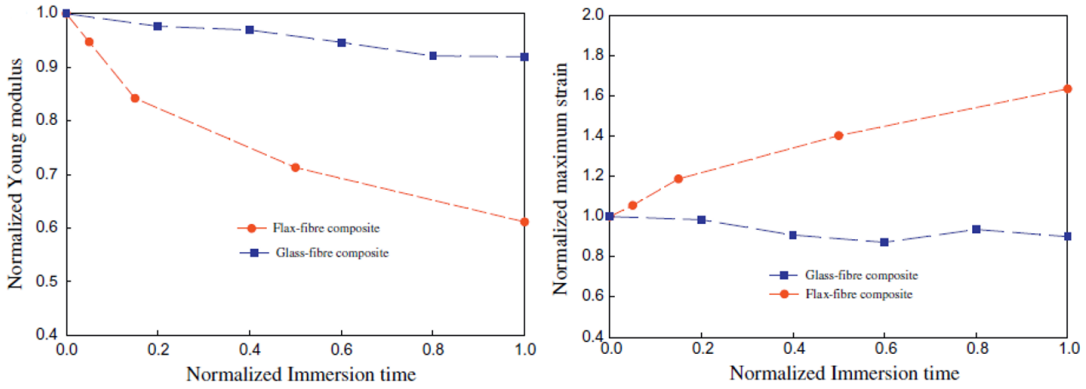

Figure 4.3: Moisture absorption effect on glass and flax composites (adopted from [5])

In Table 4.5 a summary of literature findings on the effect of moisture on flax composites is presented.

In all of the presented cases in Table 4.5, full immersion of the tested samples into water until full specimens saturation has been used . It is not easy to come up with a conversion factor for humidity based on the presented data. The reasons for that are the diversity of the results and the arguable testing conditions (in a real application the structure will

Table 4.5: Tensile modulus and strength change after water ageing of flax FRP

Citation	Type of resin	V_f %	Modulus change %	Strength change %	Fail strain change %	Ageing standard
[27]	Bio-Epoxy	40	−28.0	+10.0	+51.0	UNE-EN ISO 62
		55	−21.0	+35.0	+55.0	
[28]	Epoxy	≈ 55	−22.6	−22.6	−32.5	ASTM D570
[5]	Epoxy	51	-39.0	-15	+63	Immersion (40days up to saturation)

never experience a full immersion in water plus the coating applied highly protects the material against moisture).

The adopted conversion factor that accounts for the humidity effect in flax FRP is 0.8 for both SLS and ULS verification which also coincides with the one proposed in [15].

4.2.4 Fatigue η_{cf}

The great advantage of FRP for fatigue loading is that they usually work on low percentages of the Ultimate Tensile Strain (UTS) and that appears to be beneficial for fatigue resistance. Recent research studies reveal that flax FRP have comparable fatigue resistance to that of glass FRP and also that the fatigue resistance can be increased if the interface properties are enhanced, [29, 30, 31]. Those studies although they examine flax fiber epoxy polymers they can give a qualitative impression compared to glass FRP. The adopted fatigue conversion factor for the purposes of this thesis is 0.9 for flax FRP. However, as mentioned already in Section 4.1.4 specific investigation including experiments needs to be carried out for each separate project/application considering the variability in different resins and quality of the fibers themselves in order to quantify the fatigue resistance of the used composite material.

Table 4.6: Material safety and conversion factors for anisotropic flax FRP

Factor	Strength (ULS)	Stability (ULS)	Local stability (ULS)	Creep (SLS)	Momentary deflection (SLS)
γ_{M1}	1.35	1.35	1.35	1.0	1.0
γ_{M2}	1.35	1.35	1.5	1.0	1.0
η_{ct}	0.9	0.9	0.9	0.9	0.9
η_{cm}	0.8	0.8	0.8	0.8	0.8
$\eta_{c\nu}$	0.6	0.6	0.6	-	-
$\eta_{c\nu,1}$	-	-	-	0.5	-
$\eta_{c\nu,2}$	-	-	-	0.4	-
$\eta_{c\nu,12}$	-	-	-	0.4	-
η_{cf}	-	0.9	0.9	0.9	0.9

Part II

Design optimization

Chapter 5

FRP in bridge deck applications

5.1 Introduction

A bridge structure consist of two main components, the superstructure and the substructure. The superstructure consist of everything above the bearings while the substructure includes all the parts below. The superstructure usually consist of two parts as well, namely the main deck and the girder/beam/stringer system. In Figure 5.1 an illustration of the parts of the superstructure is presented.

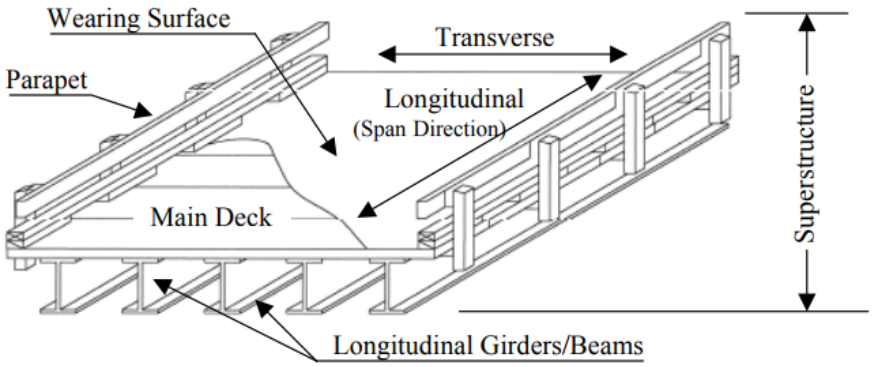

Figure 5.1: Typical parts of a bridge superstructure (adopted from [6])

FRP applications on bridges can be distinguished in three main categories based on the part of the superstructure that they appear. Those are:

- FRP modular decks
- FRP girders
- FRP complete superstructure as one module

5.2 Modular FRP decks

Following the principal of prefabricated concrete slabs/decks, the use of full composite modular decks has gained increased interest. The main reasons for this increased development are:

1. *Lightweight*: An FRP deck typically weighs 80% less compared to a reinforced concrete deck. That appears to be a major advantage in case of existing bridge deck

replacement as it allows for additional capacity but also in cases of movable bridges where weight is critical for the mechanical apparatus used.

2. *Corrosion resistance*: In cold and coastal regions deicing or sea salts interact with the structural elements. Sequentially, corrosion of steel or steel reinforcement becomes an issue that gradually degrades the structure. Considering also that the deck of the bridge is the part mostly exposed to corrosion, the non corrosive properties of FRP decks have been proven to be an optimum alternative for extending the service life of the bridge.

3. *High strength*: GFRP has increased strength when compared to concrete and steel. However, its stiffness is lower than that of steel but still comparable to that of concrete. As a result, the design of those decks is predominantly deflection/strain driven.

4. *Rapid installation*: Due to their modular nature, FRP decks can be rapidly installed and thus minimize the traffic disruption and construction costs.

However, apart from those attractive characteristics there are some challenges that need to be surpassed. Those consist of: the high initial cost compared to alternatives solutions (almost 2-3 times more), long term properties and lack of mature guidelines for their applications.

5.2.1 Manufacturing process

Among the most widely used manufacturing methods for FRP decks one can find the following:

1. *Sandwich construction*: Typical sandwich constructions consist of: (a) stiff faces that carry flexural loads and (b) a lighter core material that ensures the composite action of the panel. Faces are made of FRP laminates, while for the core many alternatives exist like rigid foams, thin-walled cellular structures (honeycomb) or corrugated FRP panels with internal transverse diaphragms. The faces and the core are produced separately and at a next stage are glued together to build the sandwich structure.

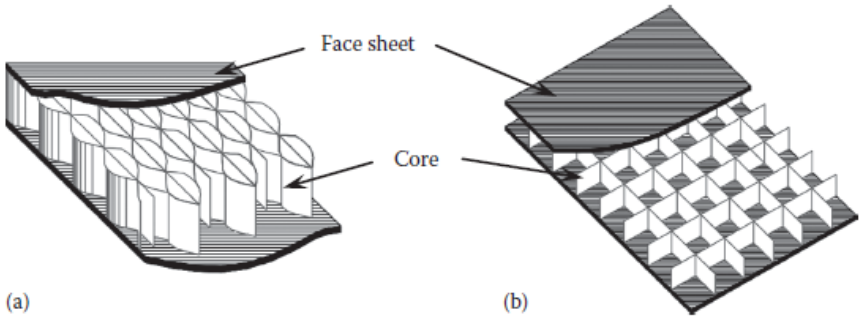

Figure 5.2: (a) Honeycomb core panel and (b) truss (web) core panel, Revised from Cheng, L., Steel-free bridge decks reinforced with FRP composites, FRP Composites for Infrastructure Applications, Springer, NY, 2012, pp 143-162.

2. *Assembly of pultruded sections*: This is the mostly used method for construction of composite bridge decks. The pultruded parts are easy and cheap to produce. They are adhesively or mechanically bonded together. Most of the available commercially decks of this kind include a top and bottom face laminate in order to increase strength

and stiffness. Among their advantages are the low fabrication cost and the ease for repair since it is the top plate that usually experience damage and that can be relatively easily replaced. Examples of such assemblies are presented in Figure 5.3.

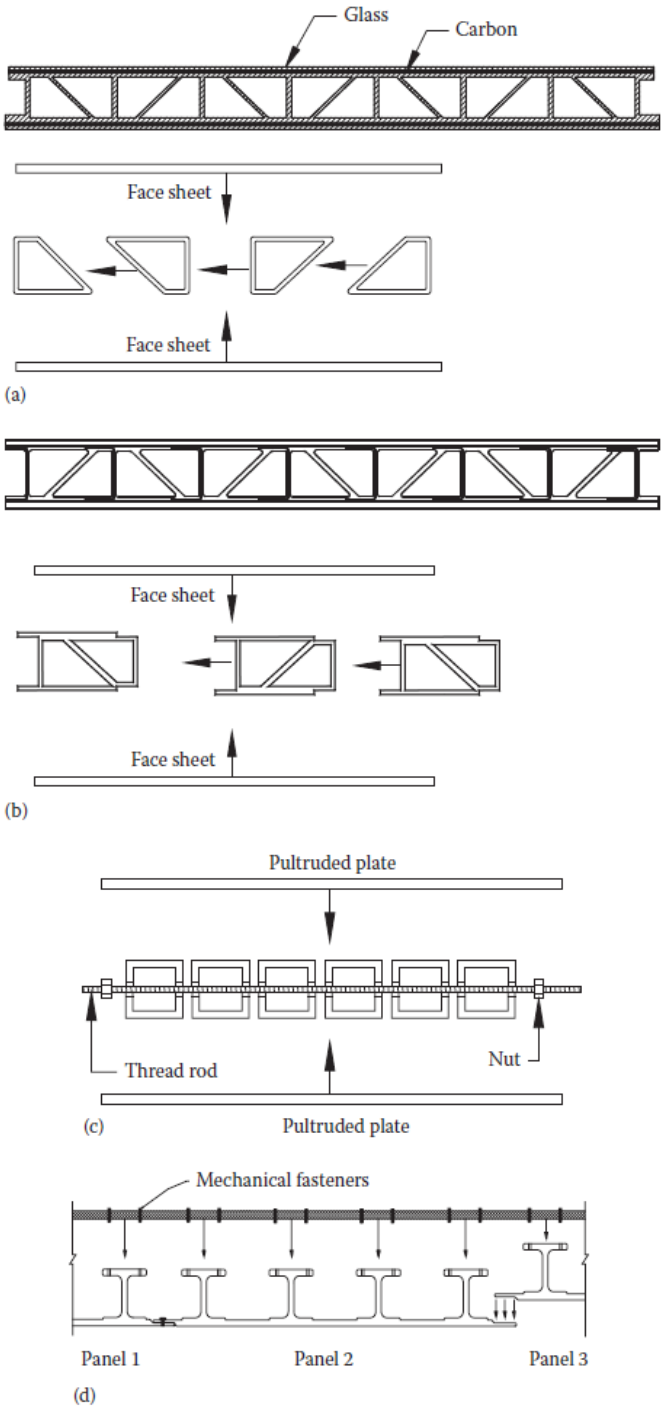

Figure 5.3: Assembly examples of pultruded shapes. (a) Lockheed Martin, (b) DuraSpan by Martin Marietta, (c) Virginia Tech by Strongwell and (d) ZellComp.

Among their disadvantages are the need for on site drilling and mechanical fastening which induces holes and thus defects in the structural elements. Those defects need to be taken into account for premature failure due to stress concentrations or because they can be seen as moisture sensitive spots.

5.2.2 Structural aspects

The properties of FRP composite decks are highly orthotropic. They have usually high strength and stiffness in the longitudinal direction of the panels. The strong primary axis is typically positioned perpendicular to the girders, see Figures 5.4 and 5.5. Finally, when steel or reinforced concrete girders are used, the composite action between the girders and the deck is conservatively neglected as the stiffness of the deck is rather low. However, this is not the case when FRP girders are used [32].

Figure 5.4: Wickwire Run Bridge during installation, Taylor County, West Virginia, 1997 (Crative Pultrusions Inc., Alum Bank,PA.)

Figure 5.5: Installation of Laurel Lick Bridge, West Virginia, the United States, 1997 (Creative Pultrusions Inc., Alum Bank,PA.)

5.3 FRP girders

Bridge girders made of FRP usually have a circular, I-beam, channel rectangular or trapezoidal shape. The reasoning for that is to exploit geometry in order to compensate for the low Young's modulus of FRP compared to steel. So far there are no economic justifications for using FRP girders as those have to be quite deep considering that the

stiffness of FRP is 10% to that of steel. The fact that the weight of a bridge is dominated by the weight of the deck is also a reason why FRP girders are not that widely used compared to FRP decks. No specific guidelines are available for designing FRP girders for a bridge. Proprietary FRP girder sections produced by by Strongwell are presented in Figures 5.6a and 5.6b. Finally recent experience for bridges and footbridges applications in Spain reveals that FRP hybrid girders can be proven to be feasible candidates for spans between 20 and 50m when durability and rapid installation are the objectives [33].

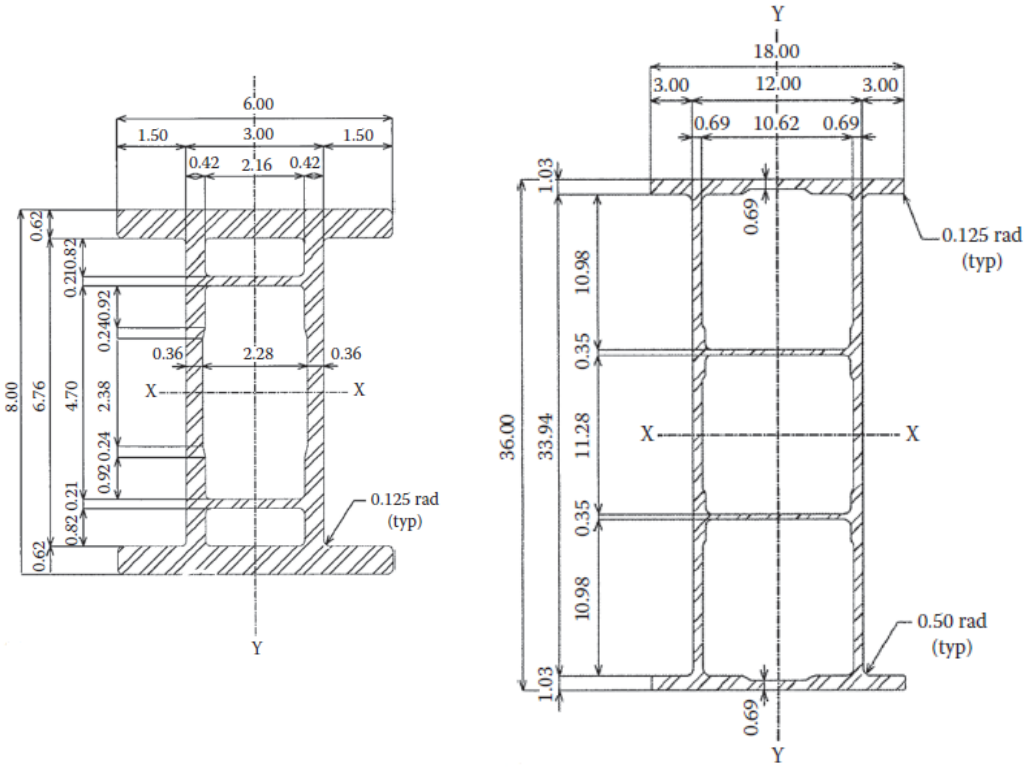

(a) 8 in. (203.2mm) section

(b) 36 in. (914.4mm) section

Figure 5.6: Strongwell pultruded girders (From Strongwell Corporation, *EXTREN DWB® Design Guide,* Bristol, VA,2000)

5.4 FRP superstructure as one module

In 1995, NFESC installed a fully composite pier deck at Port Hueneme in California, see Figure 5.7. The FRP materials used consist of E-glass fibers, isophthalate polyester and vinylester composites. The configuration of the cross-section consists of rectangular box frames and plates where pultruded parts are glued together and rods transversely connect the longitudinal webs. The top finishing of the deck contains an epoxy and grit coating in order to provide a non-skid surface. According to [34], 10 years after the installation, the deck was performing well. No details about the manufacturing method could be found about the specific application. However, it can be assumed that the superstructure was either built using pultrusion in one step, or the FRP laminates of the web, top and bottom face were produced separately and then were assembled/glued together. Judging from Figure 5.7, the absence of the foam material in the core and the presence of transverse rods, drives us to the conclusion that VARTM was not used to manufacture the bridge module in one single infusion process. Recent advances of VARTM method producing FRP

Figure 5.7: NFESC, Port Hueneme, California 1995

elements has led engineers to manufacture at once the module of the bridge. The advances of VARTM include infusion of thick laminates up to 150mm. The superstructure of the

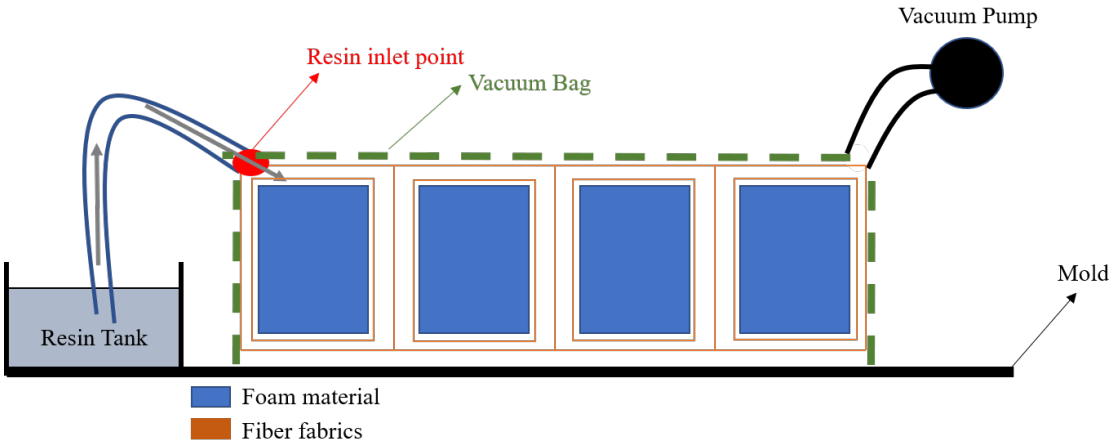

Figure 5.8: Single step manufacturing process of the bridge (Cross sectional view)

bridge is manufactured in one step as a single piece/module. The sequence of the steps through the manufacturing are presented below and can be seen in Figure 5.8:

- Place the foam parts in the predefined places from the design (spacing of the web, thickness of the laminates).
- Place the predefined fabrics from the design around the foam material.
- Seal airtight the mold with a flexible bag and apply vacuum.
- Injection of the resin takes place when opening the resin inlet point and the fabrics start to impregnate.
- Let the resin to cure and remove the end module off the mold.

The end product of the process can be seen in Figure 5.9. Advantages of this methods are: (i) freedom for tailoring the fiber orientation for the face and web laminates, (ii) no need for formwork as the foam material serves for this purpose, (iii) superstructure is created as one module which means that no further gluing or mechanical fastening is needed with other structural parts and (iv) the foam offers lateral support to the web laminate preventing

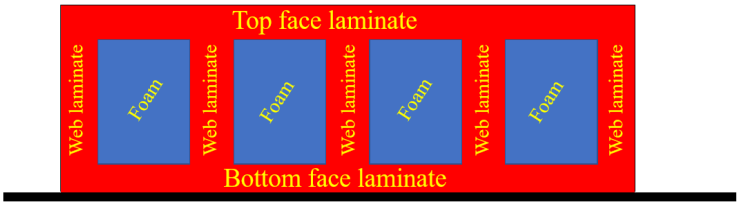

Figure 5.9: Bridge cross section using a single step VARTM process

thus lateral buckling.
However, among their disadvantages one can find: (i) difficulties during the production method and especially in infusing those big scale laminates, (ii) extensive use of foam core which due to unpredictable long term properties, they are usually not taken into account during the design process.

Engineers, trying to reduce the use of the foam in the aforementioned have proposed different cross sectional superstructure configurations as can be seen in Figure 5.10. The advantage of this configuration is that is minimizing the use of the foam which is only limited in the top face. The top face has the form of a sandwich panel with longitudinal integrated webs, while the core and the bottom face consist of simple FRP laminates. The disadvantage of this cross sectional configuration though is its assembly. The top face, the web laminates and the bottom face are produced separately and at a next stage the are glued together. In addition the web laminates are not restrained laterally from a foam material as in case of Figure 5.9 and they can more easily buckle. However, the absence of massive foam blocks in the core can be proven to provide lighter end superstructures. Both, configurations need to be investigated and analyzed to have a more clear insight and comparison including experimental sessions.

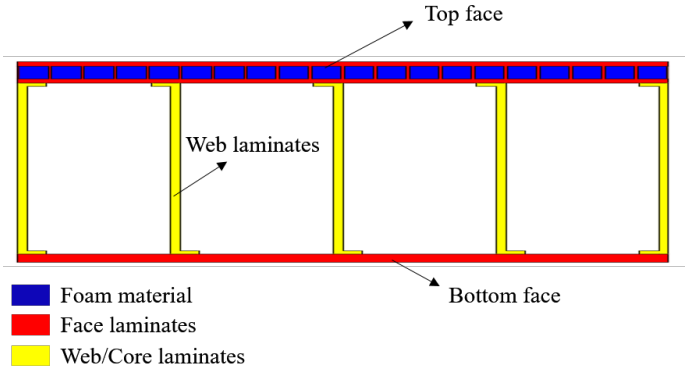

Figure 5.10: Alternative bridge cross section

In the following chapters of this report, the bridge cross sectional configuration using the single step VARMT process as presented in Figures 5.8 and 5.9 will be examined, analyzed and optimized for the design of a road traffic bridge.

Chapter 6

FEM of FRP longitudinally stiffened panel

6.1 Introduction

The case of a road traffic bridge consist of a case with high load cases for the deck. The typical SP configuration which consist of foam core which is between two FRP laminates, see Figure 6.1, will either not suffice for that application of will have a rather low deck slenderness. That can be attributed to the low shear modulus of the foam core and its low compressive strength, which is needed considering the existence of the wheel local loading.

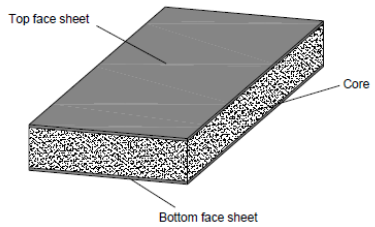

Figure 6.1: Typical SP configuration

Several alternative structural configuration of the SP have been proposed and used that incorporate FRP laminates into the core to cope the low shear modulus of foams and the resistance in patch loading, see Figures 5.2 and 5.3. The majority of those systems are produced in modules using pultrusion and at a later stage are glued together. However, those systems are mostly used as deck systems that usually lie on longitudinal girders and stringers.

Recent advances in the VARTM manufacturing method have given the opportunity to infuse thick FRP laminates up to 150mm. The scope of this thesis is to look for the optimization of an FRP cross section that will be not only the deck of the bridge but the entire superstructure as well, as already discussed in Chapter 5, section 5.4. The core in this case consists of longitudinal FRP laminates who provide considerably higher shear modulus to the core compared to the foam and is easy to produce using VARTM.

In the following section the response of a longitudinally stiffened SP is analyzed. Firstly, a mesh sensitivity analysis is performed in order to determine the minimum required mesh density of the FE and the type of FE. In a second stage, the failure modes of the superstructure that arise from the truck loading of a road traffic bridge are identified and the verification of the response of FE analysis with analytical formulas is performed. In order to accomplish the aforementioned goals, a simple case is chosen which is presented below.

6.2 Simple case description

It is assumed that the superstructure of the presented simple case has been produced using a single step VARTM process, see Figure 5.8. However, due to unpredictable long term properties of the foam that is included, the last one is not generally taken into account during the design face. This assumption is also adopted through this report and thus the contribution of the foam in the structural performance is neglected.

As it is quite known, in FRP applications, deflections drive the design due to the low Young's modulus compared to steel. In addition to that, the stiffness properties of the FRP laminates differ in different directions based on the fiber orientation arrangement. The presence of the wheel loading induces high local vertical and shear stresses to the web. Sequentially, the web FRP laminates are becoming prone to local buckling due to the application of the wheel loading. Shear buckling and local vertical buckling are examined in the section Webs instability of this chapter.

6.2.1 Model's geometry

The geometrical characteristics of the longitudinally stiffened SP are presented in Table 6.1 and depicted in Figures 6.2a and 6.2b.

Table 6.1: SP geometry

Parameter	Symbol	Value $[mm]$
Length	L	4000
Width	b	1000
Face thickness	t_f	15
Core/web height	h_c	200
SP height	h_{SP}	230
Spacing of the webs	s_w	50
Web's thickness	t_w	5
Number of webs	n_w	21
Side of area of concentrated load	a_Q	200

6.2.2 FRP laminate

In this case, the same FRP laminate properties are selected for the facing and the web. An anisotropic GFRP laminate is thus selected $[55\%0°/15\%90°/15\%+45°/15\%-45°]$ with a fiber volume content of $V_f = 50\%$ as prescribed in Table 11.13 [9]. The stiffness values of the laminates are presented in the table below.

Table 6.2: FRP laminate stiffness properties

FRP type	Density $[kg/m^3]$	E_1 $[MPa]$	E_2 $[MPa]$	G_{12} $[MPa]$	v_{12}
GFRP	1835	25800	15900	5600	0.32

6.2.3 BCs and load cases

The sandwich panel is simply supported at both ends considering a line support. In order to avoid numerical singularities in the FE model the application of the BCs is accomplished through 2 neoprene pads of $150mm$ width each see figure 6.3. Two load cases

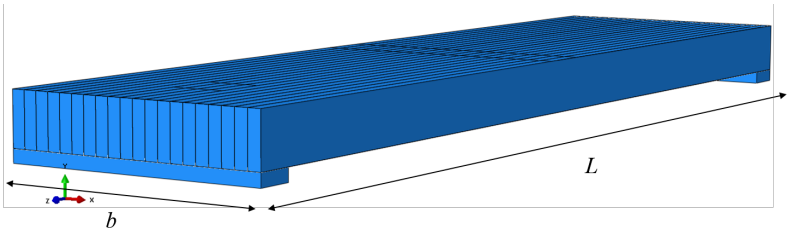

(a) Axonimetric view

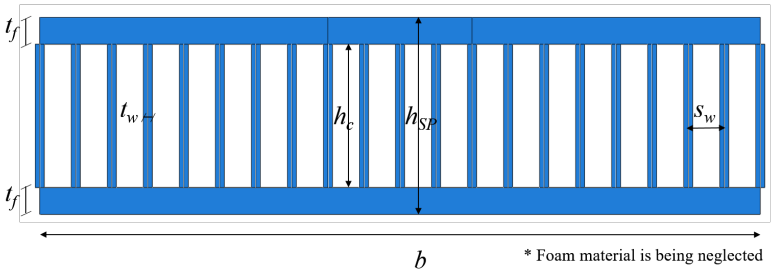

(b) Cross section

Figure 6.2: Simple case superstructure model

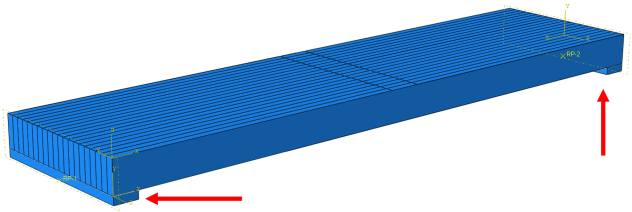

Figure 6.3: Case visualization, arrows indicate the Neoprene pads

will be examined. In the first case a uniformly distributed load of $10kN/m^2$ will be applied at the whole area of the sandwich panel and in the second case, a concentrated load of $40kN$ centralized at the midspan of the panel. The concentrated load will be applied in a square area with a $a = 200mm$ side length. The pressure load at the square area is $1N/mm^2$ which is comparable to the pressure load of the patch loading of the TS for LM-1, $\left(150000/(400 \cdot 400) = 0.9375N/mm^2\right)$ or LM-2, $\left(200000/(350 \cdot 600) = 0.9524N/mm^2\right)$ see Chapter *Basis of design*.

Table 6.3: Load cases

Load case	Uniform q $[kN/m/m]$	Concentrated Q $[kN]$
LC-1 see Figure 6.4	10	x
LC-2 see Figure 6.5	x	40 $(1N/mm^2)$
LC-3 see Figure 6.6	x	40 $(1N/mm^2)$

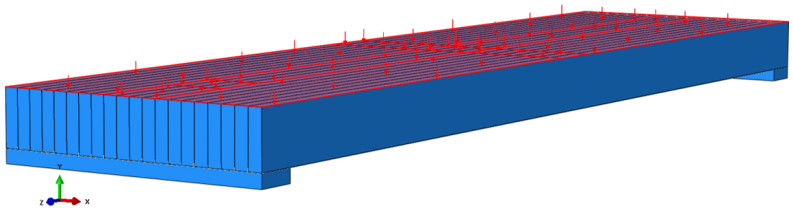

(a) Axonometric view

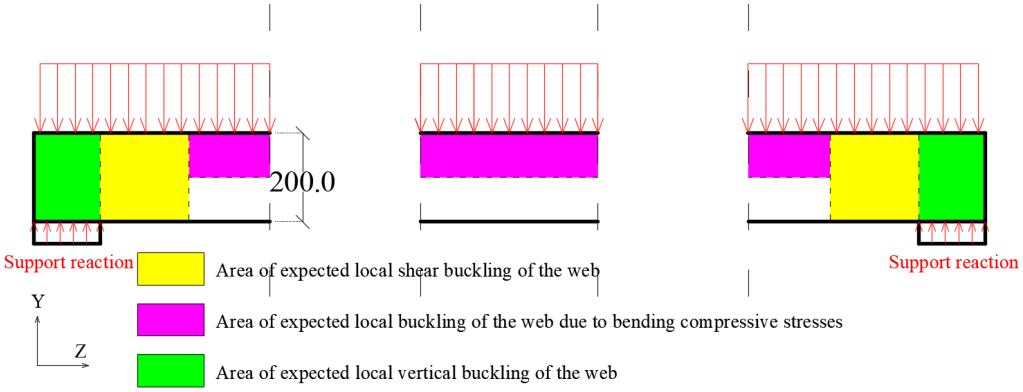

(b) Side view

Figure 6.4: LC-1 UDL $10KN/m^2$

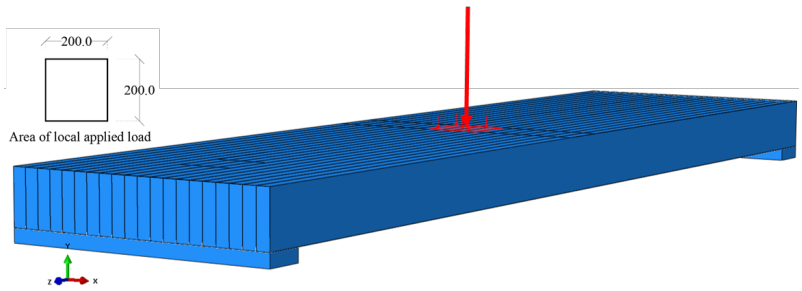

(a) Axonometric view

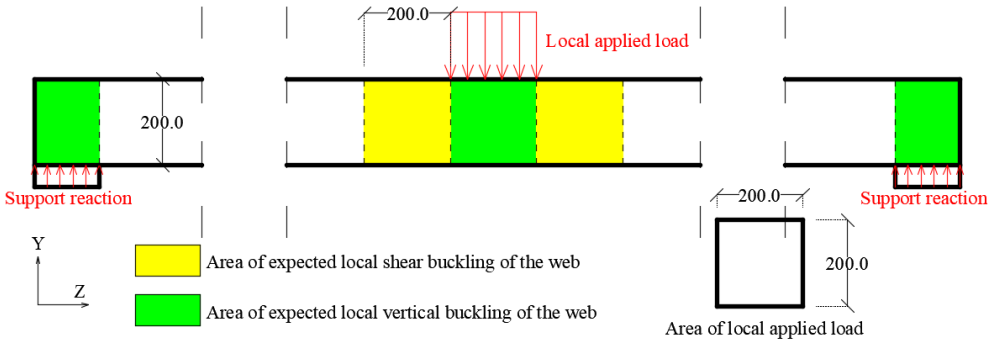

(b) Side view

Figure 6.5: LC-2 $40kN$ applied in a square area

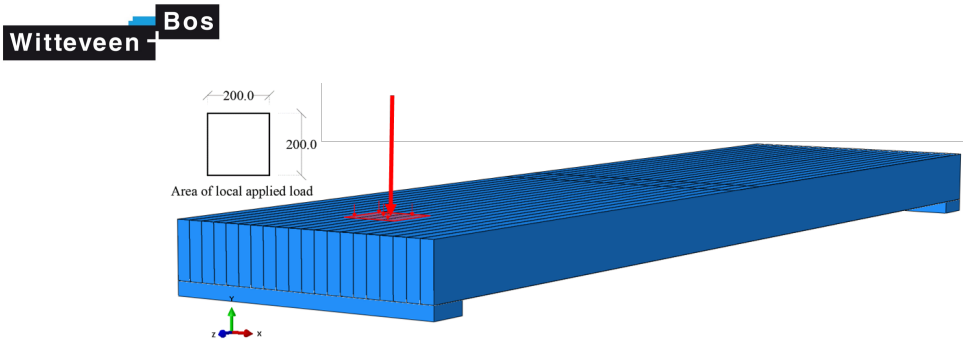

(a) Axonometric view

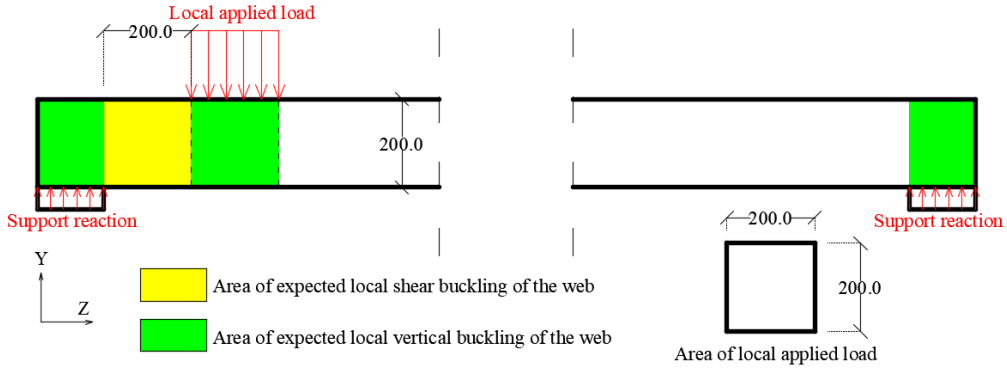

(b) Side view

Figure 6.6: LC-3 $40kN$ applied in a square area

6.3 Mesh sensitivity analysis

Development of computer power nowadays has given the opportunity to academic researchers and to the industry to make use of numerical methods for structural analysis. The FE analysis is one of those methods and the one used for the sake of this thesis through Abaqus software. Finite element method is a powerful tool when investigating the response of FRP sandwich panels and especially when one is investigating the buckling resistance of the laminates.

6.3.1 Type of FEs used

The element type used through all the analyses run in this MSc project regarding the FRP laminates is S4R for the faces and S8R for the web. S4R are deformable shell 4 noded linear elements while S8R are deformable shell 8 noded quadratic elements. Quadratic elements are also advised to be used for buckling analysis from [35]. Finally, the FRP laminates in this section are modeled as equivalent orthotropic sections, according to E.J.Barbero [26], using as engineering constants the stiffness values as presented in Table 6.2.

6.3.2 Mesh fineness for convergence

The decisive criteria for mesh fineness in this case appears to be the convergence of the prediction of critical buckling resistance of the web due to local applied load, LC-2 and LC-3. Two sessions of analysis have been performed. The difference between those is the type of elements used for the web that they are prone to buckle.

1. S4R type of elements for both the face and the we laminates
2. S4R type of elements for the face and S8R for the web laminates

Investigations on modelling wrinkling elements reveal that elements with a quadratic shape function are preferred over linear ones and convergence is being reached with fewer elements. Finally for a good estimate of the buckling load and mode shape, at least 4 elements per wavelength should be used, [35].

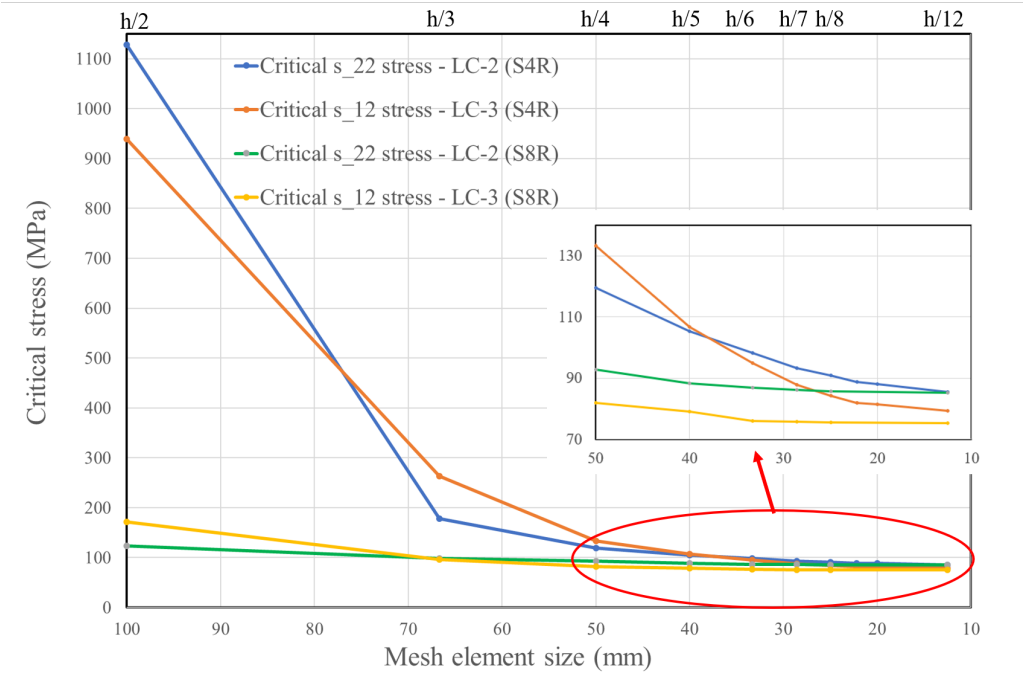

Figure 6.7: Mesh sensitivity analysis

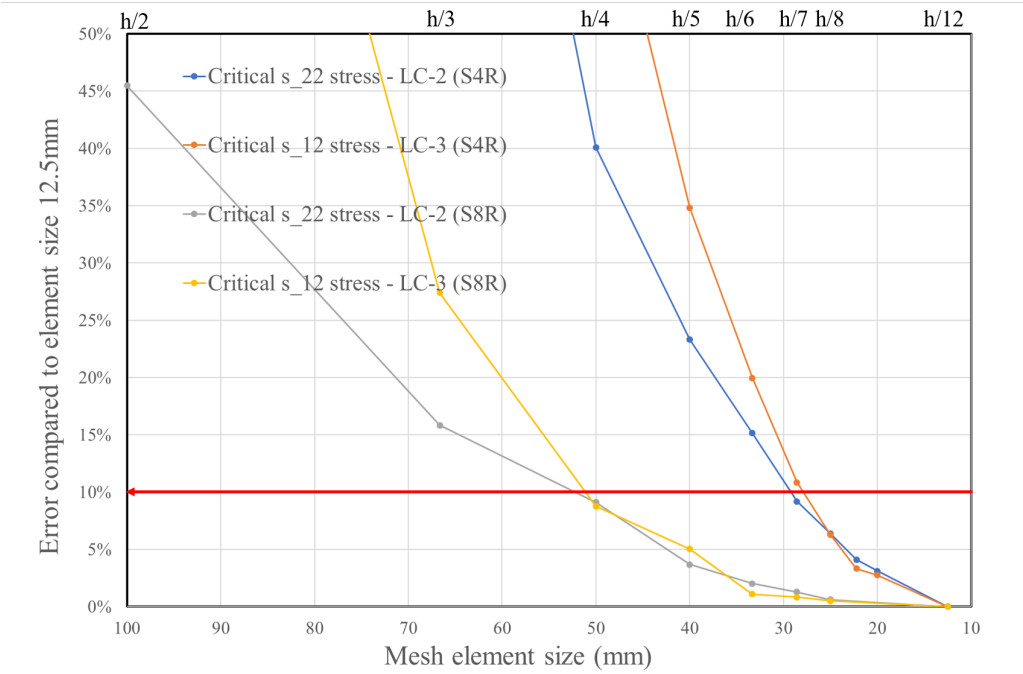

Figure 6.8: Mesh sensitivity analysis

In Figure 6.7 the critical stresses over the element size is plotted. Element size varies according to number of elements over the height of the web (see top x-axis). Since quadrilateral elements are used the elements get smaller in both directions, height and length of

the web. As a reference point for convergence the element size of 12.5mm has been chosen, see Figure 6.7. In Figure 6.8 the error of using different mesh size element compared to the reference point is depicted. The accepted error is set to 10%. One can see that in order to achieve that, has to use 50mm ($h_c/4$) element size for S8R, or 25mm ($h_c/8$) element size for S4R. Comparing those two cases, from the computational point of view the choice of S4R and $h_c/8$ element size appears to be more expensive assuming that one maintains the same element size for the entire model. In addition to that. the case of S4R elements should get a finer mesh in order to achieve the level of convergence of S8R, but that appears to be computationally expensive holding the assumption for same size of element for the wntire model.

6.4 Analytical and FE analysis response

In this section a straight comparison between the analytical solution and the FE prediction of the stresses and deflections due to the load cases described in Table 6.3 is presented.

6.4.1 LC-1 Normal facing stress σ_{11}

The second moment of inertia of the sandwich panel is calculated as follows:

$$I_{SP} = 2\Big(b\frac{t_f^3}{12} + bt_f(\frac{h_c + t_f}{2})^2\Big) + n_w t_w \frac{h_c^3}{12} = 417 \cdot 10^6 mm^4 \tag{6.1}$$

Consequently the resulting stress on the facing lies:

$$\sigma_{11} = \frac{M}{I_{SP}}\frac{h_{SP}}{2} = \frac{qL^2/8}{I_{SP}}\frac{h_{SP}}{2} = 5.51MPa \tag{6.2}$$

The FE model gives a normal σ_{11} stress of $5.60MPa$ as shown in figure 6.9 at the upper and lower fiber of the structure.

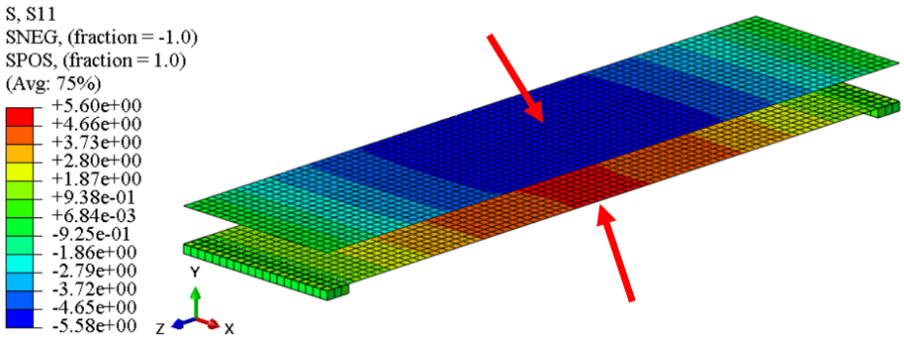

Figure 6.9: σ_{11} stress at the facings for LC-1

6.4.2 LC-2 Normal facing stress σ_{11}

Analytical approach 1

It is assumed that the Local applied load is supported by the entire width of the panel.

$$\sigma_{11} = \frac{M}{I_{SP}}\frac{h_{SP}}{2} = \frac{QL/4}{I_{SP}}\frac{h_{SP}}{2} = 11.03MPa \tag{6.3}$$

Analytical approach 2

It is assumed that the concentrated load is supported only by a strip of the panel that has a width equal to the width of the applied load.

$$n_{w,Q} = \frac{a_Q}{s_w} + 1, \qquad \text{number of webs under the loaded area} \tag{6.4}$$

The second moment of inertia of the strip of the panel with a width of $w = a_Q = 200mm$, can be found as:

$$I_{SP,Q} = 2\Big(a_Q \frac{t_f^3}{12} + a_Q t_f (\frac{h_c + t_f}{2})^2\Big) + n_{w,Q} t_w \frac{h_c^3}{12} = 86.1 \cdot 10^6 mm^4 \tag{6.5}$$

$$\sigma_{11} = \frac{M}{I_{SP,Q}} \frac{h_{SP}}{2} = \frac{QL/4}{I_{SP,Q}} \frac{h_{SP}}{2} = 53.42MPa \tag{6.6}$$

The two simplified analytical approaches (6.5,6.6) give quite different results. The FE model gives a stress $\sigma_{11} = -20.2MPa$ for the top face and $\sigma_{11} = 18.3MPa$ for the bottom face as shown in figure 6.10 at the extreme fibers of the structure. The difference between

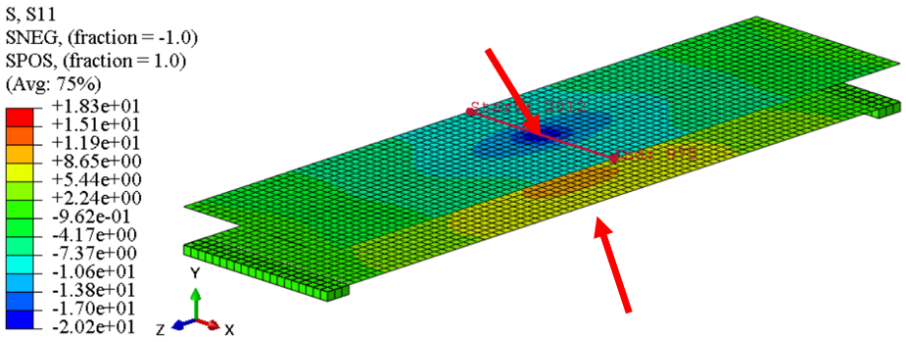

Figure 6.10: σ_{11} stress at the facings for LC-2

the simplified analytical approaches and the FE model stress prediction lies on the fact that the formers are not considering the transverse redistribution of the concentrated load which depend on the local transverse bending stiffness of the facing laminates. The FE model give a better insight into more accurate distribution of the stresses. In Figure 6.11 the analytical and FE σ_{11} stress distributions of the top face along the width of the SP are plotted at the along the red line shown in Figure 6.10.

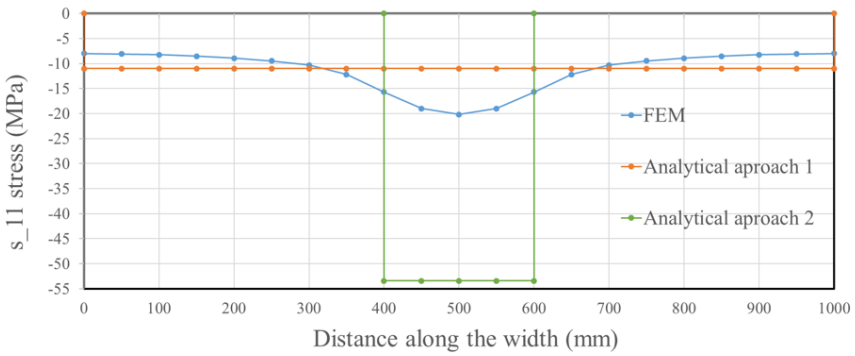

Figure 6.11: σ_{11} distribution along the width for LC-2

6.4.3 LC-1 Transverse shear stress of webs σ_{12}

This is a shear stress on webs which can be analytically found as:

$$\sigma_{12} = \frac{bql/2}{n_w t_w h_c} = 0.95MPa \tag{6.7}$$

The FE model gives a shear σ_{12} stress of $1.07MPa$ right next to the support pad as shown in Figure 6.12. The analytical prediction uniformly distributed shear stress along the height of the webs while this is not the actual case.

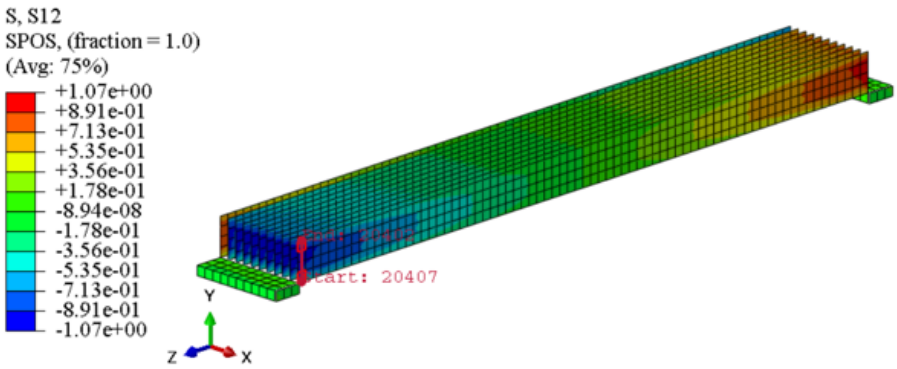

Figure 6.12: σ_{12} stress at webs

The analytical and FE σ_{12} stress distribution along the height of the web (ref line in Figure 6.12) is depicted in Figure 6.13

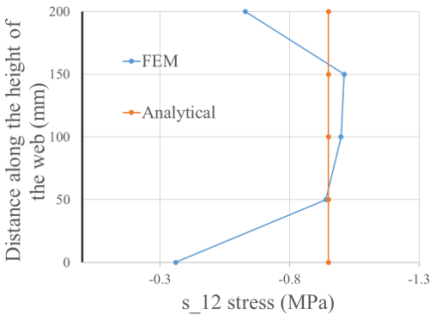

Figure 6.13: σ_{12} stress at web LC-2

6.4.4 LC-2 Transverse shear stress of webs σ_{12}

This is a shear stress on webs which can be analytically calculated considering only the webs below the surface of the applied local load:

$$\sigma_{12} = \frac{Q/2}{(a_Q/s_w + 1)h_c t_w} = 4.00MPa \tag{6.8}$$

The FE model returns a max shear stress $\sigma_{12} = 4.62MPa$. The difference compared to the analytical prediction is due to the facts that:

1. The analytical formula assumes a uniform distribution of shear stresses along the heght of the web
2. Based on the stiffness of the faces, the contribution of the webs on load transferring may differ to the one initially assumed.

Plotting σ_{12} at top points of webs along the width of the SP, see red line in Figure 6.14, one can see the FE relative contribution of each web towards the local load.

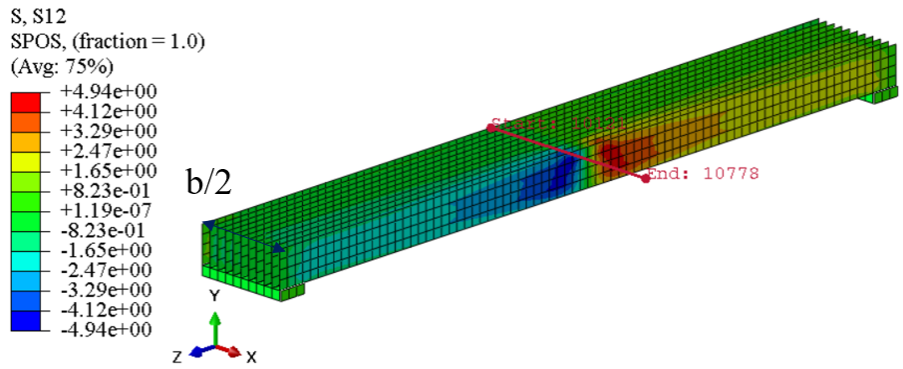

Figure 6.14: σ_{12} stress at webs

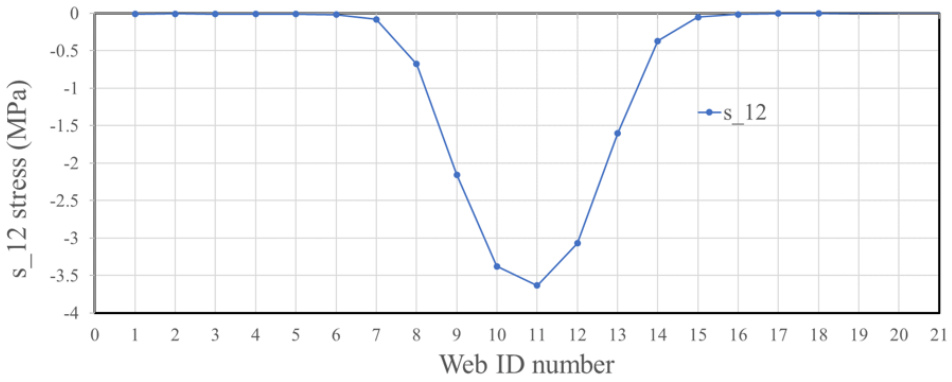

Figure 6.15: σ_{12} stress at top webs along the width of the SP

6.4.5 LC-1 Deflection

$$f_1 = \frac{5}{384} qL^4, \qquad f_2 = q\frac{L^2}{8},$$

$$w = w_1 + w_2 = \frac{f_1}{E_1 I_{SP}} + \frac{f_2}{G_c h_{SP}} = 3.1 + 0.2 = 3.3mm \tag{6.9}$$

Where:

$$G_c = \frac{n_w t_w}{w} G_{12} = 588MPa$$

The FE model returns a deflection of $3.32mm$ as shown in figure 6.16.

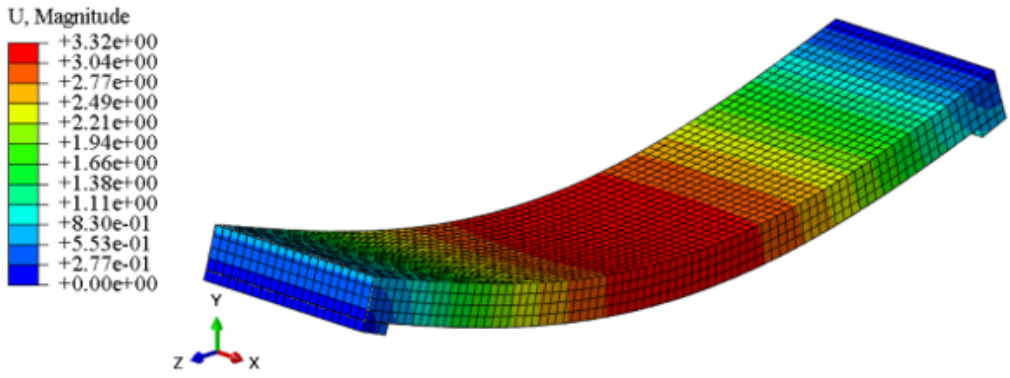

Figure 6.16: SP deflections LC-1

6.4.6 LC-2 Deflection

In case of local applied load for the analytical prediction using 3 different approaches are presented.

$$f_1 = \frac{QL^3}{48}, \qquad f_2 = Q\frac{L}{4},$$

Analytical approach 1

It is assumed that the Local applied load is supported by the entire width of the panel.

$$w = w_1 + w_2 = \frac{f_1}{E_1 I_{SP}} + \frac{f_2}{G_c h_{SP}} = 5.0 + 0.4 = 5.4mm \tag{6.10}$$

Where:

$$G_c = \frac{n_w \cdot t_w}{w} G_{12} = 588.0MPa$$

Analytical approach 2

It is assumed that the concentrated load is supported only by a strip of the panel that has a width equal to the width of the applied load.

$$w = w_1 + w_2 = \frac{f_1}{E_1 I_{SP,Q}} + \frac{f_2}{G_{c,Q} h_{SP}} = 24.0 + 1.6 = 25.6mm \tag{6.11}$$

Where:

$$G_{c,Q} = \frac{n_{w,Q} \cdot t_w}{a_Q} G_{12} = 700MPa$$

Analytical approach 3

It is assumed that only the webs under the loaded area are resisting the shear stresses while the whole face contributes in taking over bending.

$$w = w_1 + w_2 = \frac{f_1}{E_1 I_{SP}} + \frac{f_2}{G_{c,Q} h_{SP}} = 5.0 + 1.5 = 6.5mm \tag{6.12}$$

Where:

$$G_{c,Q} = \frac{n_{w,Q} \cdot t_w}{a_Q} G_{12} = 700MPa$$

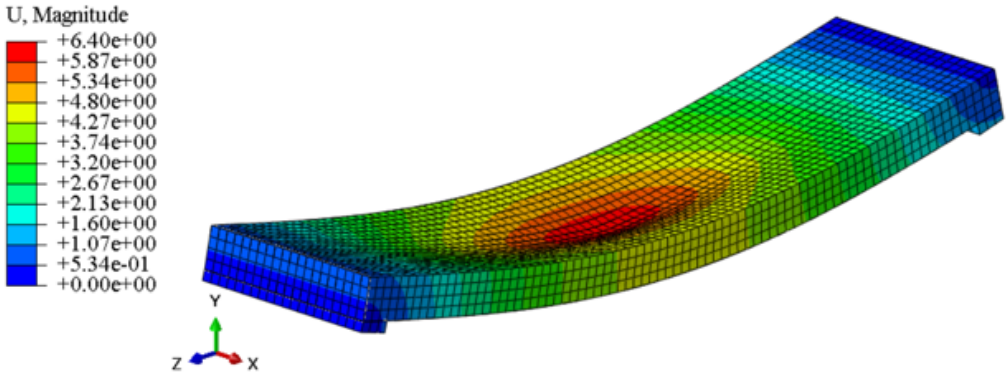

Figure 6.17: SP deflections LC-2

The FE model returns a deflection of $6.4mm$ as shown in Figure 6.17. The advantage of FE analysis is that takes into account the face stiffness and redistributes the stresses coming

from the applied load more accurately not only in the longitudinal but also in the traverse direction. Stress distribution in the transverse direction is not possible using analytical shear beam theory. This is also the reasoning for the different approaches as presented above that try to tune the beam so as to act like a plate. However, a more advanced analytical theory, which is quite intensive, should be used in order to get a better insight on the analytical prediction of the deflections due to local applied load on the panel.

In Figure 6.18 the displacement along the width of the panel at midspan are presented.

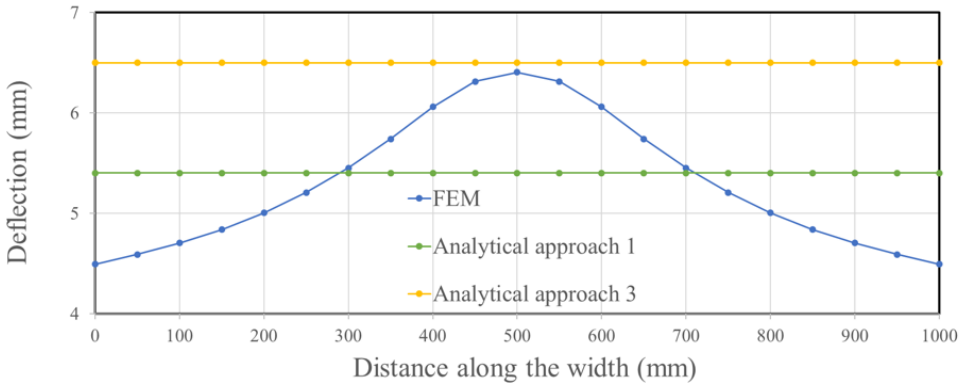

Figure 6.18: LC-2 deflections along the width at midspan

6.5 Web instability

Formulas that exist in literature are not always in accordance with the buckling loading prediction of FE analysis. In addition, existing formulas work for individual loading hence this is not the case for the web panels of the cross section of the bridge. It is always a combination of normal stess (s_{11}, s_{22}) and shear stress s_{12}.

6.5.1 FE and linear buckling analysis

Linear buckling analysis is employed to predict the critical buckling load of the web laminates.The linear buckling solver calculates the buckling load factors and corresponding mode shapes for a structure under given loading conditions. It assumes that there is a bifurcation point where the primary and secondary loading paths intersect, and before this point is reached, all element stresses change proportionally with the load factor.

A linear buckling solution is obtained by solving the following eigenvalue problem:

$$(K - \lambda K_G)x = 0 \tag{6.13}$$

Where:

- K: Global stiffness matrix
- λ: Buckling load factor
- x: Buckling mode vectors
- K_G: Global geometric stiffness matrix

For beam and plate bending structures, the geometric stiffness matrix represents the stiffening effect of the tensile axial/membrane stresses.

The buckling solution is possible only when an existing solution is available for determining the current stress state (reference load) of the structure, which is required for the calculation of the element geometric stiffness matrix. The critical stress is calculated as:

$$\sigma_{cr} = \lambda \cdot \sigma_{ref} \tag{6.14}$$

and thus,

$$\text{for} \quad \lambda < 1 \quad \text{the structure is safe from buckling} \tag{6.15}$$

$$\text{while for} \quad \lambda > 1 \quad \text{buckling occurs} \tag{6.16}$$

Linear buckling analysis can estimate the maximum load that can be supported prior to structural instability or collapse. When the type of structure isn't covered by the design code, and where P-delta, lift-off and yielding effects are not significant in the loading range up to buckling, a linear buckling analysis should give a more accurate assessment of member resistance than would be obtained from a code of practice. However, imperfections and nonlinearities tend to prevent most 'real' structures from achieving their theoretical elastic, also called "Euler", buckling strength, so the eigenvalue buckling load factors are therefore somewhat overestimated. In order to get a more accurate answer nonlinear analysis should be performed, however this is beyond the scope of this project.

6.5.2 Local vertical buckling due to local applied load

This is a buckling mode due to vertical stresses at the web induced by local applied load.

LC-2 (Figure 6.5)

As shown in Figure 6.19, the maximum vertical stress, from FE analysis is $\sigma_{y.max.FEA} = 10.29MPa$ and the buckling factor for vertical local buckling is $\lambda_{cr} = 9.027$.

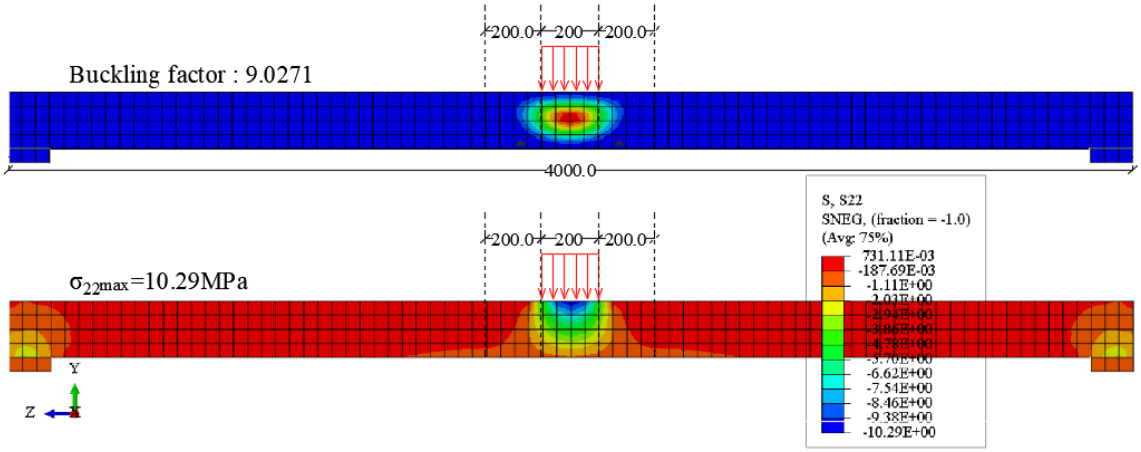

Figure 6.19: Buckling mode and σ_{22} for LC-2

The critical buckling stress from the linear buckling analysis of the FE model can be obtained as follows:

$$\sigma_{22cr.FEA} = \lambda_{cr.FEA} \cdot \sigma_{y.max.FEA} = 92.9MPa \tag{6.17}$$

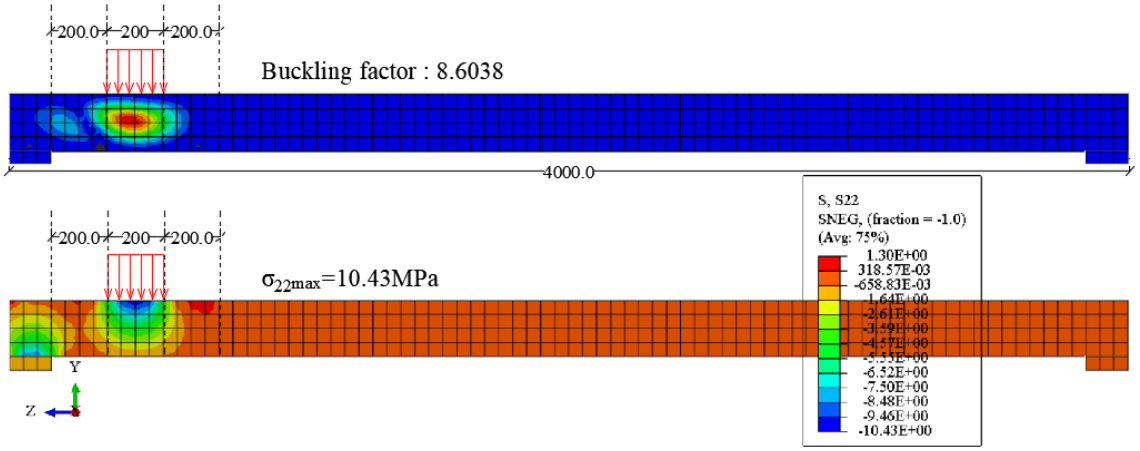

Figure 6.20: Buckling mode and σ_{22} for LC-3

LC-3 (Figure 6.6)

As shown in Figure 6.20, the maximum vertical stress, from FE analysis is $\sigma_{y.max.FEA} = 10.43MPa$ and the buckling factor for vertical local buckling is $\lambda_{cr} = 8.604$.

The critical buckling stress from the linear buckling analysis of the FE model can be obtained as follows:

$$\sigma_{22cr.FEA} = \lambda_{cr.FEA} \cdot \sigma_{y.max.FEA} = 89.7MPa \tag{6.18}$$

6.5.3 Shear buckling due to local applied load

This is a buckling mode due to shear stresses at the web induced by local applied load.

LC-2 (Figure 6.5)

As shown in Figure 6.21, the maximum vertical stress, from FE analysis is $\sigma_{zy,max,FEA} = 4.94MPa$ and the buckling factor for vertical local buckling is $\lambda_{zy,cr} = 16.478$.

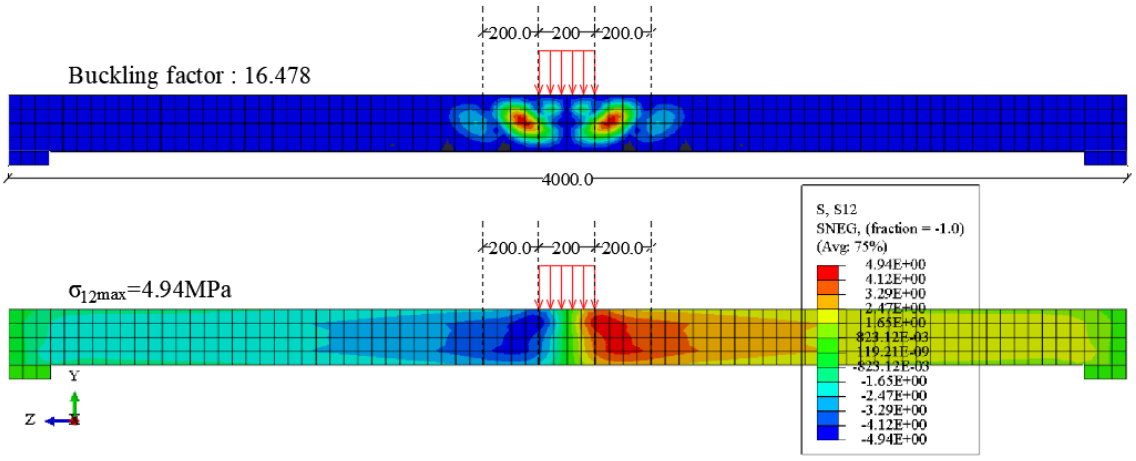

Figure 6.21: Buckling mode and σ_{12} for LC-2

The critical buckling stress from the linear buckling analysis of the FE model can be obtained as follows:

$$\sigma_{12cr,FEA} = \lambda_{cr.FEA} \cdot \sigma_{y.max.FEA} = 81.4MPa \tag{6.19}$$

LC-3 (Figure 6.6)

As shown in Figure 6.22, the maximum vertical stress, from FE analysis is $\sigma_{zy.max.FEA} = 7.73MPa$ and the buckling factor for vertical local buckling is $\lambda_{zy,cr} = 10.59$.

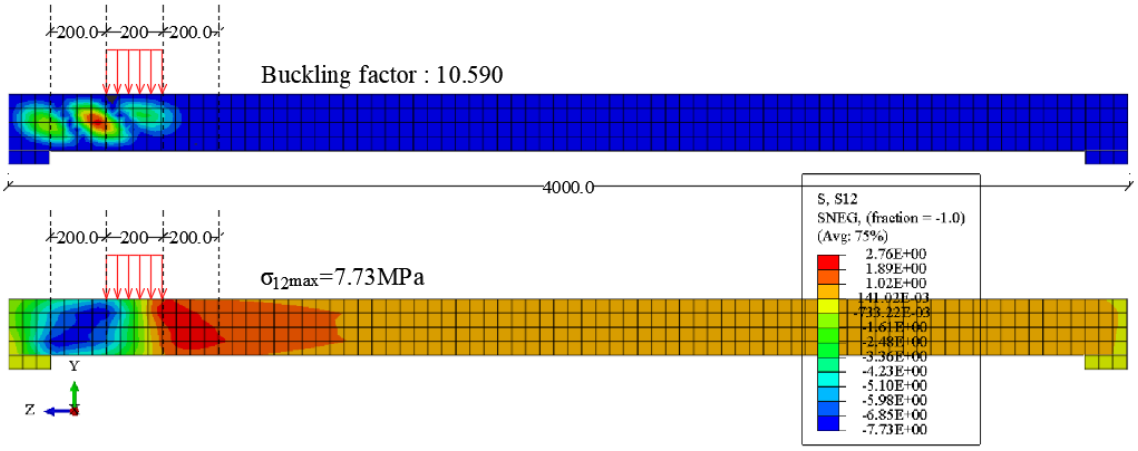

Figure 6.22: Buckling mode and σ_{12} for LC-3

The critical buckling stress from the linear buckling analysis of the FE model can be obtained as follows:

$$\sigma_{12cr,FEA} = \lambda_{cr.FEA} \cdot \sigma_{zy.max.FEA} = 81.9MPa \tag{6.20}$$

6.5.4 Analytical buckling analysis

The stiffness constants of the web are presented in Table 6.2. In the coordinate system of the profile the following relations occur:

$$E_{Lc} = E_1, \qquad E_{Tc} = E_2, \qquad G_{LT} = G_{12}, \qquad \nu_{LT} = \nu_{12}, \qquad \nu_{TL} = \nu_{LT}\frac{E_{Tc}}{E_{Lc}}$$

The stiffness constants of the web are obtained from Annex E of JRC2016 [9] as follows:

$$D_{11} = \frac{E_{Lc}t_w^3}{12(1-\nu_{LT}\nu_{TL})} = 286852.4Nmm, \quad D_{22} = \frac{E_{Tc}t_w^3}{12(1-\nu_{LT}\nu_{TL})} = 176781.1Nmm$$

$$D_{12} = \nu_{LT}D_{22} = 56570.0Nmm, \qquad D_{66} = \frac{G_{LT}t_w^3}{12} = 58333.3Nmm$$

For the stress in the vertical direction of the web the stiffness constants need to be rotated by an angle of 90°. In that case, they appear in the following form:

$$D_{11y} = D_{22} = 176781.1Nmm, \qquad D_{12y} = D_{12}\frac{D_{11}}{D_{22}} = 91792.8Nmm$$

$$D_{22y} = D_{11} = 286852.4Nmm, \qquad D_{66y} = D_{66} = 58333.3Nmm$$

According to [7] the actual support condition the faces offer to the web are depended on the ratio of thicknesses of the face and the web, see Figure 6.23. In the case selected the ratio of the thicknesses is $\frac{t_f}{t_w} = 3$, see Table 6.1, and thus we can consider the BCs of the web at the junctions with the faces clamped.

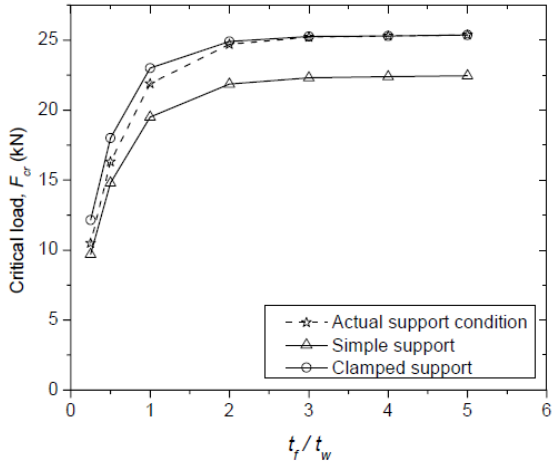

Figure 6.23: Critical loads corresponding to web buckling for different face-web ratios [7]

Effective width

The analytical formulas for compressive load work for uniform applied load at the plate. For local vertical buckling of the web due to local applied load, the distribution is not uniform. One needs to calculate the equivalent effective width, b_{eff}, assuming as stress the maximum obtained from FE analysis, in order to compare analytical with FE prediction of critical stress.

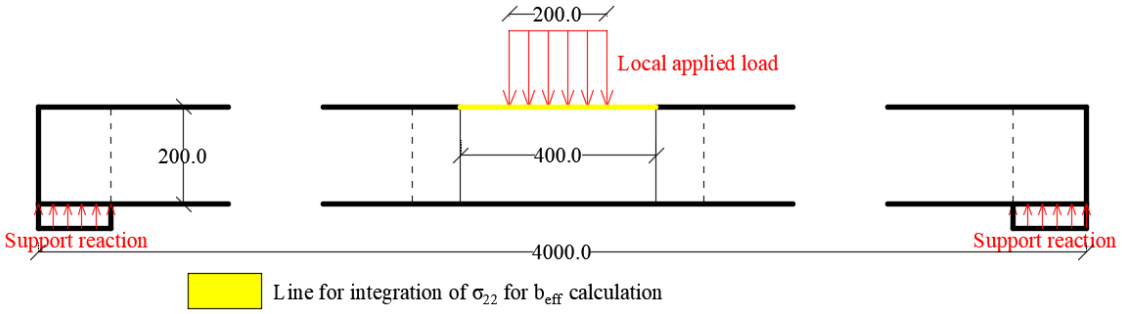

Figure 6.24: Side view of LC-2 for effective width

$$b_{eff} = \frac{\sigma_{int}}{\sigma_{22,max}} = \frac{-1890}{-10.29} = 183.6mm \tag{6.21}$$

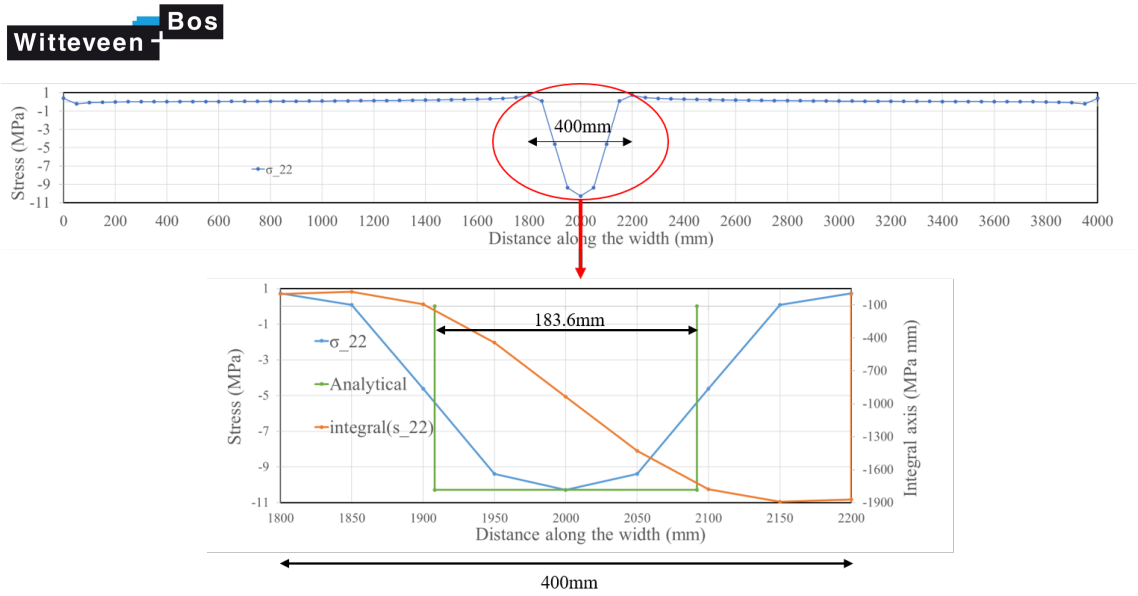

Figure 6.25: σ_{22} distribution for LC-2, integral and analytical 6.24

Local vertical buckling according to JRC2016

Equations for calculating critical stresses of flat plates given in JRC2016 are valid for infinitely long plates where the aspect ration is more than 5.

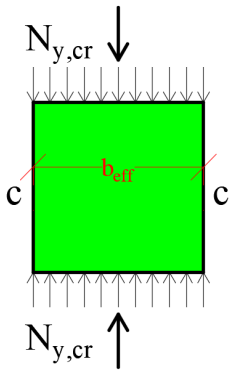

Figure 6.26: Plate configuration from JRC2016, see also equation 6.22

$$N_{y.cr} = \frac{\pi^2}{b_{eff}^2} \cdot \left[4.53 \cdot \sqrt{D_{11.y} D_{22.y}} + 2.44 \cdot \left(D_{12.y} + 2 \cdot D_{66.y}\right)\right] = 447.6 \frac{N}{mm} \tag{6.22}$$

$$\sigma_{cr.JRC} = \frac{N_{y.cr}}{t_w} = 89.5 MPa \tag{6.23}$$

Local vertical buckling according to Kassapoglou Clamped - Simply supported

This analytical method that takes into account not only the finite aspect ratio of the plate but also the ration of the stiffnesses in the two main directions, is taken from Table 6.1 of [8]. Simply supported boundary conditions is assumed at the edges of the considered segment having the effective width b_{eff}. Clamped conditions at the junctions with the web are assumed as further explained in Figure 6.23.

$$\lambda = \frac{a}{b_{eff}} \cdot \sqrt[4]{\frac{D_{22.y}}{D_{11.y}}} = 1.229 \tag{6.24}$$

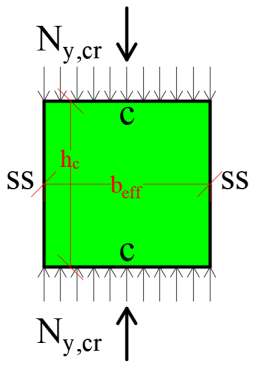

Figure 6.27: Plate configuration from Kassapoglou [8], see also equations 6.24 to 6.26.

$$K = \begin{cases} \frac{4}{\lambda^2} + \frac{2\left(D_{12.y}+2\cdot D_{66.y}\right)}{\sqrt{D_{11.y}D_{22.y}}} + \frac{3}{4}\cdot\lambda^2 = 5.63 & \text{for } 0 < \lambda < 1.662 \\ \frac{m^4+8m^2+1}{\lambda^2\left(m+1\right)} + \frac{2\left(D_{12.y}+2\cdot D_{66.y}\right)}{\sqrt{D_{11.y}D_{22.y}}} + \frac{\lambda^2}{m^2+1} & \text{for } \lambda > 1.662 \end{cases} \tag{6.25}$$

$$N_{y.cr} = \frac{\pi^2}{b_{eff}^2}\cdot\sqrt{D_{11.y}D_{22.y}}\cdot K = 371.3\frac{N}{mm} \tag{6.26}$$

$$\sigma_{cr.Kass.1} = \frac{N_{y.cr}}{t_w} = 74.3MPa \tag{6.27}$$

Shear buckling according to JRC2016 [9]

For the analytical calculation of shear buckling it is assumed that a square plate with width equal to the height of the web is prone to buckle.

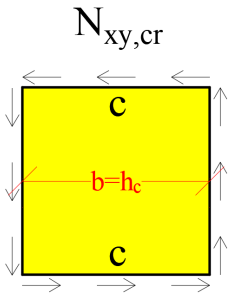

Figure 6.28: Plate configuration from JRC 2016 [9], for shear buckling, see also equations 6.24 to 6.26.

$$K = (2D_{66} + D_{12})/(\sqrt{D_{11}D_{22}} = 0.769 < 1 \tag{6.28}$$

$$N_{xy.cr} = \frac{4}{b^2}\cdot\sqrt[4]{D_{11}D_{22}^3}(15.07 + 7.08\cdot K) = 409.4\frac{N}{mm} \tag{6.29}$$

$$\sigma_{xy,cr,JRC} = \frac{N_{xy,cr}}{t_w} = 81.9MPa \tag{6.30}$$

Table 6.4: Critical stress calculation using different methods

Type of analysis	Shear buckling critical stress [MPa]	Local vertical buckling critical stress [MPa]
FE analysis LC-2	81.4	92.9
FE analysis LC-3	81.9	89.7
JRC2016 [9]	81.9	89.5
Kassapoglou CC - SS[8]	-	74.3

6.5.5 FE advantages

The advantage of using FE analysis for the prediction of buckling due to local applied loading lies to the facts that:

- Analytical formulas do not take into account the rotational stiffness at the junction of the web and the faces.
- FE analysis has a better insight to the distribution of vertical stresses at the web accounting for face stiffness something that analytical formulas are not able to do in order to predict the effective width.
- Analytical formulas work for solely pure loading (pure shear, pure compression etc.), while in reality there is always a combination of actions.

6.6 Stacking sequence

Up until now in this chapter the FRP laminates are modeled as equivalent orthotropic sections. In reality, the stacking sequence of the plies is distinct and it is expected to have an effect on load distribution. The simple case as described in section 6.2 is going to be used, however this time the section definition is going to be a composite layup, referred also as LSS in [26]. The cases examined are presented in the table below: In this section an investigation of the plies stacking sequence is presented.

Table 6.5: Models examined for stacking sequence investigation

Model	Face LSS (mm)	t_f	Web LSS (mm)	t_w (mm)	$s_{22,cr}$ (MPa)	u_{max} LC-1	u_{max} LC-2
LSS-1.1	[0]	15	[0]	5	65.8	2.8	6.3
LSS-2.1	$[0/90]_s$	15	$[0/90]_s$	5	43.7	4.1	8.2
LSS-2.2	$[90/0]_s$	15	$[90/0]_s$	5	107.3	4.1	7.7
LSS-3.1	$[90/\pm 45/0]_s$	15	$[90/\pm 45/0]_s$	5	89.4	3.7	7.0
LSS-3.2	$[90/0/\pm 45]_s$	15	$[90, 0/\pm 45]_s$	5	75.0	3.7	7.1
LSS-3.3	$[90/0/\pm 45]_s$	15	$[90/\pm 45/0]_s$	5	89.7	3.7	7.0

The laminates of the first model, LSS-1.0 consist of one ply of 0°orientation. The laminates of the model LSS-2.1 and LSS-2.2 are 50% 0°and 50% 90°fibers. The 3rd session of the models are anisotropic laminates with fiber percentages: 55% for 0°and 15% for 90°, 45°, -45°. The critical buckling stress of the web due to LC-2 is also presented for all cases.

6.6.1 [0/90]s versus [90/0]s

The laminates in a SP configuration exhibit mostly axial stresses. This is the principle of box sections: the webs serve to keep the faces at a distance (lever arm) so as to create maximum bending resistance by the axial forces (tensile and compressive) generated at the top and bottom faces. Following that, it is expected that the 0°ply will not matter if it is centralized in the laminate or not since the laminate is not experiencing bending. However, the 90°ply will have a significant effect both for the face and the web as explained below:

Effect on the faces

The effect can be visualized while one plots the displacements along the width of the panel at mid span due to local applied load, LC-2, over the displacements due to UDL, LC-1. In Figure 6.29 the ratio of LC-2 over LC-1 displacements at midspan is presented. Already the existence of the 90°ply helps on distributing the load towards the transverse direction, since the transverse bending stiffness of the laminate is increased, if one compares with the LSS-1.1 case green line. This also means that more webs manage to contribute in carrying the load as it is more evenly transversely distributed.
Looking now to the LSS-2.1 (orange line) and LSS-2.2 (blue line) in Figure 6.29 the same explanation as before fits here. However, this time the stacking sequence matters and indeed placing the 90°ply at the top of the laminate is more beneficial for the load distribution and for minimizing the deflection since more material contributes in this way, see Table 6.5.

Effect on the webs

Buckling resistance of the web increases in case of LSS-2.2 compared to case LSS-2.1. That can be explained if one considers that local buckling of the web laterally displaces

the laminate and the maximum resistance to that is given by the the stiffest , lengthwise, fiber which in this case is the 90°ply.

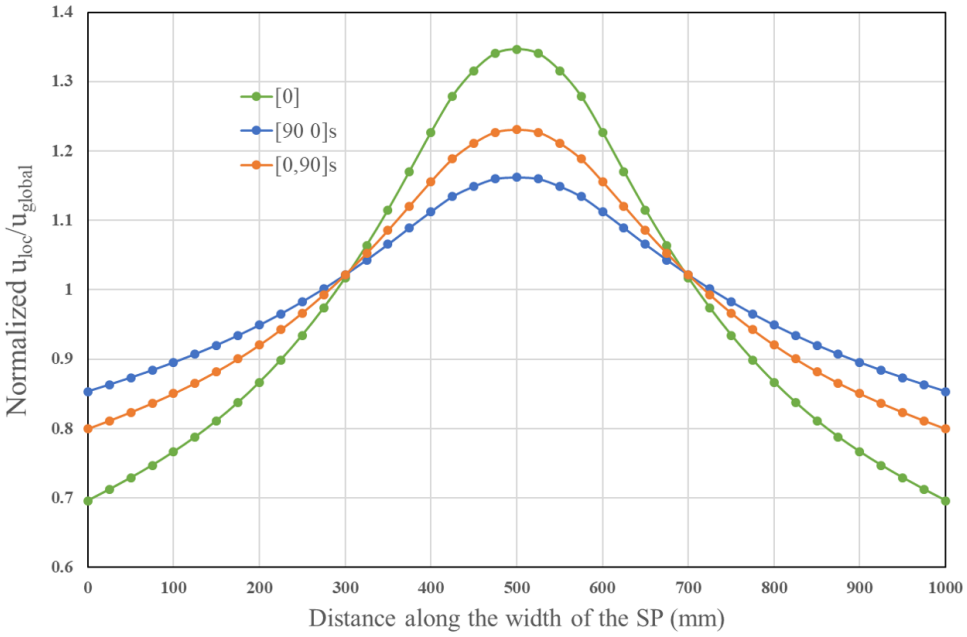

Figure 6.29: LSS-1.1,2.1 and 2.2 LC-2 over LC-1 normalized displacements

6.6.2 [90/0/±45]s versus [90/±45/0]s

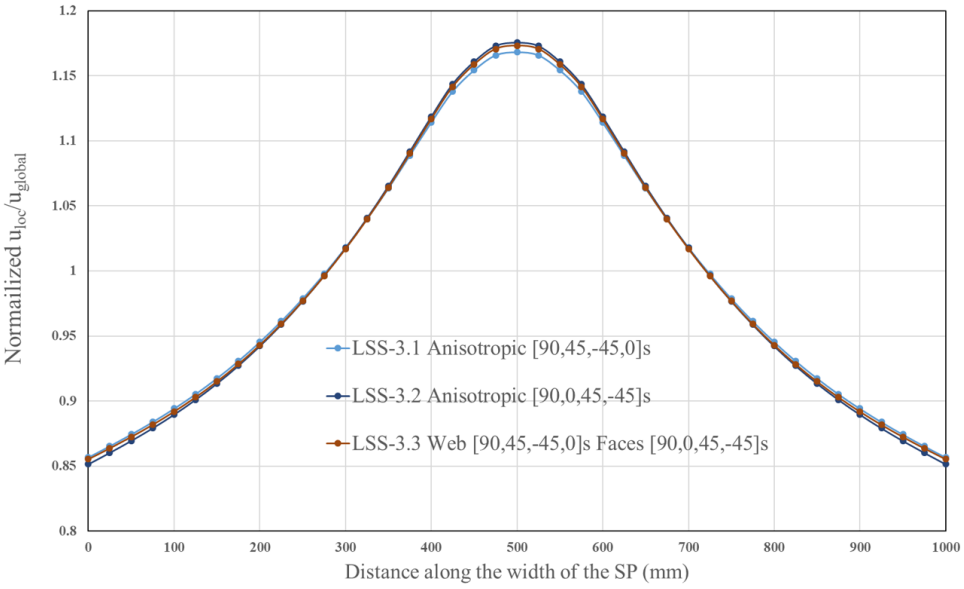

Figure 6.30: LSS-1.1,2.1 and 2.2 LC-2 over LC-1 normalized displacements

Effect on the faces

No clear difference can be observed in Figure 6.30 or in Table 6.5 regarding the displacements and their distribution for models LSS-3.1,3.2 and 3.3. It will be decided for the face to have the stacking sequence of [90/0/±45]s. The reasoning for that is that due

to local applied load the faces may experience local bending and thus the 0°ply is more beneficial to be closer to the edges rather than at the center of the laminate.

Effect on the webs

Comparing the models LSS-3.1,3.2 and 3.3 in Table 6.5 one can realize that for buckling resistance of the web, the 90°and ±45°plies are more beneficial to be on the outer side of the laminate. As already discussed ±45°and 90°plies are stiffer compared to the 0°ply in resisting the lateral displacement of the web and thus buckling.

6.7 Optimization of the simple case

In this section an approach for optimization of the simple case selected is presented. The objective of the optimization is to maintain the same amount of material used and maximize the deflection performance. Rearrangement of the material through the cross section (faces vs webs) is considered in order to fully exploit the given amount of material. The area of the material used per unit meter, considering a constant cross section along the length of the unit bridge is:

$$A = A_f + A_w = 2 \cdot b \cdot t_f + n_w \cdot t_w \cdot h_c = 51000mm^2 \tag{6.31}$$

Where A_f and A_w are the cross sectional areas of the faces and the webs respectively.

As it is already known, the design of FRP structures is deflection driven. This is also the reason why cross sectional configurations as the one examined (sandwich panel with integrated longitudinal webs) are attractive for FRP structures because they take advantage of geometrical arrangement to compensate for their low material stiffness.

The design principle of the sandwich panel with integrated webs is that the faces resist to bending actions while the webs take over the shear stresses and create the lever arm between the two faces. The webs should also be thick enough in order not to buckle. Shear deformation theory is usually used to calculate deflections because the shear modulus of FRP is rather low and thus shear deformations become significant.

In fact, there is a trade off between shear and bending deformations based on the two terms of equation 6.32.

$$f_1 = \frac{5}{384} q L^4, \qquad f_2 = q \frac{L^2}{8},$$

$$w = w_1 + w_2 = \frac{f_1}{E_1 I_{SP}} + \frac{f_2}{G_c h_{SP}} \tag{6.32}$$

For two cases of bridge slenderness (a) $L/h_c = 20$ and (b) $L/h_c = 16$ the deflection over A_w/A for uniform loading case LC-1 (see Table 6.3) is presented in Figure 6.31

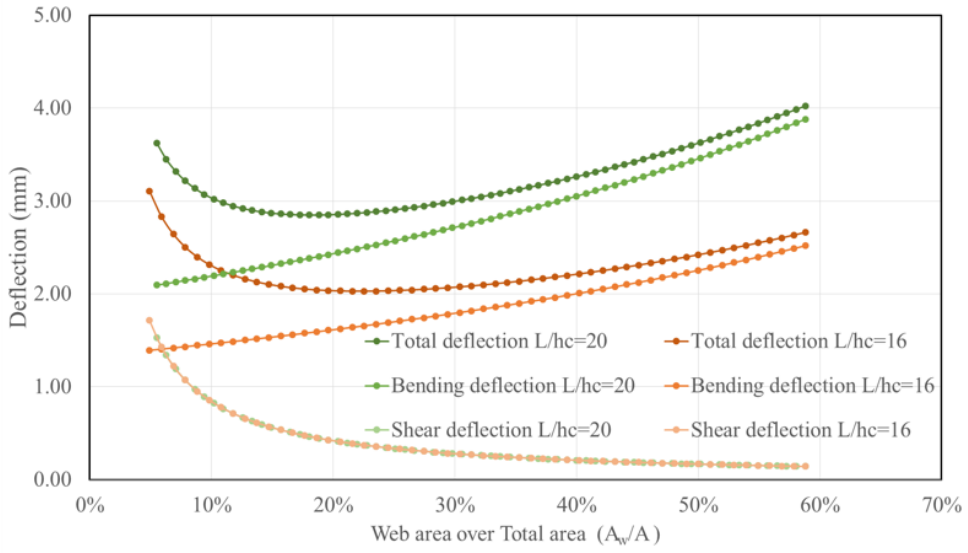

Figure 6.31: Contributions of bending and shear deflections for LC-1

One can see in Figure 6.31 the contributions of shear and bending deflection while varying the areas of the web and that of the faces. There is a range of A_w/A ratio where the total deflection becomes minimum, for the given amount of cross-sectional area in

equation 6.31 and for the given laminates' properties as given in Table 6.2. In addition the lines of shear deflection for both unit bridge slenderness cases coincide since such does the web area that takes over the shear stresses A_w/A.

6.7.1 Spacing of the web

The rule of thumb used till now, for engineering practice, for the spacing of the web, s_w, in the specific cross section is $h_c/s_w \simeq 4$. The cross section has the form of a vierendeel truss having faces as chords and webs as posts. According to vierendeel girder analysis, the closer the posts are, the lower the moments at the chords meaning transverse bending moments in the faces in our case [36].

Criterion for the choice of the spacing of the web is the following: the webs should be as close as possible retaining the optimum Aw/A ratio and with the condition that the webs should not buckle. As buckling limit the buckling factor from linear buckling analysis is used for the last verification as:

$$\lambda_{cr} \geq 1 \tag{6.33}$$

The selected cases for unit bridge slenderness is the one presented in Table below:

Table 6.6: Optimum selected cases from Figure 6.31

Unit bridge slenderness case	A_w/A (%)	h_c/s_w	s_w (mm)	t_f (mm)	t_w (mm)	$min(\lambda_{cr})$ from LC-2 & LC-3
(a)	19.6	4	50	20.5	2.381	1.08
(b)	24	3	62.5	19.5	2.824	1.11

6.7.2 Conclusion

In Tables 6.7 and 6.8, a summary of the optimum range of cases is presented for the unit bridge examined.

Table 6.7: Data obtained from FE and Figure 6.31

Unit bridge slenderness	Optimum A_w/A ratio	λ_{cr} for $h_c/s_w > 4$	λ_{cr} for $h_c/s_w = 4$	λ_{cr} for $h_c/s_w < 4$
(a), see Table 6.6	$16 - 20\%$	<1	1.08	>1

Table 6.8: Data obtained from FE and Figure 6.31

Unit bridge slenderness	Optimum A_w/A ratio	λ_{cr} for $h_c/s_w > 3$	λ_{cr} for $h_c/s_w = 3$	λ_{cr} for $h_c/s_w < 3$
(b), see Table 6.6	$20 - 25\%$	<1	1.11	>1

6.8 Web Instability Including the Foam Core

In this section the effect of the foam core in buckling resistance of thew longitudinal webs will be examined. In this type of structure built with the single step VARTM process, see Figure 5.9, the foam parts are there for manufacturing purposes using VARTM. In fact, they play the role of the formwork for the entire structure. As already explained, the fibers are laid or wrapped around the foam parts and the whole set-up is sealed and resin is infused and impregnates the fibers creating thus the desired designed laminates.

In common design practice the contribution of the foam material is completely neglected since the long term effects and material properties are difficult to predict and identify. Since the foam material is in general a light and weak kind of material compared to the FRP laminates, neglecting it through the design phase is not a that conservative approach. However, when it comes to web buckling the contribution of the foam can have a significant advantageous effect that is being neglected, since it prevents out of plane deformation of the web and thus increasing the buckling resistance of the web.

To have an impression of the effect of foam on buckling resistance of the webs, the lightest and weakest foam is chosen for this analysis. The foam material used is a polyurethane as indicated in Table 11.3 in JRC2016 with the following parameters:

$$d_{PUR} = 50kg/m^3, \qquad E_{PUR} = 10MPa, \qquad G_{PUR} = 5MPa$$

The foam material is assumed to be tie connected with surrounded laminates. Linear 8-node brick elements are used for modeling the foam parts.

It is observed that, the stresses at the web laminates in the model including the foam material are identical to the one excluding it. However, deflection due LC-2 has reduced by 8% and the buckling mode is different. Critical buckling factor, is 2-3 times bigger than before although, the reasoning for this could be that, more than one webs contribute to the buckling mode shape and that is not usually the case in reality due to imperfections.

It is however an indication that, the foam offers an elastically distributed vertical support to the faces and lateral support to the webs. This can more evenly distribute the load transversely and increase the buckling resistance of the webs.

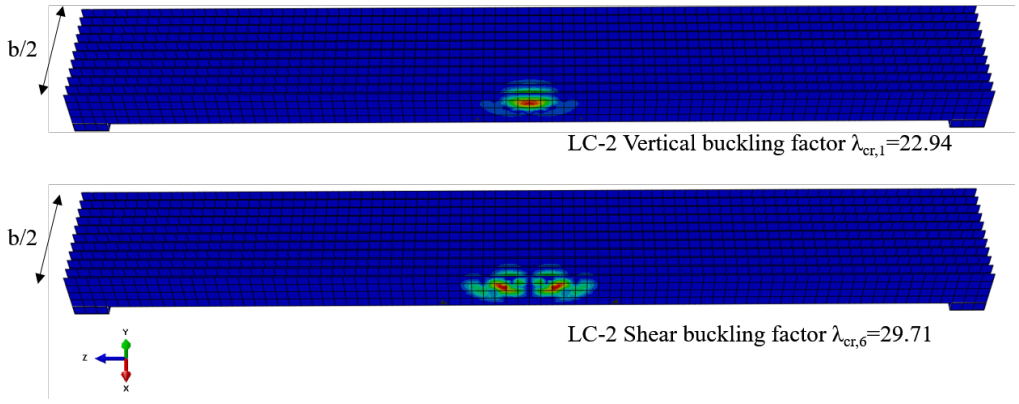

Figure 6.32: Buckling of the web for LC-2 including the foam material

Further research in combination with experimental work is needed for the investigation of foam FRP laminates interaction long term properties in order to be able to take advantage of the beneficial contribution of the former in such types of structures.

Chapter 7

Basis of design for the composite bridge

7.1 Bridge geometrical configuration

The geometrical configuration of the bridge is identical to that of the simple model presented in section 6.2. An FE model of it is shown in Figure 7.1. Also in this case, as in the simple case, the supports are modeled as line supports using neoprene pads. The selected width of the bridge is chosen to be $6m$, so as to be able to include 2 traffic lanes and to broaden the application of this MSc project. The length and the height of the bridge will vary and the will be mentioned in the next chapter.

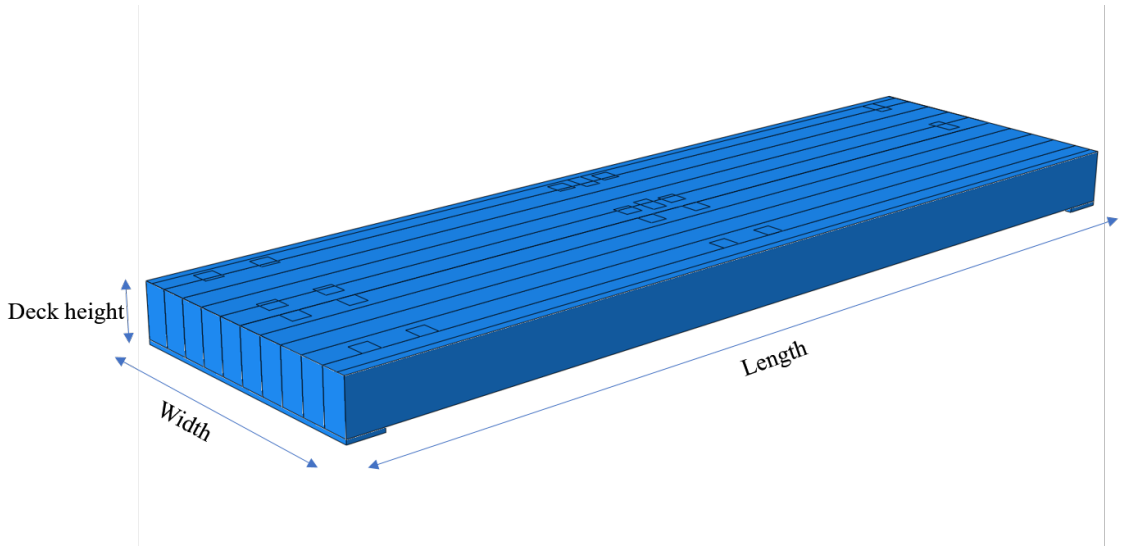

Figure 7.1: FE model of the bridge

7.2 Actions on the bridge

In this section the actions taken into account for the design of the bridge are presented. Those consider the selfweight of the structure, an additional permanent loading that consists of the top finishing of the deck and the traffic loading. For the traffic loading LM-1 and LM-2 are employed, as prescribed in EN1991 Part 2 *Traffic loads on bridges*.

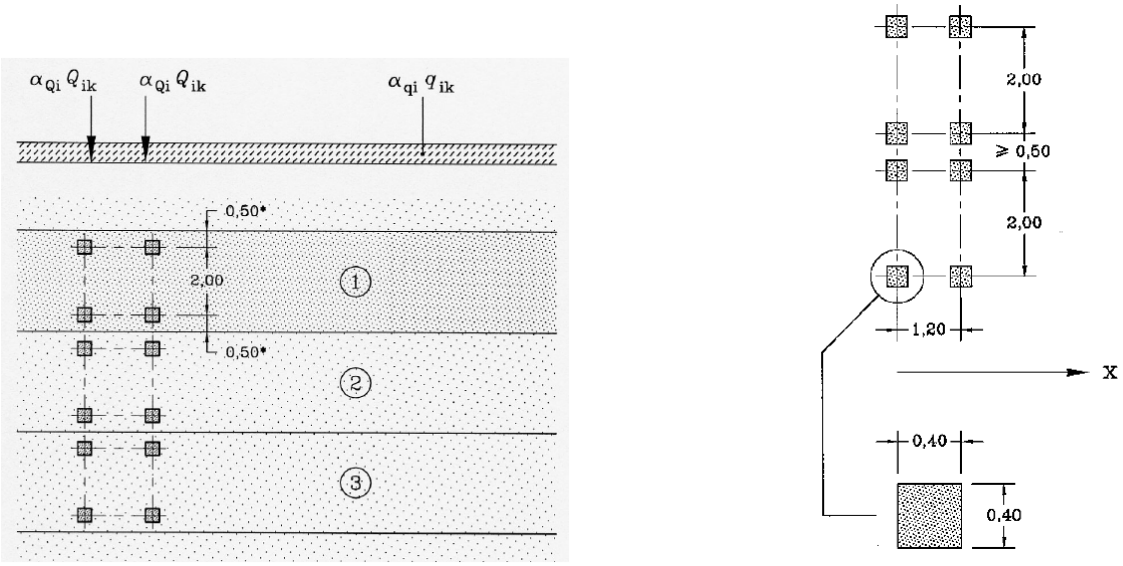

(a) Global verification

(b) Local verification

Figure 7.2: LM-1 application

7.2.1 Permanent loading

1. Selfweight $-9.81 m/s^2$ multiplied by density
2. Railings (typical $1-1.5 KN/m$) applied in $200 mm$ width at the side non constrained edges, returns a pressure load of $7.5 KN/m^2$.
3. Wearing layer $12 mm$ of epoxy nongrit of $23 KN/m^3$, returns a pressure load of $0.276 KN/m^2$.

7.2.2 LM-1

LM-1 is used fot global and local verification and consist of two partial systems:

1. A double-axle concentrated load, namely TS.
2. A UDL that differs per notional lane.

Table 7.1: LM-1 : Characteristic values

Location	TS Axle loads Q_{ik} (kN)	UDL system q_{ik} (kN/m^2)
Lane Number 1	300	9
Lane Number 2	200	2.5
Lane Number 3	100	2.5
Other Lanes	0	2.5
Remaining area	0	2.5

7.2.3 LM-2

LM-2 is employed for local and global verification. It consists of a single-axle TS equal to $400KN$ and is presented below.

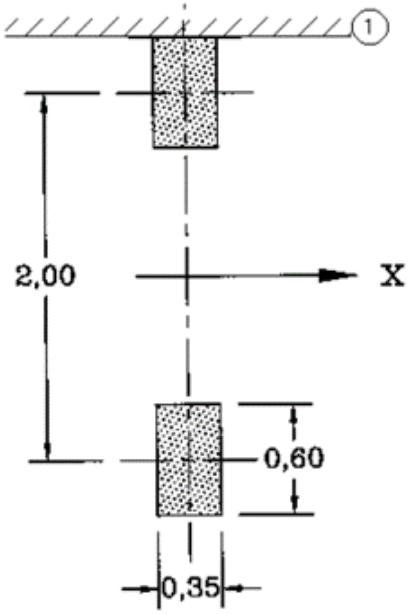

Figure 7.3: LM-2 application

7.3 Load combinations

Loads that are accounted in the current project are the dead load of the bridge and the variable load of traffic. Hence, the selected load combinations as prescribed in EN1990 are listed below:

7.3.1 ULS

The load combination used is referred as persistent and transient and lies as shown below:

$$\sum_{j\geq 1} \gamma_{G,j} G_{k,j} \ \{+\} \ \gamma_P P \ \{+\} \ \gamma_{Q,1} Q_{k,1} \ \{+\} \ \sum_{i>1} \gamma_{Q,1} \psi_{0,i} Q_{k,i} \tag{7.1}$$

According to table A2.4(B) - *Design values of actions (STR/GEO) (SET B)* of EN1990 Annex A2 partial safety factors for actions are defined as:

$$\gamma_G = 1.35$$
$$\gamma_Q = 1.35$$

7.3.2 SLS

Since the only variable loading that is being accounted in this project is the action due to traffic on the bridge, the two following combinations are considered.

Characteristic

$$\sum_{j\geq 1} G_{k,j} \ \{+\} \ P \ \{+\} \ Q_{k,1} \ \{+\} \ \sum_{i>1} \psi_{0,i} Q_{k,i} \tag{7.2}$$

The third term of the combination is not going to be used since the only variable loading taken into account is the traffic loading as already mentioned.

Frequent

$$\sum_{j\geq 1} G_{k,j} \ \{+\} \ P \ \{+\} \ \psi_{1,1} Q_{k,1} \ \{+\} \ \sum_{i>1} \psi_{2,i} Q_{k,i} \tag{7.3}$$

Where:

$$\begin{aligned} \psi_1 &= 0.75, \qquad \text{for TS} \\ \psi_1 &= 0.40, \qquad \text{for UDL} \end{aligned}$$

Quasi-permanent

$$\sum_{j\geq 1} G_{k,j} \ \{+\} \ P \ \{+\} \ \sum_{i\geq 1} \psi_{2,i} Q_{k,i} \tag{7.4}$$

According to Table A2.1 - *Recommended values of ψ factors for road bridges* of EN1990 Annex A2 partial safety factors for actions are defined as:

$$\psi_2 = 0$$

7.4 Truck positioning and Structural checks

In this section the different load combinations are presented and the structural checks applied for each one of them are presented. For the case of ULS combination, stresses in the laminates and buckling resistance of longitudinal webs is performed while for the case of SLS the maximum deflection plays the role of the decisive criterion.

7.4.1 SLS combinations

1. Quasi-permanent load combination. The permanent loading is only applied and the long term maximum deflection of the bridge is found. The conversion and material safety factors for creep load combination are used, as presented in Tables 4.3 and 4.6. According to SIA260 the appearance criteria that concerns the permanent condition of the bridge, considers the quasi-permanent load combination and the limit for the reversible deflection follows as:

$$w_2(G_k) \leq \frac{L}{700} - w_0 \tag{7.5}$$

Where:

- w_2: long term deflection under the effect of permanent actions
- G_k: characteristic value of the corresponding permanent actions
- w_0: precamber of the beam

2. Frequent load combination. The frequent load combination is used and the trucks are positioned at the mid-span of the bridge in order to account for maximum deflection. The conversion and material safety factors for the momentary deflection combination are used, as presented in Tables 4.3 and 4.6. In the Eurocode there are no specific requirements for the deflection limit of a road traffic bridge. However, according to SIA260 the deflections, w_{31}, due to traffic loading should be limited for the comfort criterion as presented below.

$$w_{31}(\psi_1 Q_{k1}) \leq \frac{L}{500} \tag{7.6}$$

Where:

- w_{31}: deflection under traffic loading
- ψ_1: reduction factor applied to the representative value for traffic loading
- Q_{k1}: characteristic value of the traffic action, LM-1
- L: the span of the bridge

7.4.2 ULS combinations

Strength

1. The persistent and transient combination is used incorporating LM-1 placed at the mid-span of the bridge.
2. The persistent and transient combination is used incorporating LM-1 placed at the mid-span of the bridge. This time only the 60tn TS is considered.
3. The persistent and transient combination is used incorporating LM-1 placed close to the support of the bridge in order to obtain maximum shear.
4. The persistent and transient combination is used incorporating LM-1 placed close to the support of the bridge in order to obtain maximum shear. This time only the 60tn TS is considered.
5. The persistent and transient combination is used incorporating LM-2 placed at the mid-span of the bridge.
6. The persistent and transient combination is used incorporating LM-2 placed close to the support of the bridge in order to obtain maximum shear.

The conversion and material safety factors for the strength combination are used, as presented in Tables 4.3 and 4.6. First ply strain failure criteria is applied for the plies of the selected laminates.

$$\varepsilon_{ij,ply} \leq \varepsilon_{ij,failure}, \qquad i,j = 1,2 \tag{7.7}$$

Buckling

1. The persistent and transient combination is used incorporating LM-1 placed at the mid-span of the bridge.
2. The persistent and transient combination is used incorporating LM-1 placed close to the support of the bridge in order to obtain maximum shear.
3. The persistent and transient combination is used incorporating LM-2 placed at the mid-span of the bridge.

4. The persistent and transient combination is used incorporating LM-2 placed close to the support of the bridge in order to obtain maximum shear.

The conversion and material safety factors for the local stability combination are used, as presented in Tables 4.3 and 4.6. As discussed in chapter FEM modeling and section Web instability the structural to fulfill the buckling criterion is selected as follows:

$$\begin{aligned} \sigma_{22.max} &\leq \sigma_{cr} \cdot \frac{\eta_c}{\gamma_m} \Rightarrow \\ \sigma_{22.max} &\leq \sigma_{22.max} \cdot \lambda_{cr} \cdot \frac{\eta_c}{\gamma_m} \Rightarrow \\ \lambda_{cr} &\geq \frac{\gamma_m}{\eta_c} \end{aligned} \tag{7.8}$$

In Figure 7.4 a visualization of the 2 different TSs positioning cases, mid-span and close to the support, is presented.

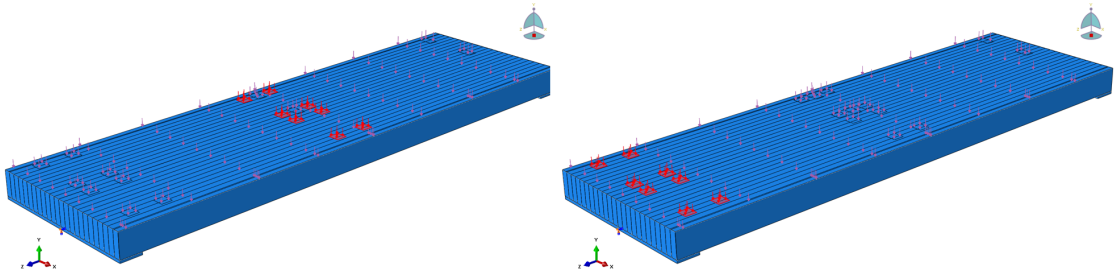

Figure 7.4: LM-1 Mid-span (left) and support (right) positioning of the TSs

7.5 Support pad width

An optimization approach for the width of the support is presented in this section. The support reaction is also a concentrated load that induces local buckling to the webs equally well as the local applied loads. In order not to promote vertical buckling at the support compared to the places where the footprints of the TSs are applied the following inequality has been taken into account, see Figure 7.5 and considering $Q = 150KN$ and $q = 9KN/m^2$ from LM-1.

$$\sigma_B \leq \sigma_A \tag{7.9}$$

$$\frac{Q \cdot (1 + (L - 1200)/L)}{w_p \cdot t_w} + \frac{q \cdot L/2}{t_w \cdot w_p} \leq \frac{Q}{w_{LM1} \cdot t_w} + \frac{q}{t_w} \tag{7.10}$$

$$w_p \geq \frac{Q \cdot (1 + (L - 1200)/L) + q \cdot L/2}{Q/w_{LM1} + q} \tag{7.11}$$

Plotting equation 7.11 for various bridge spans, one can get the corresponding pad width, see Figure 7.6.

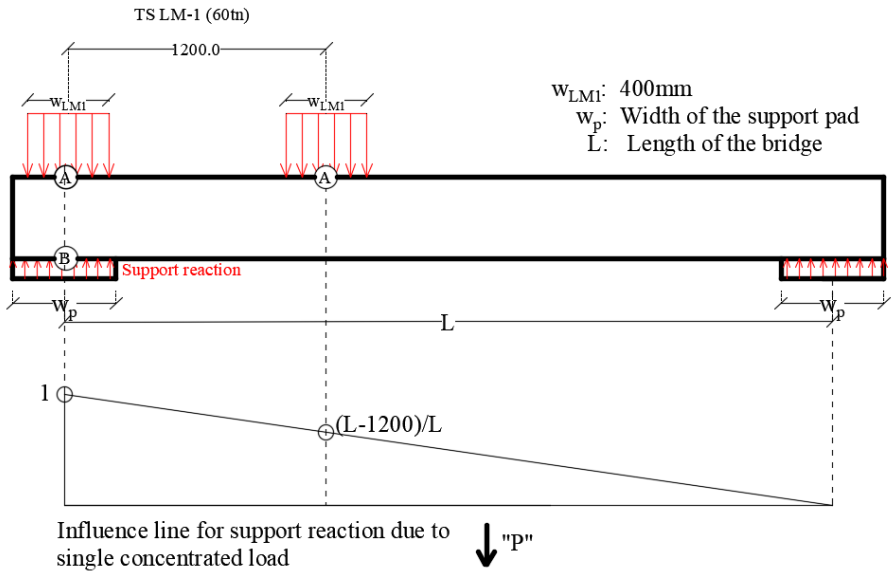

Figure 7.5: Support pad width and influence line

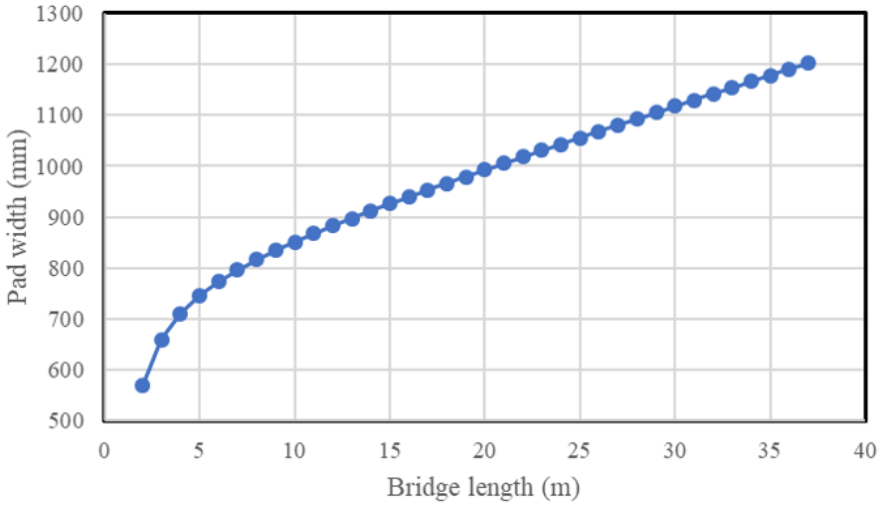

Figure 7.6: Width of support pad over span of the bridge, according to equation 7.11

7.6 Material properties

In order to define/predict the material properties of an FRP laminate, one has to consider material properties of both fiber and resin, the fiber volume fraction V_f and the orientation of the fibers into the laminate. The approach followed along this chapter is described in steps below:

1. Knowing fiber's, resin's properties and V_f, the following formulas are employed in order to define the UD ply properties. These equations are derived from the semi-

empirical Halpin and Tsai equations.

$$E_{1UD} = [E_R + (E_{F1} - E_R) \cdot V_f] \cdot \phi_{UD} \tag{7.12}$$

$$E_{2UD} = \left[\frac{1 + \xi_2 \eta_2 V_f}{1 - \eta_2 V_f} \cdot E_R\right] \cdot \phi_{UD} \tag{7.13}$$

$$G_{12UD} = \left[\frac{1 + \xi_G \eta_G V_f}{1 - \eta_G V_f} \cdot G_R\right] \cdot \phi_{UD} \tag{7.14}$$

$$v_{12UD} = v_R - (v_R - v_F) \cdot V_F \tag{7.15}$$

Where:

$$\eta_2 = \frac{E_{F2}/E_R - 1}{E_{F2}/E_R + \xi_2}, \quad \xi_2 = 2; \qquad \eta_2 = \frac{G_F/G_R - 1}{G_F/G_R + \xi_G}, \quad \xi_G = 1; \qquad \phi_{UD} = 0.97$$

Table 7.2: Vinylester resin, glass fiber [9] and flax fiber properties [14]

Material	E_1 (%)	E_2 (MPa)	G_{12} (MPa)	ν_{12} (MPa)	Density (kg/m^3)
Glass fiber	73100	73100	30000	0.24	2570
Flax fiber	55000	55000	1600	0.25	1250
Vinylester resin	3550	3550	1350	0.32	1100

2. After obtaining the elastic constants of the UD ply the section of the laminates is modeled in Abaqus as a composite layup or LSS. This has been decided in order to apply the first ply strain failure criterion. This way of modeling the FRP laminates is also advisable for stress verification by E.J.Barbero in [26]. The ply-stack is symmetric and contains plies in $0°, 45°, -45°, 90°$ angle directions. In Figures 7.7 and 7.8, the definition of the ply-stack for the facing and the web laminate as input in Abaqus and as decided and discussed in section 6.6.

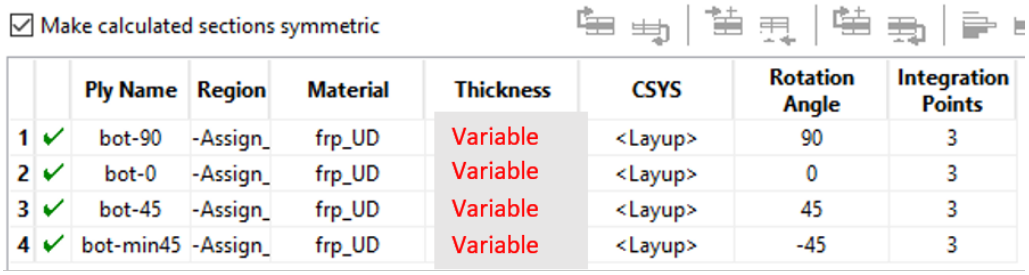

		Ply Name	Region	Material	Thickness	CSYS	Rotation Angle	Integration Points
1	✔	bot-90	-Assign_	frp_UD	Variable	<Layup>	90	3
2	✔	bot-0	-Assign_	frp_UD	Variable	<Layup>	0	3
3	✔	bot-45	-Assign_	frp_UD	Variable	<Layup>	45	3
4	✔	bot-min45	-Assign_	frp_UD	Variable	<Layup>	-45	3

Figure 7.7: LSS of the face as input in Abaqus

Make calculated sections symmetric

		Ply Name	Region	Material	Thickness	CSYS	Rotation Angle	Integration Points
1	✔	web-90	Assign-S	frp_UD	Variable	<Layup>	90	3
2	✔	web-45	Assign-S	frp_UD	Variable	<Layup>	45	3
3	✔	web-min45	Assign-S	frp_UD	Variable	<Layup>	-45	3
4	✔	web-0	Assign-S	frp_UD	Variable	<Layup>	0	3

Figure 7.8: LSS of the web as input in Abaqus

7.6.1 UD laminate cases examined

As already examined in the previous chapters, glass, flax and BioMid FRP is going to be considered, using a vinyl-ester type of resin, for the application of the road traffic bridge. Below the UD stiffness properties of the selected laminates are presented as input in Abaqus for the relevant limit states.

Table 7.3: UD laminate stiffness properties of Glass FRP

Limit state	V_f (%)	$E_{1,UD}$ (MPa)	$E_{2,UD}$ (MPa)	$G_{12,UD}$ (MPa)	$\nu_{12,UD}$	Density (kg/m^3)
ULS	50	37200	11400	3800	0.29	1835
SLS Frequent	50	26784	8208	2736	0.29	1835
SLS Quasi-permanent	50	26784	3283	1094	0.29	1835

Table 7.4: UD laminate stiffness properties of Flax FRP

Limit state	V_f (%)	$E_{1,UD}$ (MPa)	$E_{2,UD}$ (MPa)	$G_{12,UD}$ (MPa)	$\nu_{12,UD}$	Density (kg/m^3)
ULS	50	28400	10750	1425	0.32	1175
SLS Frequent	50	18403	6966	923	0.32	1175
SLS Quasi-permanent	50	9202	2786	369	0.32	1175

For the case of BioMid fibers, there are even less available data compared to Flax fibers. In addition BioMid fibers have almost the same mechanical properties as Flax fibers. Although there are some indications that BioMid could have better environmental performance, that remains to be seen by future experimental work. For this reason, only the FFRP will be considered in order to represent the natural fiber composite in this project.

The fiber volume fraction considered is 50% for both UD laminate properties. This might be more difficult to achieve when flax fibers are used. However, as presented in Table 3.4 form early stage experimental work, the laminate composite with BioMid fibers reaches a fiber volume fraction of 55%. It is thus reasonable to assume a $V_f = 50\%$ for the natural fiber polymer accounted in this report.

Chapter 8

Design optimization

8.1 Introduction

Design optimization of structural configurations is a big chapter in engineering. The main purpose for that may vary depending on the objective every time. However, most of the time the optimization ends up to be the maximum exploitation of the structural materials and the minimization of the cost without sabotaging on the other side the safety criteria that need to be fulfilled.

In this chapter the model of the bridge is parameterized and optimized. In order to deal with this complex optimization procedure, because of the amount of variables, dependencies and constraints, advanced optimization algorithms are employed. Having understood the effects of the each parameter in chapter 6 to a certain extend, modeFrontier is used which offers the possibility of creating a workflow incorporating Abaqus and subject the created workflow into optimization. The aim of this chapter is to present and analyze the optimum design of the bridge for a certain range of bridge length (10-30m) and a bridge slendernesses of $L/h_{SP} = 16$.

8.2 Definition of the optimization problem

In order to clearly describe an optimization problem one has to define the following:

1. Objective function. An objective is a numerical value that is to be maximized or minimized.
2. Design constraints. A constraint is a condition that must be satisfied in order for the design to be feasible.
3. Design variables. A design variable is a specification that is controllable from the point of view of the designer.

In one sentence the outcome of the optimization process can be stated as follows: *Finding the set of input variables that minimizes or maximizes the objective function by satisfying at the same time all imposed constraints.*

In the following subsections, the explicit definition of the optimization problem for the case of the bridge is presented.

8.2.1 Variables

Since the main goal is to optimize the SP with the integrated longitudinal webs, the geometrical parameters of the SP are considered as variables. Those are presented in Table

8.1 together with their lower and upper bounds.

Table 8.1: Design variables of the optimization process

Variable	Lower bound	Upper bound	Description
t_{0f}	0	100	thickness of the 0°ply at the face (mm)
t_{45f}	0	100	thickness of the 45°ply at the face (mm)
t_{-45f}	0	100	thickness of the -45°ply at the face (mm)
t_{90f}	0	100	thickness of the 90°ply at the face (mm)
t_{0w}	0	100	thickness of the 0°ply at the web (mm)
t_{45w}	0	100	thickness of the 45°ply at the web (mm)
t_{-45w}	0	100	thickness of the -45°ply at the web (mm)
t_{90f}	0	100	thickness of the 90°ply at the web (mm)

From Table 8.1 one can understand that implicitly also the the laminate thicknesses of the we and the faces are variables. In fact these are functions of the thicknesses of the sum of the thicknesses of their plies as presented below.

$$t_f = 2 \cdot (t_{0f} + t_{45f} + t_{-45f} + t_{90f}) \tag{8.1}$$

$$t_w = 2 \cdot (t_{0w} + t_{45w} + t_{-45w} + t_{90w}) \tag{8.2}$$

8.2.2 Constants

The parameters presented here may vary through this section however they remain constant along each optimization run. The parameters that remain constant through each optimization run are called from now on Defined Before each Run (DFBR). A summary of these parameters are presented in Table 8.2. In addition to those parameters all conversion

Table 8.2: Design variables of the optimization process

Parameter	Value	Description
ρ_F	2570	glass fiber density kg/m^3
ρ_R	1100	vinyl ester density kg/m^3
V_f	50	fiber volume content %
L	DFBR	length of the bridge (m)
b	6	width of the bridge (m)
h_{SP}	DFBR	height of the SP
s_w	DFBR	spacing of the webs (mm)
n_w	DFBR	number of webs

and material factors stated in Table 4.3 are also considered constants. Exception to that is the conversion factor that accounts for creep since is a different for every different ply orientation and is a function of the its percentage in the laminate. Finally, constant variables are also considered the loading cases and the actions on the bridge as explicitly stated in chapter 7.

8.2.3 Constraints

The considered constraints that limit the output of the process and thus determine the set of variables are presented in the table below. Constraints are either derived from manufacturing limitations, design codes or the basis of the design as stated in chapter 7.

The prospect for new guidance in the design of FRP, JRC2016 and the dutch fibre-reinforced polymers in civil load-bearing structures recommendations, CUR96, instruct for

Table 8.3: Design constraints of the optimization process

Constraint	Description
$t_f \leq 100mm$	limit from local manufacturer
$t_w \leq 100mm$	limit from local manufacturer
$2t_{45f} \geq 12.5\% \cdot t_f$	New CUR96
$2t_{-45f} \geq 12.5\% \cdot t_f$	New CUR96
$2t_{90f} \geq 12.5\% \cdot t_f$	New CUR96
$2t_{45w} \geq 12.5\% \cdot t_w$	New CUR96
$2t_{-45w} \geq 12.5\% \cdot t_w$	New CUR96
$2t_{90w} \geq 12.5\% \cdot t_w$	New CUR96
$w_{31}(\psi_1 Q_{k1}) \leq \frac{L}{500}$	SLS frequent load combination SIA260
$w_2(G_k) \leq \frac{L}{700} - w_0$	SLS quasi-permanent load combination SIA260
$\varepsilon_{ij,ply} \leq \varepsilon_{ij,failure}, \quad i,j = 1,2$	$1^{(st)}$ ply strain failure
$\lambda_{cr} \geq \frac{\gamma_m}{\eta_c}$	buckling eigenvalue limit, see chapter 7

a minimum fiber reinforcement in each direction for FRP laminates. This minimum fiber reinforcement in each direction is intended to prevent resin failure due to fatigue, creep, impact and accidental loading.

8.2.4 Objective function

The main drawback for broader application of FRP bridges is that their weight per square meter is more or less the same as that of a steel bridge consisting of orthotropic deck. In addition to that the bigger experience of engineers on steel design compared to FRP and considering also the difficulties of the latter in the design make the choice of FRP even more rare. Based on that, the objective function through all the optimization runs is the minimization of the weight of the bridge. Since the bridge is considered to have a constant cross section along its length the design objective is suppressed to the minimization of the cross sectional weight/area.

8.3 Need for advanced optimization algorithms

The more variable parameters one accounts for an optimization problem the more complex the manual optimization gets. In order to understand further this statement, the following example is presented.

8.3.1 Trivial optimization example

Consider a prismatic steel rod subjected to tension. Given the following information, the design optimization of the rod is presented.

Constant parameters

- The applied force of 10KN.
- The ultimate stress of steel as 355MPa considering linear elastic analysis.
- The length and the fixed BC.

Design variables

- The diameter, d, of the rod is the only design variable in that case.

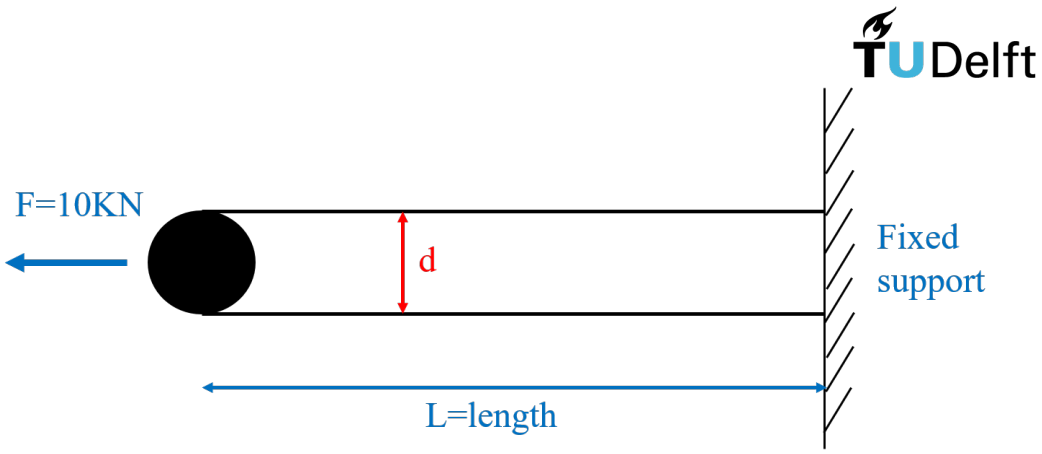

Figure 8.1: Steel rod subjected to tension

Design constraint

- The stress at the rod cannot exceed the limit of 355MPa.

$$\sigma_{rod} \leq 355MPa \tag{8.3}$$

Objective function

- The goal of the optimization is to minimize the weight (objective function).

Since the length of the rod and steel's density are constant, the minimization of the weight can be expresses as:

$$\min(Weight) = \min(Area \cdot L \cdot \rho_{steel}) = \min(Area) = \min(\pi\frac{d^2}{4}) = \min(d) \tag{8.4}$$

One can understand that maximizing the unity check for the constraint of the ultimate stress will end up optimizing the hidden (in this case) objective function of minimizing the weight of the examined structural configuration as follows.

$$\frac{F}{A} \leq 355 \Rightarrow \frac{F}{\pi d^2/4} \leq 355 \Rightarrow d^2 \geq \frac{4F}{355\pi} \Rightarrow$$

$$d \geq 5.9mm \tag{8.5}$$

8.3.2 Optimization workflow

In case of sandwich panel with longitudinal integrated webs, the optimization is not that trivial. In addition to that, lack of analytical solutions for local buckling prediction and plate response for local applied loads (TSs) make things even more difficult. For this reason the model of the bridge has been parameterized in python as an input file for Abaqus 6.14, and with the aid of ModeFrontier the following optimization workflow has been developed. The optimization workflow is driven by a Fast optimizer. This Fast optimizer uses Response Surface Models (Meta-Models) to speed up the optimization process. The MOGA-II optimization algorithm has been used (reference to the ModeFrontier manual). In the workflow, the objective function, the variables and the constraints have been incorporated as stated previously in this chapter. Schematic representation of the workflow is shown in Figure 8.2 and as appears in ModeFrontier in Figure 10.1.

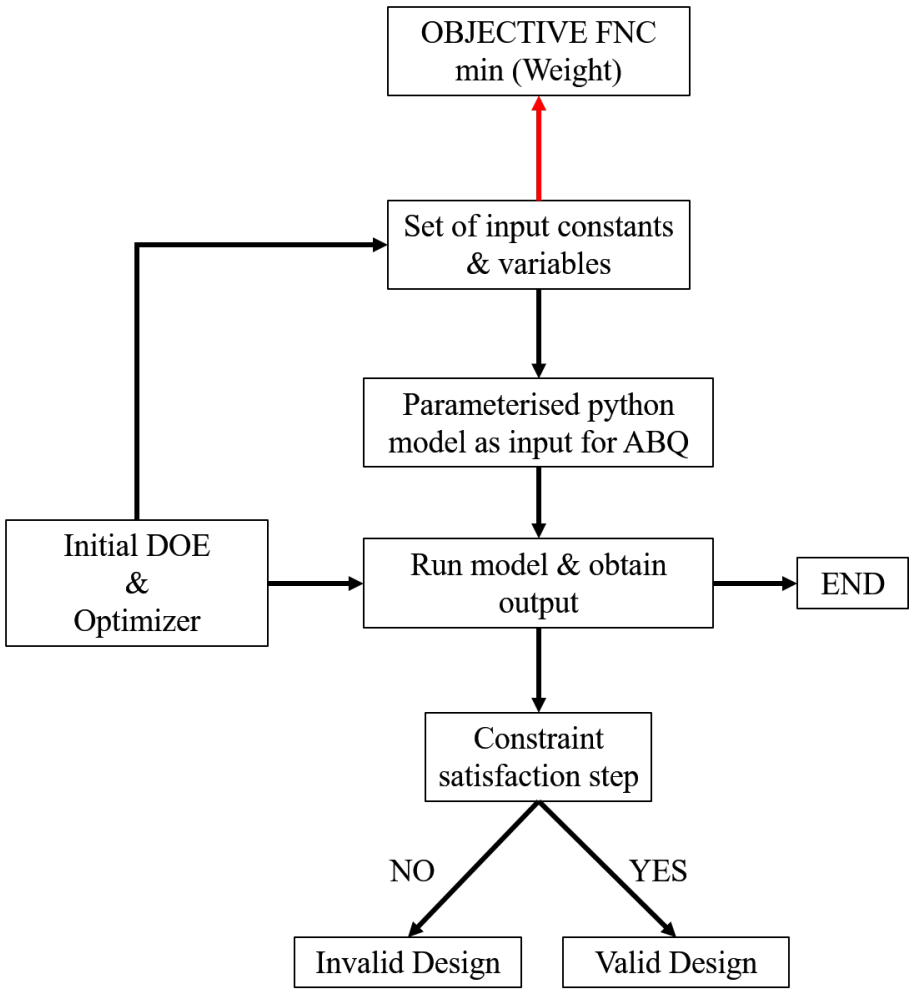

DOE: Design Of Experiment
ABQ: Abaqus
FNC: Function

Figure 8.2: Optimization workflow in modeFrontier

How does the optimization workflow works

The first step is to manually define initial experiments, also called initial population. Then the optimizer runs and from the existing population, taking into account the objective function, generates more experiments. The population is constantly updated and the optimizer "builds up knowledge" regarding the design space, meaning the relation between the input variables and the output data. For the initial population, 5 realization of constraint satisfaction and 35 randomly sets of variables have been used. For each optimization process 400 designs have been evaluated.

The optimization process is performed for an FRP that consist of (a) glass fibers and vinylester type of resin and for (b) flax fibers and vinylester type of resin . The stiffness properties and density of the selected FRPs are shown in Tables 7.3 and 7.4.

8.4 Engineering disadvantages of the optimization algorithm

The optimizer is a mathematical tool and has no engineering thought. One should be really conscious and at the same time careful about this matter. In fact, several experiments generated by the optimizer, while they satisfy all constraints and thus considered as valid designs, they have zero engineering behind them.

Example is the following realization in which, the optimizer chooses the web to be thicker than the faces, and it is not the buckling constraint that provokes that. This leads to a really heavy and inefficient use of the material and also rises failure modes that have not been considered or were unexpected. We can understand that as the face

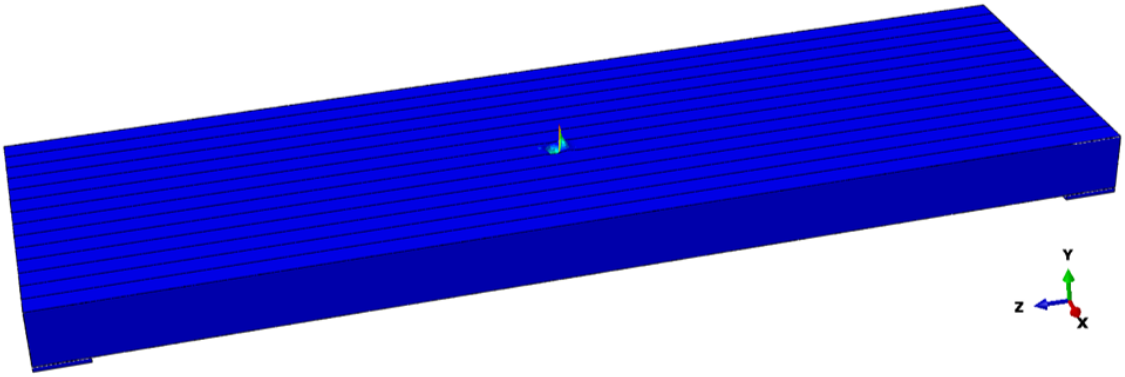

(a) Axonometric view

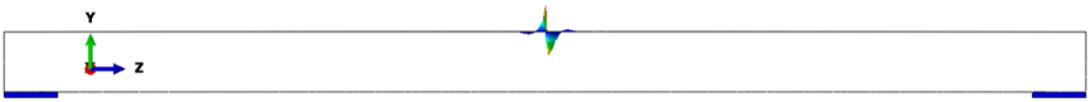

(b) Side view

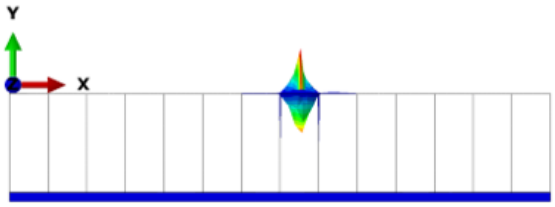

(c) Cross section

Figure 8.3: Valid realization of the optimizer

becomes thinner compared to the web, it becomes more prone to buckle. However, the case presented in Figure 8.3 does not represent the optimum solution out this optimization run (FFRP,$L = 20m$,$L/h_S P = 16$). It has a weight over area $501.4kg/m^2$, while the optimum realization out of this run returns an optimum case of $256kg/m^2$. Of course since the optimizer is set to minimize the weight, the convergence point, which is considered as the optimum point, is in accordance with the engineering principles. This means that the webs get as thin as possible as long as they take over shear deflections and they do not buckle. The main bending deflection resistance comes from the faces which are also most efficient in taking that over resulting in a lighter and more economical design.

8.5 Results

In this section, the results form the optimization runs are presented. Discussion on the results follows. As already mentioned, the goal of the optimization is to minimize the weight of the bridge, by satisfying the imposed constraints (SLS & ULS criteria). The cases of glass and flax FRP are examined for a structural height of $L/h_{SP} = 16$ for a span range of $10 - 30m$. In the design procedure, all partial, conversion and material safety factors are incorporated in order to come up with realistic design dimentions of the cross section of the bridge each time.

8.5.1 Minimum weight

As already mentioned, each bridge span consist of a different optimization process having the same constraints. In Figures 8.4 and 8.5 the optimum (minimum weight) cases that the optimizer achieved are presented, together with their governing constraints. These are the deflection for the comfort criterion, as described in equation 7.6, and the buckling criterion for the web for linear buckling analysis as presented in equation 7.8. In all cases, both for GFRP and FFRP, the ULS strength UC (1^{st} ply strain failure) is not exceeding the value of 0.5 and thus is not reported graphically.

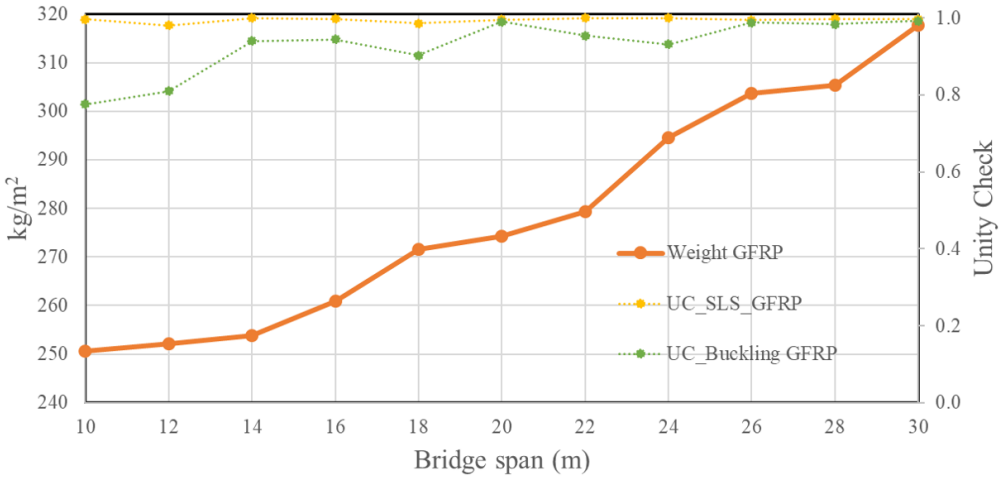

Figure 8.4: Optimum bridge weight for GFRP and structural height $L/h_{SP} = 16$

Plotting the optimum weights for FFRP and GFRP at at the same plot over the bridge span one can do a direct comparison. The spacing of the web is a function of the structural height, at a value of $s_w \approx h_{SP}/3$.

It can be seen in Figures 8.4 and 8.5 that for the case of GFRP the unity check for buckling criterion is closer to 1. That can be attributed to the fact that, shear modulus of FFRP is quite lower compared to GFRP, see Tables 7.3 and 7.4 resulting in a thicker web laminate compared to GFRP, see Figure 8.7. Consequently, this increases the buckling resistance of the FFRP bridge cases while the web laminate of the GFRP case are more slender and more prone to buckle.

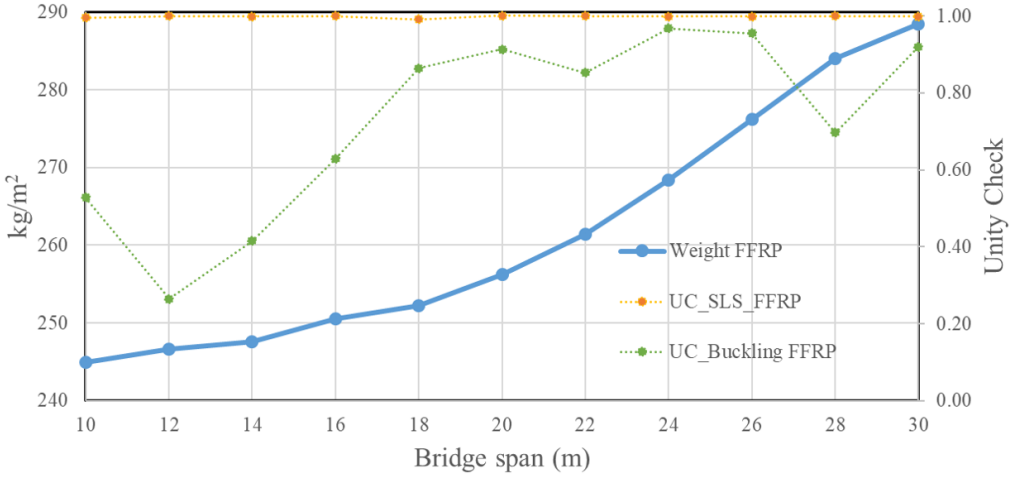

Figure 8.5: Optimum bridge weight for FFRP and structural height $L/h_{SP} = 16$

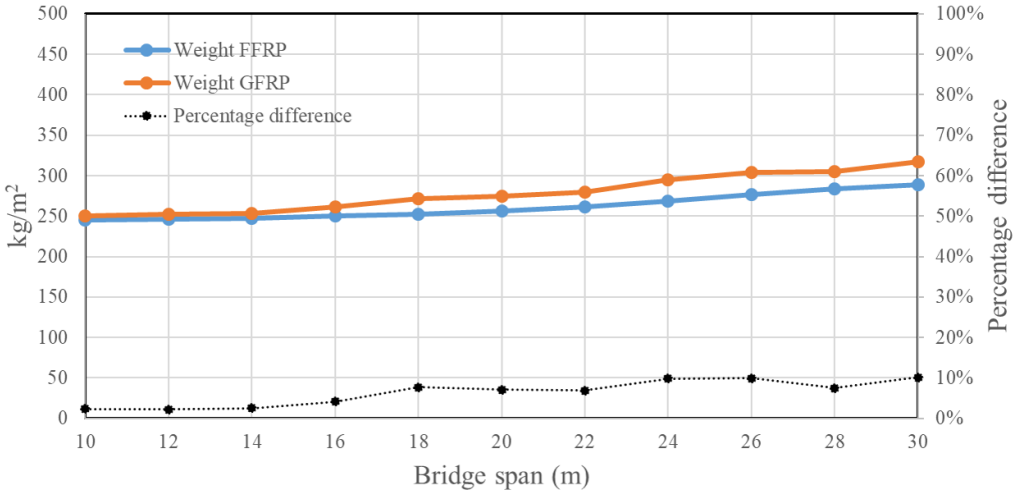

Figure 8.6: Comparison of GFRP and FFRP optimum bridge weight for structural height $L/h_{SP} = 16$

8.5.2 Thickness of laminates

In this subsection the thicknesses of the laminates are presented in Figure 8.7. One can observe that, gradually as the span increases, the thickness of the web increases as well. This is because the deck slenderness is constant and thus the web gets higher, meaning more prone to buckle. This leads to an increased web thickness to satisfy the buckling criterion. However, the increased thickness due to buckling, contributes also to the moment resistance and thus one can observe that for the optimum case the thickness of the faces can be reduced. Of course, since the efficiency of the faces in moment resistance is higher than that of the webs, the reduction of the face thickness is lower compared to the increase in the web thicknesses. This effect lead also to higher weight, as the deflection criteria is always governing, and can be observed in the change of the slope of the weight lines in Figure 8.6 after 14m for GFRP and after 18m for FFRP.

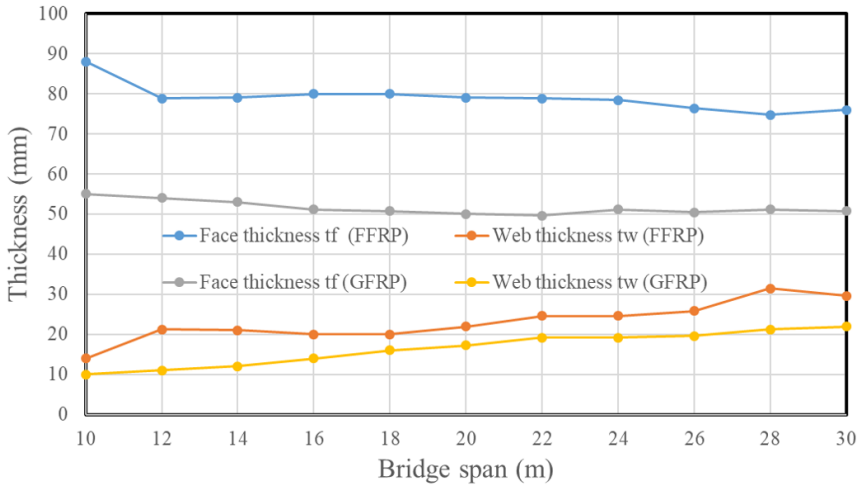

Figure 8.7: Laminate thicknesses over bridge span for GFPP and FFRP for structural height $L/h_{SP} = 16$ and web spacing $s_w = h_{SP}/3$.

8.5.3 Quasi-permanent deflection

In Figure 8.8 the maximum long term deflection, as described in equation 7.5 are plotted. The limit $L/700$ is also included which if exceeded, the initial precambering of the bridge can be calculated according to SIA260. We can conclude that no precambering of the bridge is needed for the selected span range for GFRP and that for FFRP precambering is needed for spans bigger than $28m$.

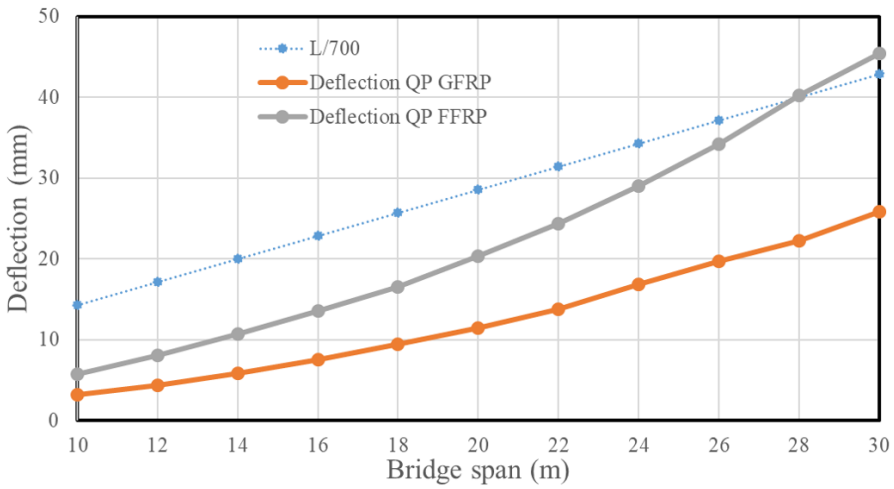

Figure 8.8: Quasi-permanent deflection over span of the bridge for optimum cases

8.5.4 Percentages of fiber orientation of optimum designs

The FRP laminates during the optimization were modeled as symmetric composite layups consisting of UD plies of $0°$,$90°$,$45°$ and $-45°$. The thicknesses of the different oriented plies were treated as variable in an attempt to investigate the optimum ply orientation for the web and the face laminate. It is found that the face laminates should be highly orthotropic with the main percentage of fibers in longitudinal direction, while the optimum fiber plystack for the webs leans closer to a quasi-isotropic laminate. In Table 8.4 the mean values for all optimum cases for each ply orientation together with the standard

deviation are presented for the sample of $10 - 30m$ span cases.

Table 8.4: Percentages of ply orientations for optimum designs in the laminates

Variable	GFRP Mean value (%) $\overline{x}$	GFRP St.Dev.(%) s	FFRP Mean value (%) $\overline{x}$	FFRP St.Dev. (%) s
p_{0f}	61.1	0.70	61.9	0.48
p_{45f}	12.9	0.45	12.6	0.11
p_{-45f}	12.9	0.45	12.6	0.11
p_{90f}	13.2	0.44	12.8	0.40
p_{0w}	35.1	15.19	30.3	6.88
p_{45w}	20.1	4.16	26.9	3.49
p_{-45w}	20.1	4.16	26.9	3.49
p_{90f}	24.6	7.64	15.9	2.43

One can observe in table 8.4 that, mean values of ± 45 plies for the case of FFRP are higher compared to GFRP. This is reasonable and expected if one considers: a)the relatively lower shear modulus of the unidirectional FFRP compared to GFRP ply, see Tables 7.3 and 7.4 and b) the efficiency of ± 45 plies in increasing the shear modulus of the laminate.

8.5.5 Buckling modes

All buckling modes that appear in the optimum designs are local buckling modes of a single web for the buckling cases examined as stated in subsection 7.4.2. More specifically the lowest buckling amplification factor is found for the load case where the LM-1 is positioned close to the support. The case of 20m span for FFRP is selected for visualization of the mode shapes. In Figure 8.9 only the loading due to TSs is depicted for ease of visualization.

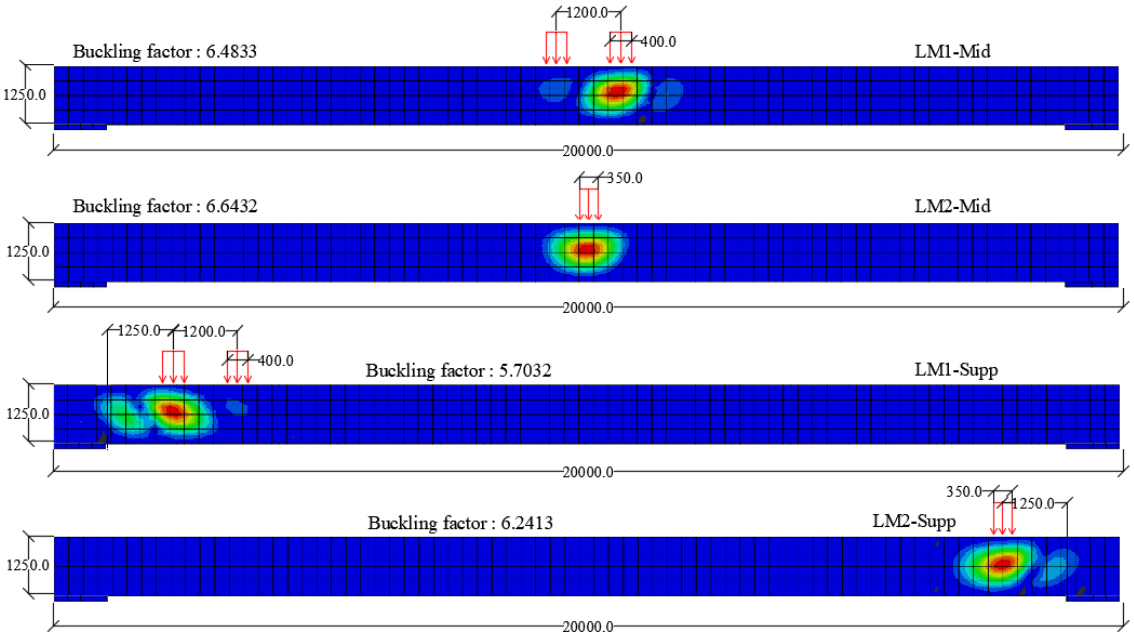

Figure 8.9: Buckling modes for 20m bridge span of FFRP

We can clearly observe that the buckling becomes more critical for the load cases where the TS is positioned close to the support. This is because local vertical buckling and local shear buckling of the web seem to interact. Interaction of buckling modes and how this affect the final buckling resistance of FRP laminates is a topic beyond the scope of this project. However, investigation of this matter is necessary because the interaction of buckling modes may lead to non-linear post buckling behavior of the laminate which makes the assumption of linear buckling weaker.

Analytically, knowing the properties of thickness of each ply, the bending stiffness matrix is found using Classical Laminate Theory for the web laminates of FFRP 20m span case.

$$D = \begin{bmatrix} 9.32 \cdot 10^7 & 5.57 \cdot 10^7 & 8.59 \cdot 10^6 \\ 5.57 \cdot 10^7 & 1.35 \cdot 10^8 & 8.59 \cdot 10^6 \\ 8.59 \cdot 10^6 & 8.59 \cdot 10^6 & 4.04 \cdot 10^7 \end{bmatrix} [MPa] \tag{8.6}$$

The equivalent stiffness constants for the vertical direction are found as:

$$\begin{aligned} D_{11y} &= 1.35 \cdot 10^8 MPa, & D_{12y} &= 8.09 \cdot 10^7 MPa \\ D_{11y} &= 9.32 \cdot 10^7 MPa, & D_{66y} &= 4.04 \cdot 10^7 MPa \end{aligned} \tag{8.7}$$

The integral of s_{22} for LM2-Buckling is found as $7628.7 N/mm$ and the maximum stress $s_{22,max} = 14.02 MPa$, see Figure 8.10. Thus, we can calculate the effective width, $(544.03 mm)$, and make use of the analytical formulas for vertical buckling of the web.

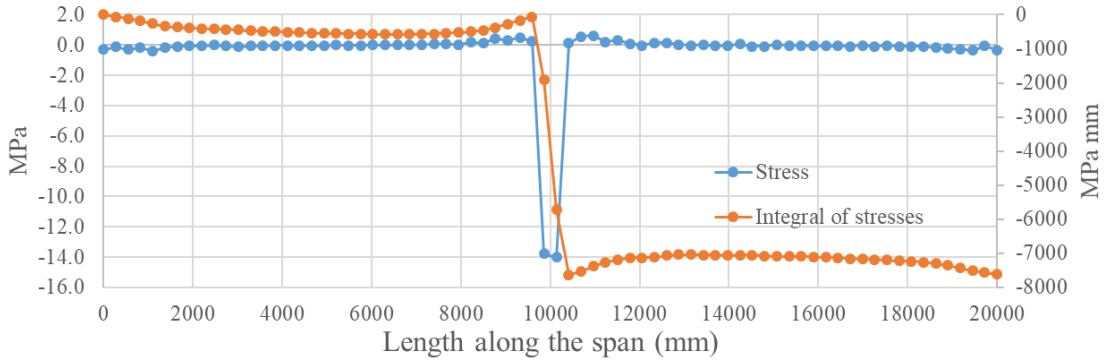

Figure 8.10: Distribution of σ_{22} for LM-2 at the web

Table 8.5: Critical stress calculation using different methods

Type of analysis	Local vertical buckling critical stress [MPa]
FE analysis LM2-Mid	93.15
JRC2016 [9]	1369.11
Kassapoglou CC - SS[8]	185.84

The discrepancy on the results reveal the incapability of analytical formulas to predict the buckling resistance of the laminate. The reasons for that have been already mentioned in subsection 6.5.5 but are also summarized below:

- Analytical formulas cannot account for the actual boundary conditions of the face-web junction.

- Existing analytical formulas account for unique type of loading, pure compression, shear or bending. In reality the laminate experiences a combination of these actions.
- The prediction of JRC2016 does not take into account the aspect ration of the laminate, while Kassapoglou formula does. This might be the reason why the latter's prediction is at the same order of magnitude compared to the FE's prediction.

8.6 $L/300$ deflection limit

The deflection limit is the design requirement which is agreed between the contractor/designer and the client. L/300, is used here alternatively as this was the limit according to the old Dutch code and is still used as a reference by some clients. As already mentioned the Eurocodes do not prescribe a deflection limit for the frequent SLS load combination and thus the $L/500$ limit was adopted from the Swiss structural codes SIA260.

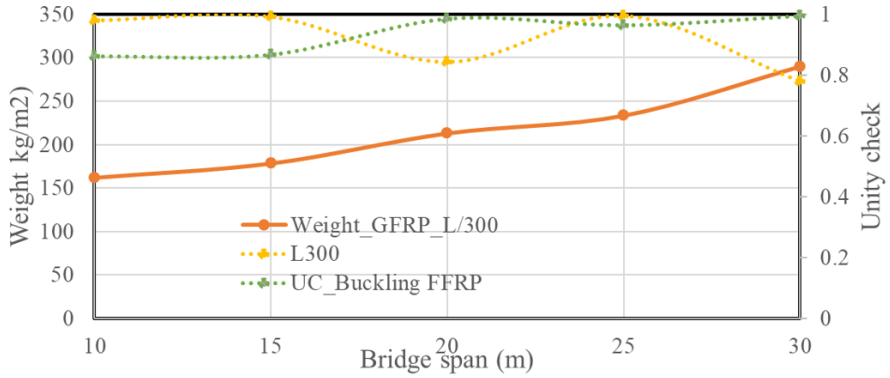

Figure 8.11: Optimum bridge weight for GFRP, structural height $L/h_{SP} = 16$, and $L/300$ comfort criterion limit

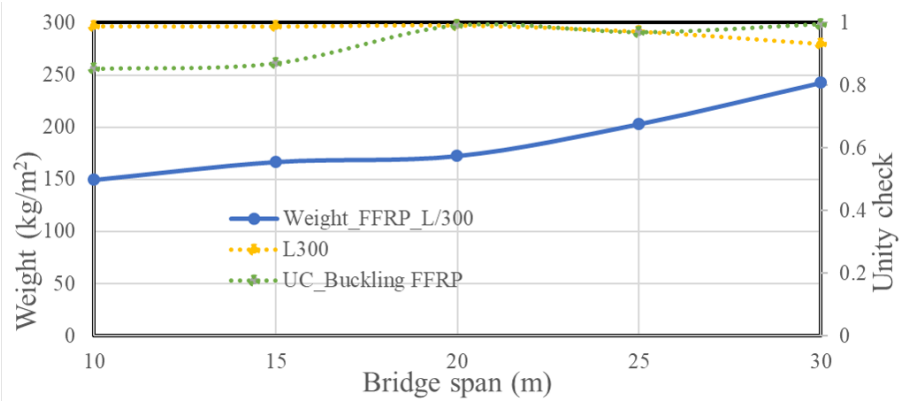

Figure 8.12: Optimum bridge weight for FFRP, structural height $L/h_{SP} = 16$, and $L/300$ comfort criterion limit

We can see in Figures 8.11 and 8.12 that for spans over 20m the unity check for the buckling criterion is always equal to the unity. In addition to that, also for smaller spans the buckling criterion is rather close to 1 in contrary with the cases where $L/500$ deflection limit was considered, see Figures 8.4 and 8.5. For all cases the ULS strength unity check which is expressed by the 1^{st} ply strain failure criterion, does not exceed the value of 0.61 for GFRP and 0.83 for FFRP and thus is not presented graphically.

Comparing the weight of the bridge this case in Figure 8.13, FFRP appears to be from $7 - 20\%$ lighter compared to GFRP.

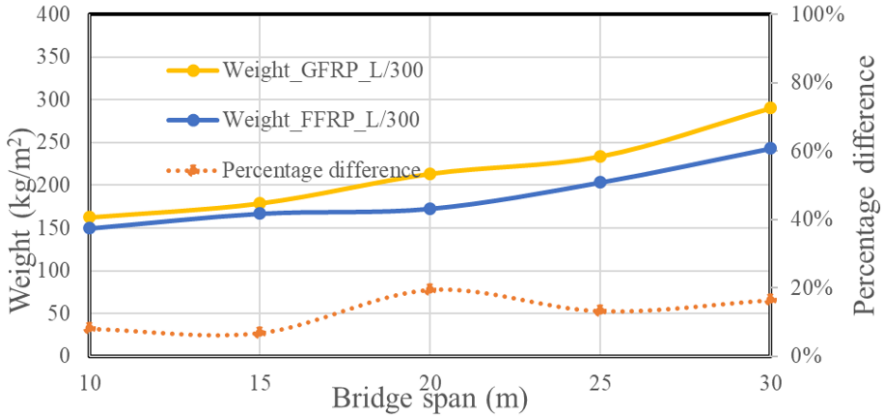

Figure 8.13: Comparison of GFRP and FFRP optimum bridge weight for structural height $L/h_{SP} = 16$ with $L/300$ comfort criterion limit

8.6.1 Quasi-permanent deflection

In Figure 8.14 the maximum long term deflection, as described in equation 7.5 are plotted. The limit $L/700$ is also included which if exceeded, the initial precambering of the bridge can be calculated according to SIA260. We can conclude that no precambering of the bridge is needed for the selected span range for GFRP and that for FFRP precambering is needed for spans bigger than $20m$.

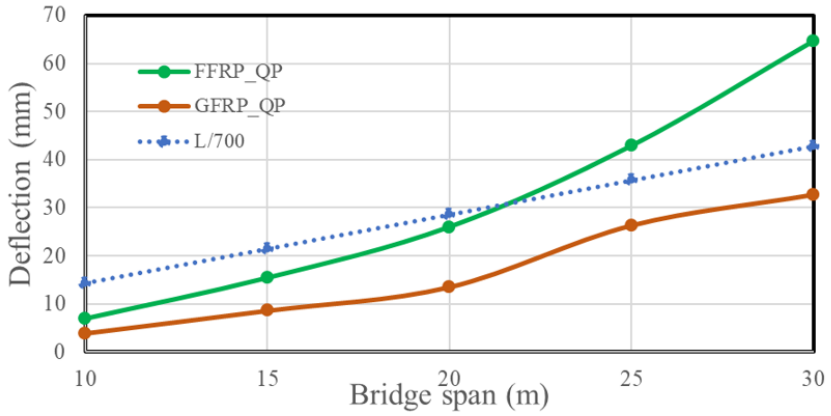

Figure 8.14: Quasi-permanent deflection over span of the bridge for optimum cases

8.6.2 Comparison with L/500 case

In Figure 8.15 the weight of the optimum cases for $L/500$ and $L/300$ deflection limit are shown. Judging by the graph, the reduction in the weight between the two cases decreases as the span increases. The reasoning for that, as already mentioned, is that the decisive criterion for spans greater than $20m$ is the ULS buckling.

Looking into the laminates thicknesses for GFRP in Figure 8.16 and FFRP in Figure 8.17, we can see that the thickness of the web for the two cases is almost the same. The thickness of the faces reduces since now the limit is 60% lower, making the web more prone to buckle since it weakens the rotational stiffness of the face-web junction increasing thus the buckling length of the web laminate.

Finally, the optimum face laminates appear to be highly orthotropic with the majority of fibers in the longitudinal direction of the bridge while the webs lean closer to a quasi-

isotropic laminate. That was also the case when the $L/500$ deflection limit was considered.

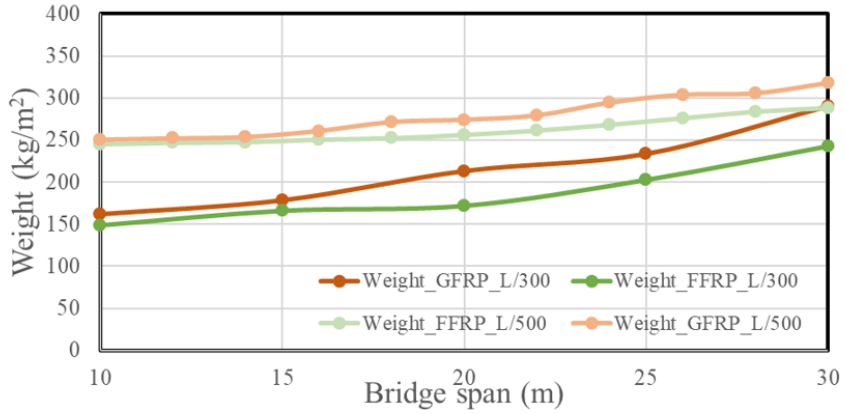

Figure 8.15: Comparison of optimum cases for $L/500$ and $L/300$ deflection limit

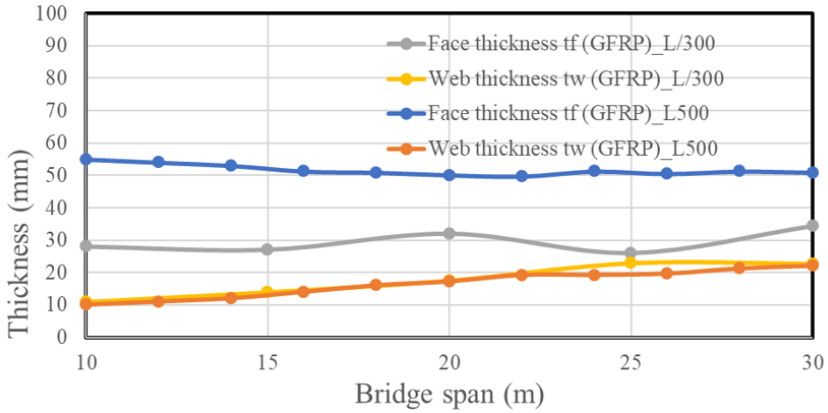

Figure 8.16: GFRP laminate thicknesses for $L/500$ and $L/300$ deflection limit

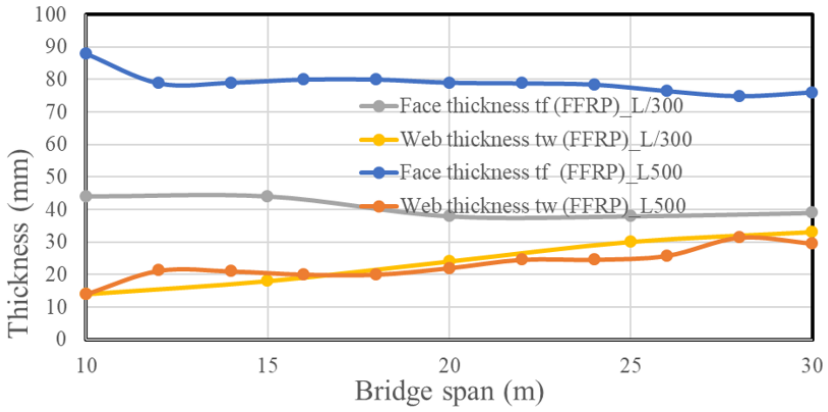

Figure 8.17: FFRP laminate thicknesses for $L/500$ and $L/300$ deflection limit

8.7 Optimum deck slenderness

The deck slenderness throughout the optimization process has been chosen to be $L/h_{SP} = 16$. However, this might not be the optimum (meaning the lightest) possible solution for all spans of the bridge. If one has used multi-objective optimization tools, then he could have set both minimization of the weight and maximization of the slenderness as objectives. Then the outcome would not be a single point but a so called *pareto font*. This is a set of points representing the optimum cases which would be a trade-off between weight and deck slenderness. The application of multi-objective optimization in this study appeared to be rather computationally demanding in order to achieve convergence and also difficult to set up. The difficulty mainly lies on the fact that the model changes in two dimensions. It is not only the height of the deck that varies but also the spacing of the webs as function of the former.

For illustration purposes, the investigation for optimum deck slenderness has been run manually (using single objective optimization, weight minimization) for the case of GFRP 12m span bridge. $L/500$ SLS frequent load combination deflection limit has been considered and a web spacing of $s_w \approx h_{SP}/3$.

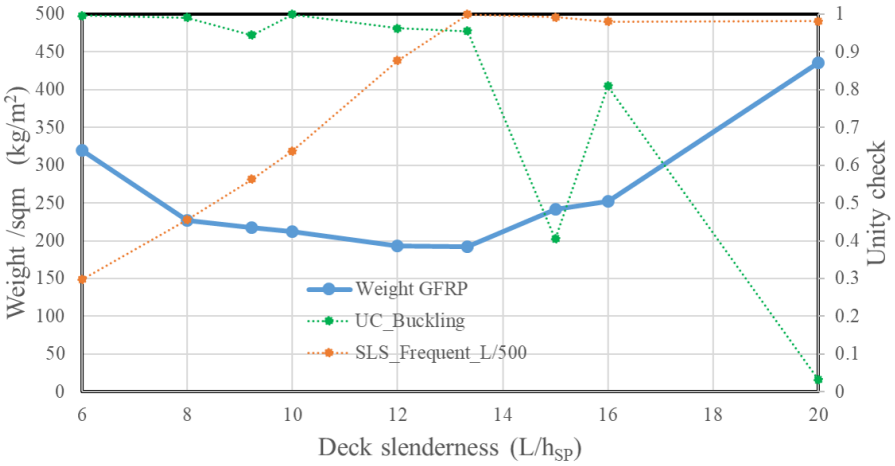

Figure 8.18: Weight of 12m span GFRP bridge varying the deck slenderness

As we can see in Figure 8.18 the optimum (minimum weight) deck slenderness for a 12m GFRP span bridge is $L/h_{SP} \approx 13.5$. **This is also the point where the two decisive design criteria turn simultaneously into the unity.** The weight of the bridge follows a parabolic path. For low values of deck slendernesses, the buckling is the decisive criterion as the slenderness of the web increases, while for higher deck slendernesses the decisive criterion becomes the SLS deflection limit. In all cases the unity check for ULS strength does not exceed the value of 0.62. In Figure 8.19 the thicknesses of the face and web laminates are presented for the run cases. The relatively increased thickness of the face laminate in low deck slendernesses can be explained due to the rotational stiffness it offers to the boundaries of the web laminate, decreasing thus the latter's buckling length. For deck slenderness $L/h_{SP} > 13.3$, the face thickness increases exponentially in order for the structure to satisfy the deflection limit of the frequent load combination, increasing thus the total weight of the bridge. The thickness of the web is driven by the buckling criterion until the optimum deck slenderness.

The quasi-permanent load combination for SLS does not exceed the $L/700$ limit and thus no initial precambering is needed according to SIA260. Quasi-permanent deflection follow the norm of frequent's load combination deflections as expected, see Figure 8.20.

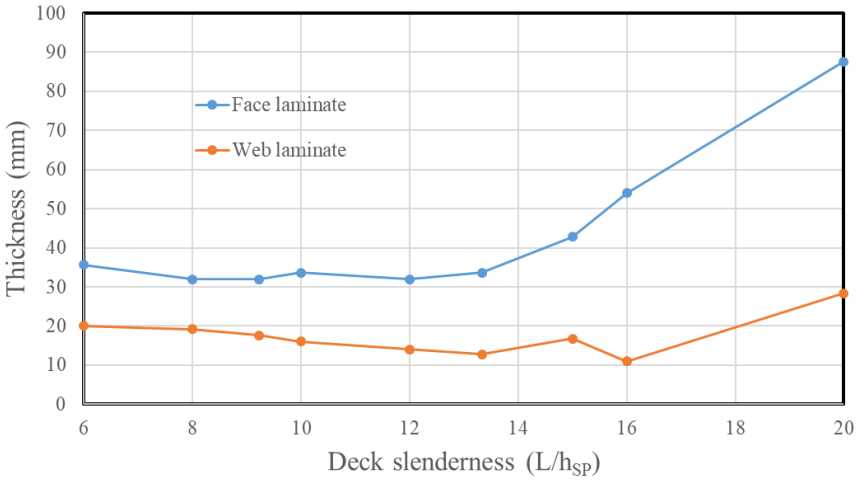

Figure 8.19: Weight of 12m span GFRP bridge varying the deck slenderness

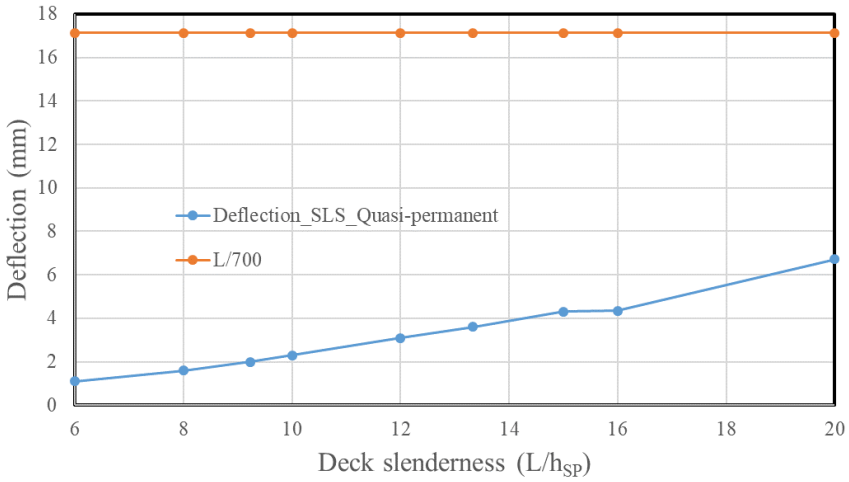

Figure 8.20: Deflection under permanent load for 12m span GFRP bridge varying the deck slenderness

Finally, it is not possible to generalize for all span and material cases that the optimum deck slenderness is $L/h_{SP} \approx 13.5$. That depends on the material properties of the FRP considered, the span of the bridge and the spacing of the web. As it can be seen in Figures 8.4 and 8.5, there are cases where both design criteria have a unity check equal to 1 which is a reliable sign that the design is very close to the theoretical optimum.

Chapter 9

Conclusions and future work

9.1 Conclusions

The following conclusions have been made considering the assumptions for material properties based on available literature. The safety factors which reduce the resistance in case of ULS while reduce the stiffness properties for SLS, are summarized in Table 9.1. Strain and shear strain failure for both materials is considered as 1.2% and 1.6% respectively.

Table 9.1: Summary of safety factors for considered laminates, see Tables 7.3 and 7.4

Limit State	GFRP	FFRP
ULS Strength	2.68	4.22
ULS Local buckling	2.98	5.21
SLS Comfort	1.39	1.54
SLS Long-term	1.39/3.45/3.45 see Table 7.3	3.09/3.85/3.85 see Table 7.4

- Flax FRP with a $V_f = 50\%$ returns a lighter bridge superstructure compared to glass FRP. The weight benefit by using flax FRP ranges from 2-10% as it is shown in Figure 9.1 and is attributed to the lower weight of FFRP.

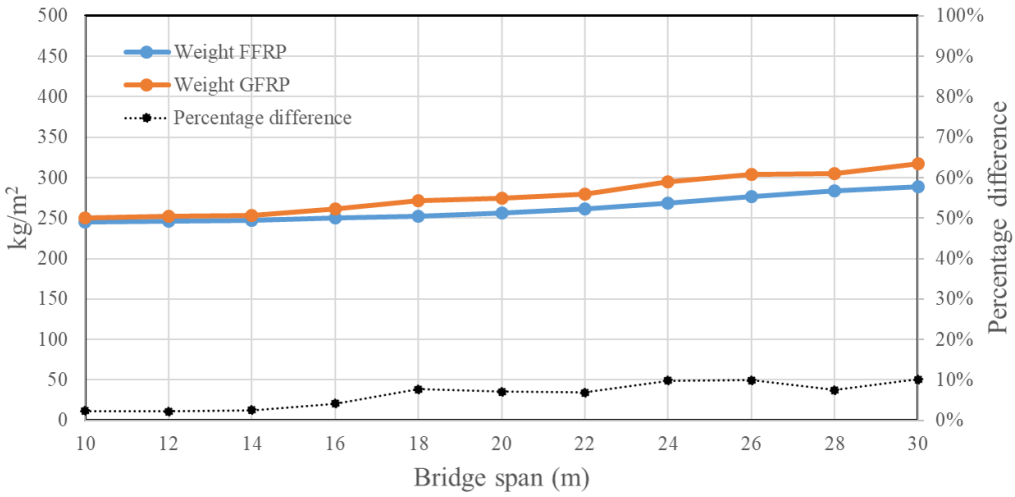

Figure 9.1: GFRP and FFRP optimum bridge weight for structural height $L/h_{SP} = 16$ and $s_w = h_{SP}/3$ spacing of the web

- Local buckling of the web drives the design, and make the structure heavier. The reason for that is that it increases the thickness of the web which are the least efficient in taking over deflections (apart from shear deflections).

- ULS strength criterion was never decisive for the examined cases, verifying the well known strain based design property of FRP structures. The maximum UC reaches the value of 0.85 for $L/300$ deflection limit, while it does not exceed the value of 0.5 for $L/500$ deflection limit.

- Accounting for the lightest possible foam material given by [9], increases $2-3$ times the buckling resistance of the web laminates since it acts as an elastic out of plane support. This can imply large weight reductions for spans larger than 20m where local buckling is the dominant design criterion.

- Changing the deflection limit from $L/500$ to $L/300$ results to almost linear 35% to 9% reduction of weight for 10 to 30m GFRP bridge span respectively, while for FFRP the reduction ranges from 40% to 16% for 10 to 30m bridge span as it is shown in Figure 9.2.

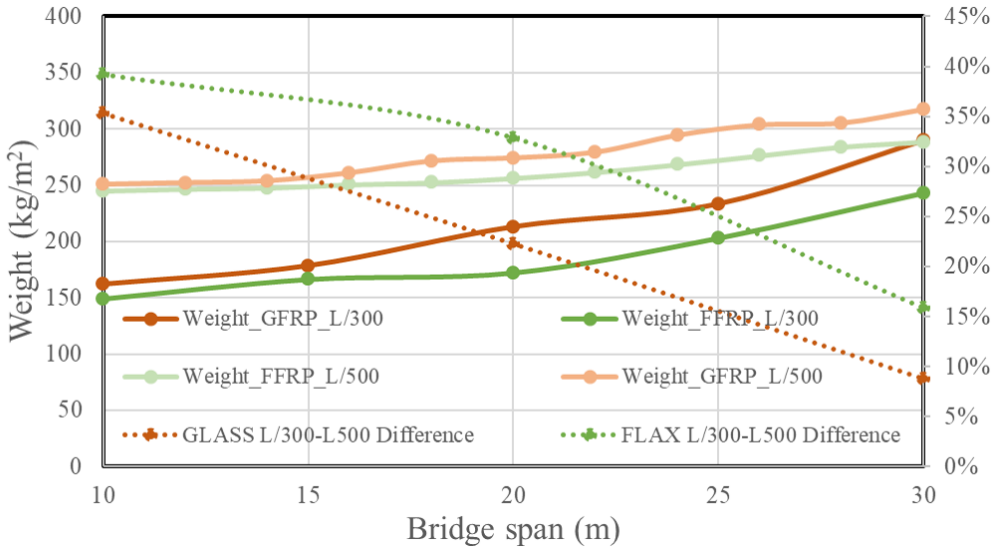

Figure 9.2: Comparison of GFRP and FFRP optimum bridge weight for $L/300$ and $L/500$ deflection limit and considering structural height $L/h_{SP} = 16$

9.2 Recommendations

- In the type of structure considered (sandwich panel with integrated longitudinal webs) face laminates should be highly orthotropic with the majority of fibers in longitudinal direction, while the optimum fiber plystack for the webs leans closer to a quasi-isotropic laminate, see Table 8.4.

- The optimum plystack sequence for the web laminates is to place the 90° fabric at the outermost fiber of the laminates, then the ±45° and finally the 0° fabric in the middle. The reasoning is that for out of plane deflections and thus buckling, this arrangement enhances the buckling resistance of the web.

- Regarding the plystack of the face laminates the 90° fabric should be places at the outermost fiber. In this way the load can be more easily transversely distributed.

- FE linear buckling analysis can give a better insight on the local buckling of the web compared to analytical formulas that need to be further developed. The advantage of FE is that it takes into account the actual rotational stiffness of the web-face junction and that returns a better insight on the distribution of stresses.

9.3 Future work

- Fatigue and interlaminar shear failure in such thick laminates need to be considered in order to have a better insight on the capabilities of FFRP.
- In order to account for the foam material during the design, not only its mechanical properties but also the durability of the foam and the interface between the foam and FRP laminates need to be investigated in experiments.
- Initial imperfections have not been considered during this project. Non-linear buckling analysis should be performed to investigate the sensitivity of buckling on geometrical initial imperfections.
- Experimental investigation upon all the aforementioned matters, including the environmental effects on bio-based FRP, is needed in order to support and verify the numerical models, especially for the case of natural fiber FRP where the available literature data are limited.

Chapter 10

Annex A

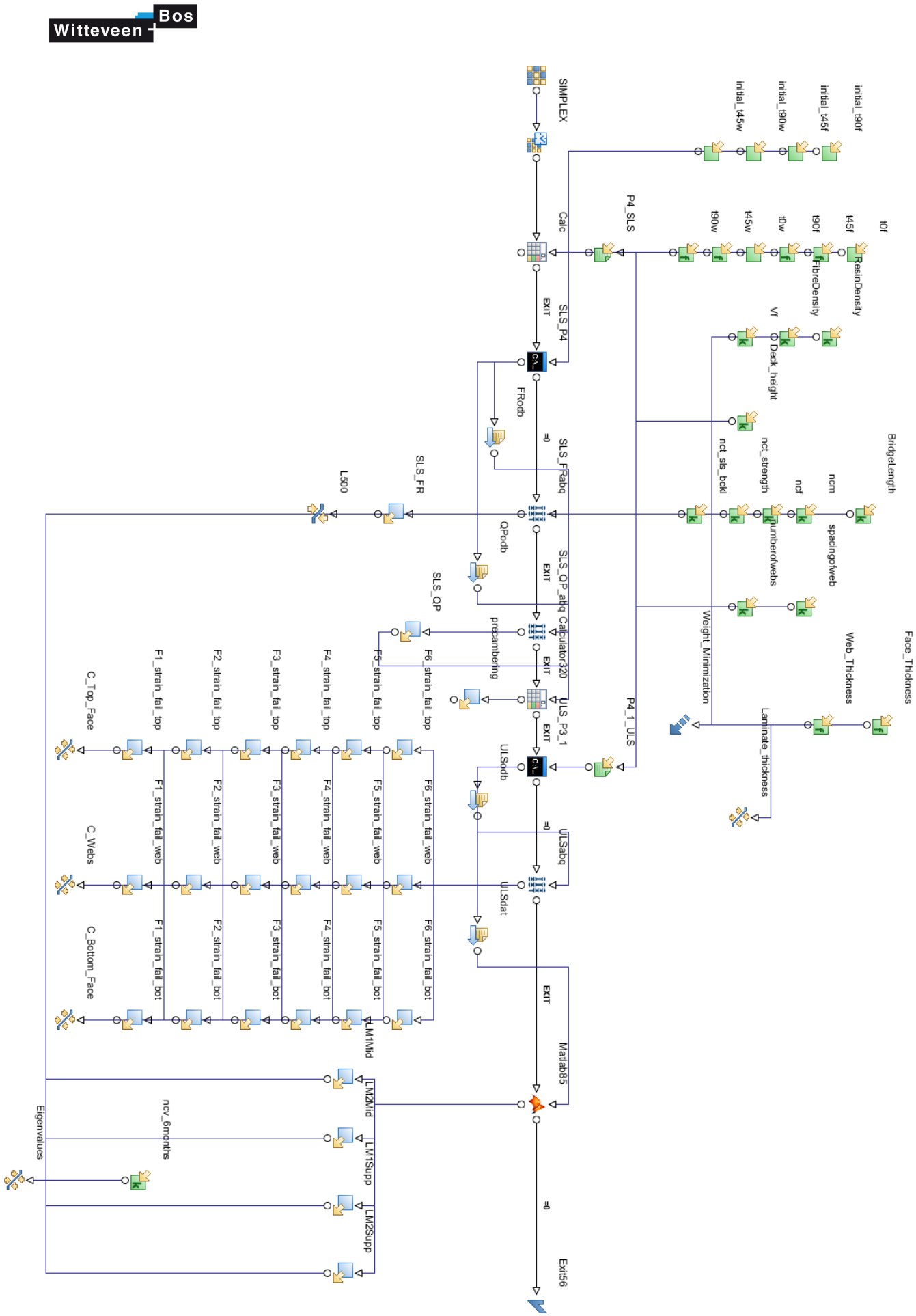

Figure 10.1: Optimization workflow in modeFrontier

Bibliography

[1] N. Jauhari, R. Mishra, and H. Thakur, "Natural Fibre Reinforced Composite Laminates - A Review," *Materials Today: Proceedings*, vol. 2, no. 4-5, pp. 2868–2877, 2015.

[2] L. Pil, F. Bensadoun, J. Pariset, and I. Verpoest, "Why are designers fascinated by flax and hemp fibre composites?," *Composites Part A: Applied Science and Manufacturing*, vol. 83, pp. 193–205, 2016.

[3] H. L. Bos, *The potential of flax fibres as reinforcement for composite materials.* 2004.

[4] A. Célino, S. Fréour, F. Jacquemin, and P. Casari, "The hygroscopic behavior of plant fibers: a review," *Frontiers in Chemistry*, vol. 1, no. January, pp. 1–12, 2014.

[5] M. Assarar, D. Scida, A. El Mahi, C. Poilâne, and R. Ayad, "Influence of water ageing on mechanical properties and damage events of two reinforced composite materials: Flax-fibres and glass-fibres," *Materials and Design*, vol. 32, no. 2, pp. 788–795, 2011.

[6] A. Zhou, "Stiffness and Strength of Fiber Reinforced Polymer Composite Bridge Deck Systems," *Engineering Mechanics*, vol. PhD, p. 249, 2002.

[7] B. D. Manshadi, "Biaxial Wrinkling of Thin-Walled GFRP Webs in Cell-Core Sandwiches," vol. 5185, 2011.

[8] C. Kassapoglou, *Design and Analysis of Composite Structures.* 2010.

[9] L. Ascione, J.-F. Caron, P. Godonou, K. Van Ijselmuijden, J. Knippers, T. Mottram, M. Oppe, M. G. Sorensen, J. Taby, L. T. Editors, E. Gutierrez, S. Dimova, A. Pinto, and S. Denton, *Prospect for New Guidance in the Design of Frp.* 2016.

[10] E. Sparnins, *Mechanical properties of flax fibers and their composites.* 2006.

[11] L. Yan, N. Chouw, and K. Jayaraman, "Flax fibre and its composites - A review," *Composites Part B: Engineering*, vol. 56, pp. 296–317, 2014.

[12] N. Saba, M. Jawaid, O. Y. Alothman, and M. T. Paridah, "A review on dynamic mechanical properties of natural fibre reinforced polymer composites," *Construction and Building Materials*, vol. 106, no. December, pp. 149–159, 2016.

[13] D. B. Dittenber and H. V. S. Gangarao, "Critical review of recent publications on use of natural composites in infrastructure," *Composites Part A: Applied Science and Manufacturing*, vol. 43, no. 8, pp. 1419–1429, 2012.

[14] W. Claassen, "Bio-based composite moveable bridge The design process," no. September, pp. 21–23, 2016.

[15] P. G. F. Bosman, "Flax fibre reinforced polymer in outdoor structures - durability,"

[16] K. L. Pickering, M. G. A. Efendy, and T. M. Le, "A review of recent developments in natural fibre composites and their mechanical performance," *Composites Part A: Applied Science and Manufacturing*, vol. 83, pp. 98–112, 2015.

[17] M. Aslan, B. F. Sørensen, and B. Madsen, *Characterisation of flax fibers and flax fiber composites. Being cellulose based sources of materials.* DTU Wind Energy, no. 0005 ed., 2012.

[18] O. Faruk, A. K. Bledzki, H. P. Fink, and M. Sain, "Biocomposites reinforced with natural fibers: 2000-2010," *Progress in Polymer Science*, vol. 37, no. 11, pp. 1552–1596, 2012.

[19] O. Faruk, A. K. Bledzki, H.-P. Fink, and M. Sain, "Progress Report on Natural Fiber Reinforced Composites," *Macromolecular Materials and Engineering*, vol. 299, no. 1, pp. 9–26, 2014.

[20] F. P. La Mantia and M. Morreale, "Green composites: A brief review," *Composites Part A: Applied Science and Manufacturing*, vol. 42, no. 6, pp. 579–588, 2011.

[21] J. Mussig, ed., *Industrial Applications of Natural Fibres.* 2010 John Wiley & Sons, Ltd, 2010.

[22] X. Song, "Vacuum Assisted Resin Transfer Molding (VARTM): Model Development and Verification," *Doctor thesis*, p. 161, 2003.

[23] C. Kong, H. Park, and J. Lee, "Study on structural design and analysis of flax natural fiber composite tank manufactured by vacuum assisted resin transfer molding," *Materials Letters*, vol. 130, pp. 21–45, 2014.

[24] F. Senese, "What is cellulose?."

[25] O. Faruk and M. Ain, *Biofiber reinforced polymer composites for structural applications.* 2013.

[26] E. J. Barbero, *Finite Element Analysis of Composite Materials using AbaqusTM.* 2013.

[27] J. García-Manrique and E. Muñoz, "Water absorption behaviour and its effect on the mechanical properties of flax fibre reinforced bioepoxy composites," *International Journal of Polymer Science*, vol. 2015, pp. 16–18, 2015.

[28] L. Yan and N. Chouw, "Effect of water, seawater and alkaline solution ageing on mechanical properties of flax fabric/epoxy composites used for civil engineering applications," *Construction and Building Materials*, vol. 99, pp. 118–127, 2015.

[29] F. Bensadoun, K. A. Vallons, L. B. Lessard, I. Verpoest, and A. W. Van Vuure, "Fatigue behaviour assessment of flax-epoxy composites," *Composites Part A: Applied Science and Manufacturing*, vol. 82, pp. 253–266, 2016.

[30] S. Liang, P.-b. Gning, L. Guillaumat, S. Liang, P.-b. Gning, and L. Guillaumat, "A comparative study of fatigue behaviour of flax / epoxy and glass / epoxy composites Science Arts & Métiers (SAM)," 2014.

[31] S. Liang, P. B. Gning, and L. Guillaumat, "Properties evolution of flax/epoxy composites under fatigue loading," *International Journal of Fatigue*, vol. 63, pp. 36–45, 2014.

[32] M. Zoghi, *The international handbook of FRP composites in civil engineering*, vol. 6012. 2014.

[33] M. Areiza Hurtado, A. Bansal, C. Paulotto, and S. Primi, "FRP girder bridges: lessons learned in Spain in the last decade," *6th International Conference on FRP Composites in Civil Engineering (CICE 2012)*, no. June, pp. 13–15, 2012.

[34] T. a. Hoffard and L. J. Malvar, "Fiber-Reinforced Polymer Composites in Bridges: A State-of-the-Art Report," no. May, p. 38, 2005.

[35] L. Fagerberg, "Wrinkling of Sandwich Panels for Marine Applications," *Doctoral Thesis at the Department of Aeronautical and Vehicle Engineering at the Royal Instite of Technology*, 2003.

[36] I. Lukačević, "COMBINED LATTICE AND VIERENDEEL GIRDER IN LONG-SPAN STEEL," no. 12, pp. 28–38, 2016.